ER-18 Final Report

AE-440: Jet Propulsion Detail Design

Course Instructor: Dr. Mark Ricklick

Authors: Anuranan Bharadwaj, Nicholas Pradilla,
Kalkamanali Satvaldy, Vincent Shi

Embry-Riddle Aeronautical University

Daytona Beach, FL, 32114-3800

April 28th, 2026

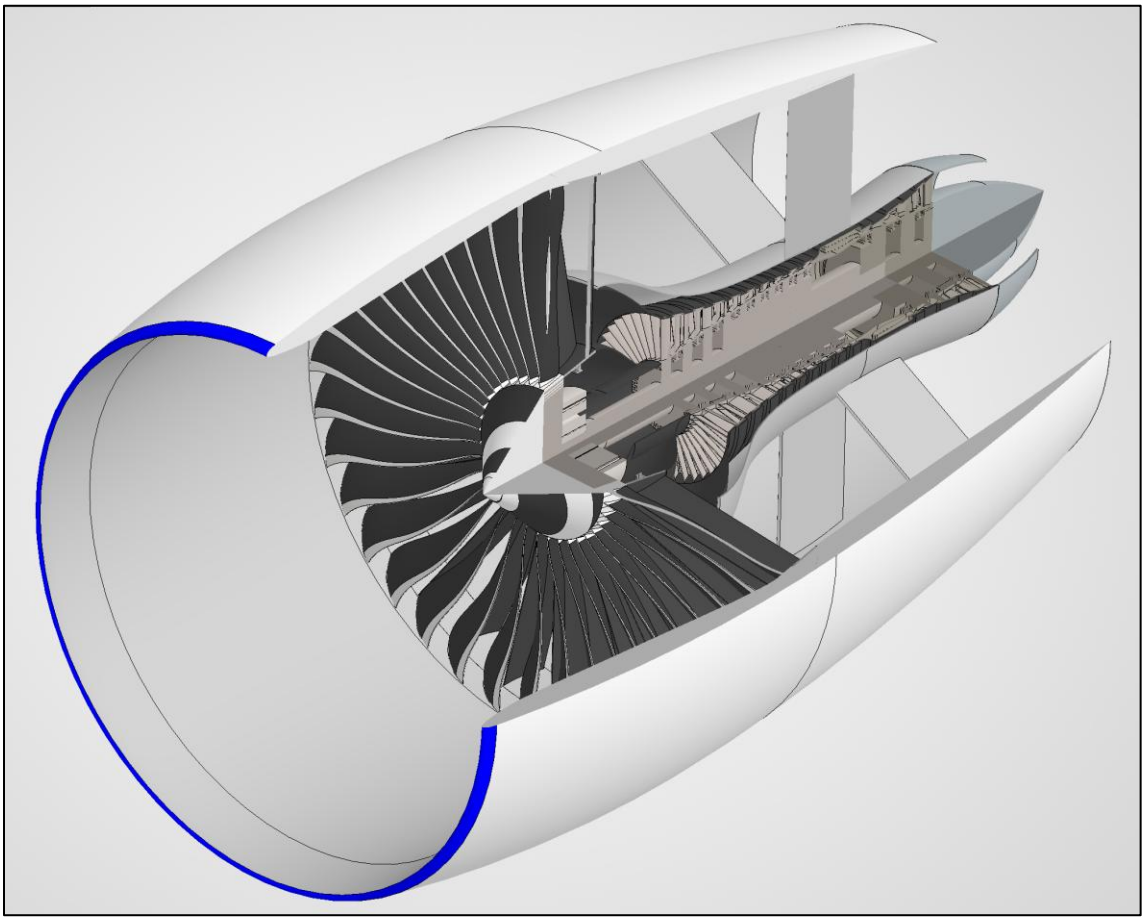

Figure 1: Proposed Engine CAD

Contents

Abstract 3
Introduction 4
Cycle Design 7
Inlet Design 9
Fan Design 17
Low-Pressure Compressor Design 22
High-Pressure Compressor Design 31
Combustor Design 41
Turbine (High-Pressure & Low-Pressure) Design 43
Nozzle Design 54
Appendix A: Engineering Ethics 60
Appendix B: Engineering Standards 60
Appendix C: Teamwork / Self-Reflection 61
Anuranan Bharadwaj 61
Nicholas Pradilla 62
Kalkamanali Satvaldy 62
Vincent Shi 63
Appendix D: Detailed Station Data 63

Abstract

The ER-18 airlifter requires a propulsion system that delivers high thrust for short-runway takeoff under hot conditions while maintaining strong fuel efficiency during long-duration cruise and loiter missions. This report presents the design of a high-bypass turbofan engine developed to meet these requirements. The primary challenge was balancing high takeoff thrust with efficient high-altitude operation, where the engine is expected to spend most of its service life.

The design was developed using an iterative process, beginning with cycle analysis and extending through the inlet, turbomachinery, combustor, and nozzle. A MATLAB-based cycle tool was created and validated against existing software like AEDsys to ensure reliable thermodynamic predictions. The turbomachinery design formed the core of the process, where parameters such as loading, flow coefficients, and rotational speeds were adjusted to achieve physically consistent velocity triangles, acceptable aerodynamic limits, and realistic geometry. Design decisions were continuously evaluated based on performance constraints, system integration, and comparison with existing engines.

The final configuration is a high bypass, separate exhaust turbofan (non-afterburning) with a bypass ratio of 11 and an overall pressure ratio of 55. The engine consists of a single-stage fan, a three-stage low-pressure compressor, a six-stage high-pressure compressor, a one-stage high-pressure turbine, and a two-stage low-pressure turbine. A gearbox with a 3.2:1 reduction ratio is used to operate the fan at a lower RPM for improved efficiency. The engine produces approximately 196 kN of thrust at takeoff and 67 kN at cruise (Mach 0.85 at 12,192 m), with a specific thrust of 84 N/(kg/s) and a TSFC of approximately 16 (g/s)/kN. The design emphasizes reduced stage count to minimize weight and complexity, while maintaining acceptable aerodynamic and thermodynamic performance.

When compared to existing engines such as the GE90 and GE9X, the proposed engine achieves similar performance trends with fewer compressor and turbine stages, resulting in a simpler configuration. While this may lead to a slight reduction in peak efficiency, the overall design provides a balanced solution that meets mission requirements with competitive fuel consumption, adequate thrust capability, and reduced system complexity. From the preliminary analysis, the proposed engine also demonstrates flat-rated characteristics, where it is capable of maintaining near-constant thrust output across a range of operating conditions, particularly during takeoff under varying ambient temperatures. This provides a more consistent and reliable performance envelope, ensuring that thrust requirements are met without significant degradation in hot-day or off-design conditions.

Introduction

This section outlines the overall design process and the key design choices made for each component, which are discussed in detail in the subsequent sections. The operation of a jet engine can be described as follows: the inlet smoothens and directs the incoming flow, while the fan draws in a large mass of air. The compressor stages then increase the pressure of the flow to levels required for efficient combustion. In the combustion chamber, fuel is injected, increasing the enthalpy of the flow and energizing it sufficiently to drive the turbine blades. The turbines extract work to power the compressor and fan, and finally, the flow expands through the nozzle, accelerating to produce thrust.

From the preliminary analysis, it was established that the proposed engine must generate sufficient thrust to enable short-runway takeoff under hot conditions, while also maintaining high fuel efficiency for long loiter missions at high cruising altitudes. These mission requirements strongly influenced the cycle design. Key outcomes included the selection of a high bypass ratio, high overall pressure ratio, significant thrust lapse at altitude, high mass flow rate, and a relatively high takeoff weight for the aircraft.

The overall design process followed an iterative approach, ensuring that parameters across all components remained consistent and compatible. The process began with refining the engine cycle, followed by the design of the inlet and nozzle. The majority of the effort was then focused on the turbomachinery components (fan, compressors, and turbines), which form the core of the engine. The combustor was designed in the final stage, using both calculated conditions and reference to existing designs.

The cycle, inlet, and nozzle were initially analyzed at both takeoff and cruise conditions. For turbomachinery design, a key design philosophy was to prioritize cruise conditions, since the engine is expected to operate most of its life in that regime. Other components were then adjusted accordingly to ensure overall consistency and performance across the operating envelope.

The following tables summarize the key engine parameters and major design features of the proposed engine.

Table 1: Engine Design Parameters

Design Variable	Value
Type	High Bypass Separate Exhaust Turbofan (Non-Afterburning)
Compressor	1 Fan, 3-stage LP, 6-stage HP
Turbine	1-stage HP, 2-stage LP
Gearbox	Star-configuration Planetary, 5-Planet, 3.2:1 reduction ratio

Combustor	Annular
Nozzle (Fan & Core)	Converging
Fan	365 cm
Length	663 cm (Inlet to Core Nozzle Exhaust Cone)
Width x Height	379 x 380 cm
Overall Pressure Ratio	55
High-Pressure Compressor Ratio	15.7
Low-Pressure Compressor Ratio	3.5
Fan Pressure Ratio	1.3
Bypass Ratio	11
Turbine Inlet Temperature	1778 K
Customer Bleed	5 %
Cooling 1	5 %
Cooling 2	5 %
Power Takeoff Coeff – LP	0
Power Takeoff Coeff – HP	0.000321
RPM	Fan 2200, LP 7000, HP 13000
Takeoff Thrust	196 kN

Table 2: Design Features at Cruise

Parameter	Value
Cruise Condition	0.85 M, 12192 m
Total Air Mass Flow	635 kg/s
Air Mass Flow – Fan	582 kg/s
Air Mass Flow – Core	52 kg/s
Thrust	67 kN
Specific Thrust	84 N/ (kg/s)
TSFC	16 (g/s) /kN

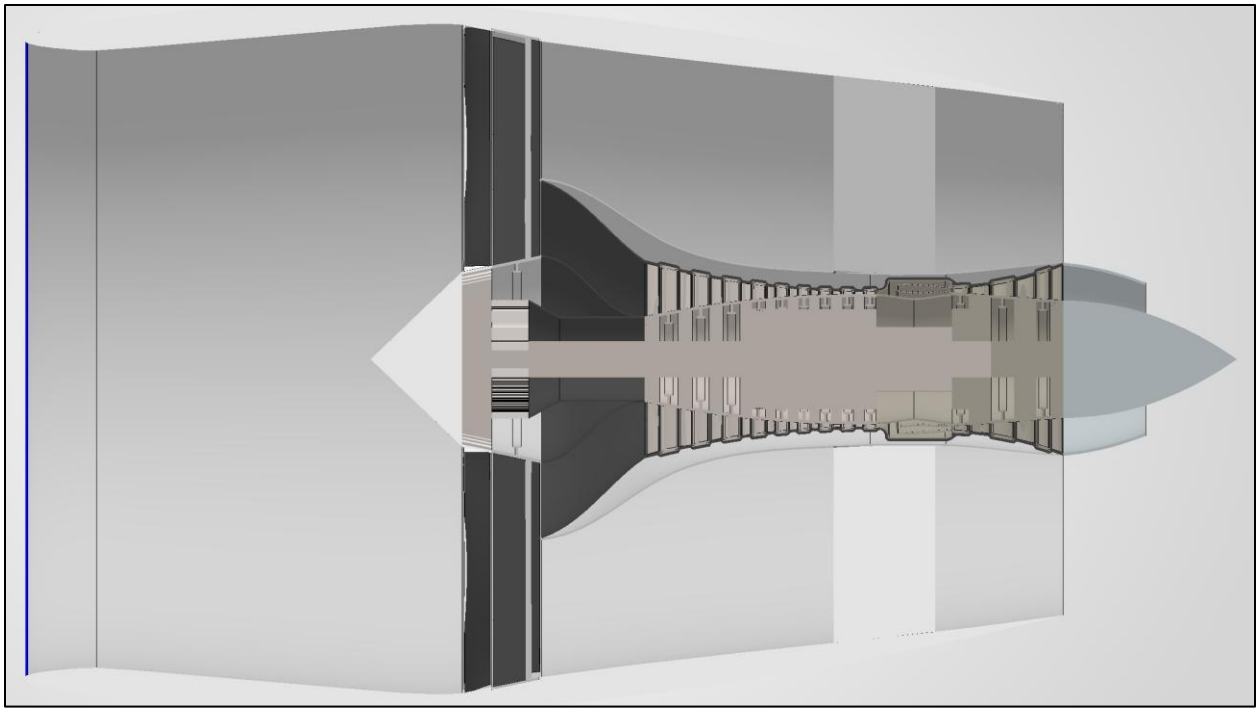

Figure 2: Engine Cross Section

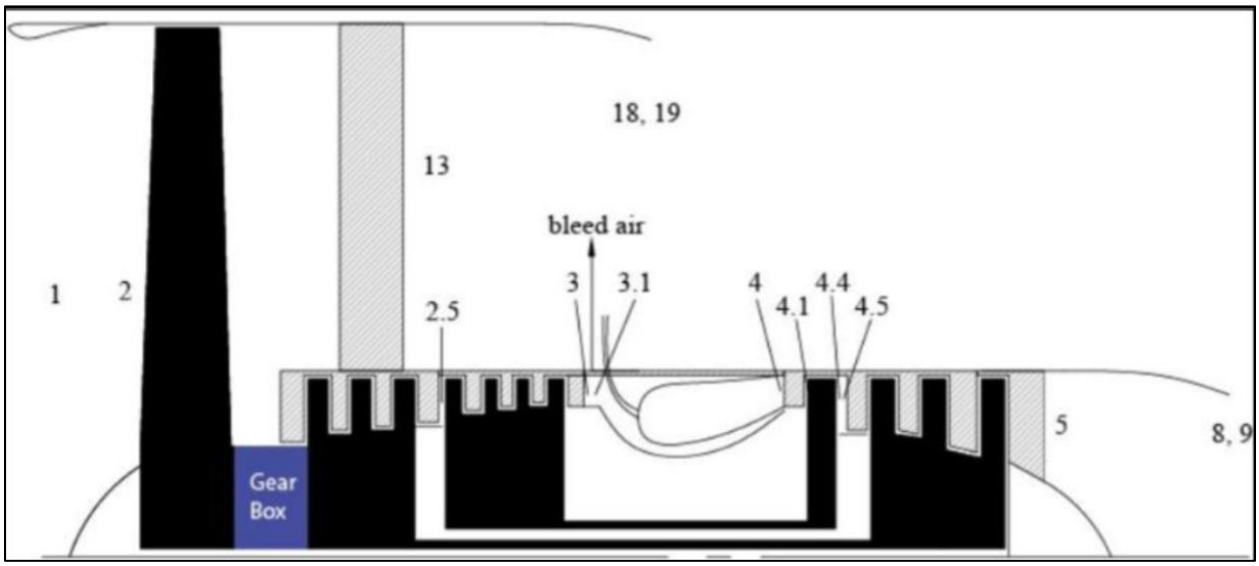

Figure 3: Engine Schematic

Throughout the design process, existing engines such as the GE90 and GE9X were referenced as sanity checks. The following table summarizes publicly available data for these engines that were used to validate and guide the design choices.

Table 3: Existing Engines Data

Parameter	GE 90-110B1	GE9x
Fan	1-stage	1-stage
LPC	4-stage	3-stage
HPC	9-stage	11-stage
HPT	2-stage	2-stage
LPT	6-stage	6-stage
LP Rotor Speed	2,355 RPM	2,355 RPM
HP Rotor Speed	9,332 RPM	9,561 RPM
Bypass Ratio	9:1	10:1
Pressure Ratio	42:1	60:1
Takeoff Thrust	492.7-513.9 kN	489.3 kN
Fan Diameter	3.3 m	3.4 m

Cycle Design

The cycle design began with the development of a MATLAB-based calculation tool intended to replicate and validate preliminary cycle results obtained using AEDsys from preliminary design analysis. The objective was to establish a reliable and flexible analysis framework that could be used to evaluate engine performance across different operating conditions.

The cycle analysis focused on two key operating conditions:

1. Design point
    - Altitude: 2134 m
    - Mach: 0.82
2. Takeoff
    - Altitude: 0 m
    - Mach: 0.1

Cycle calculations were performed in MATLAB to determine thermodynamic properties and performance metrics at these conditions. The results from the MATLAB tool were then compared against AEDsys outputs to validate accuracy. The comparison showed that the results of the MATLAB cycle analysis design tool matched AEDsys outputs with an error of one percent, confirming that the MATLAB tool reliably reproduces the expected cycle behavior. A detailed comparison between AEDsys and MATLAB results is provided in the Appendix.

The following figures illustrate the h-s diagram for the entire engine at cruise.

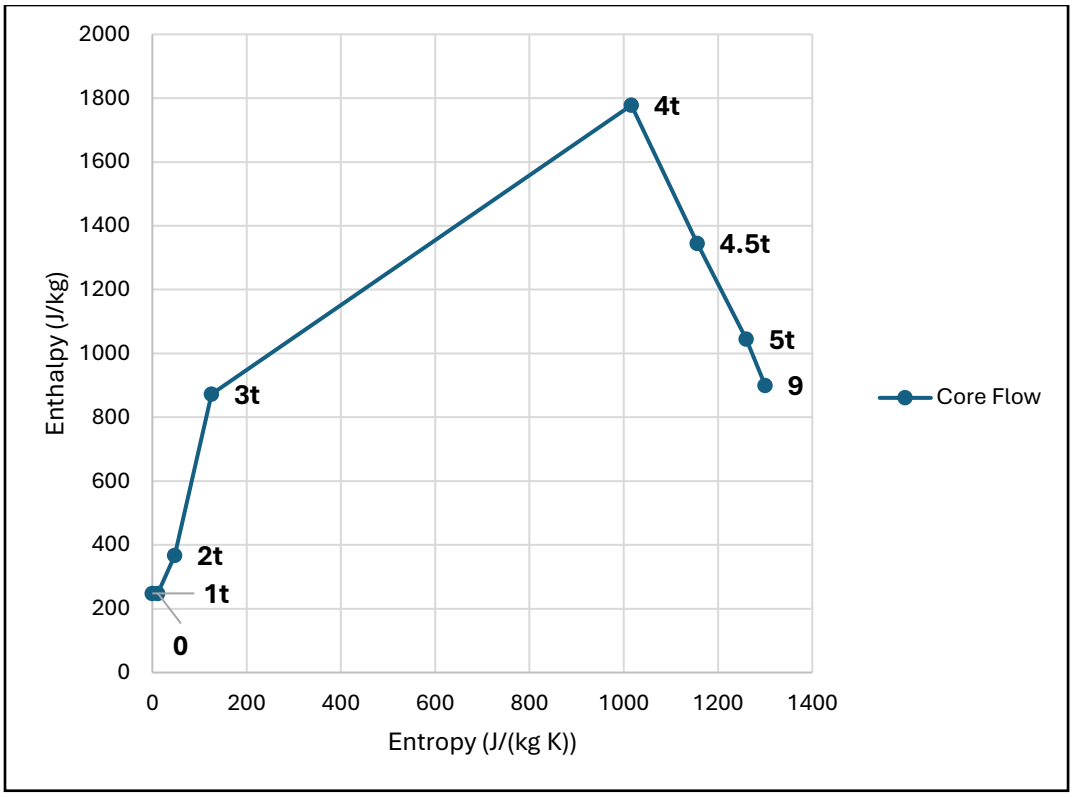

Figure 4: h-s Diagram (Core) – Cruise Condition

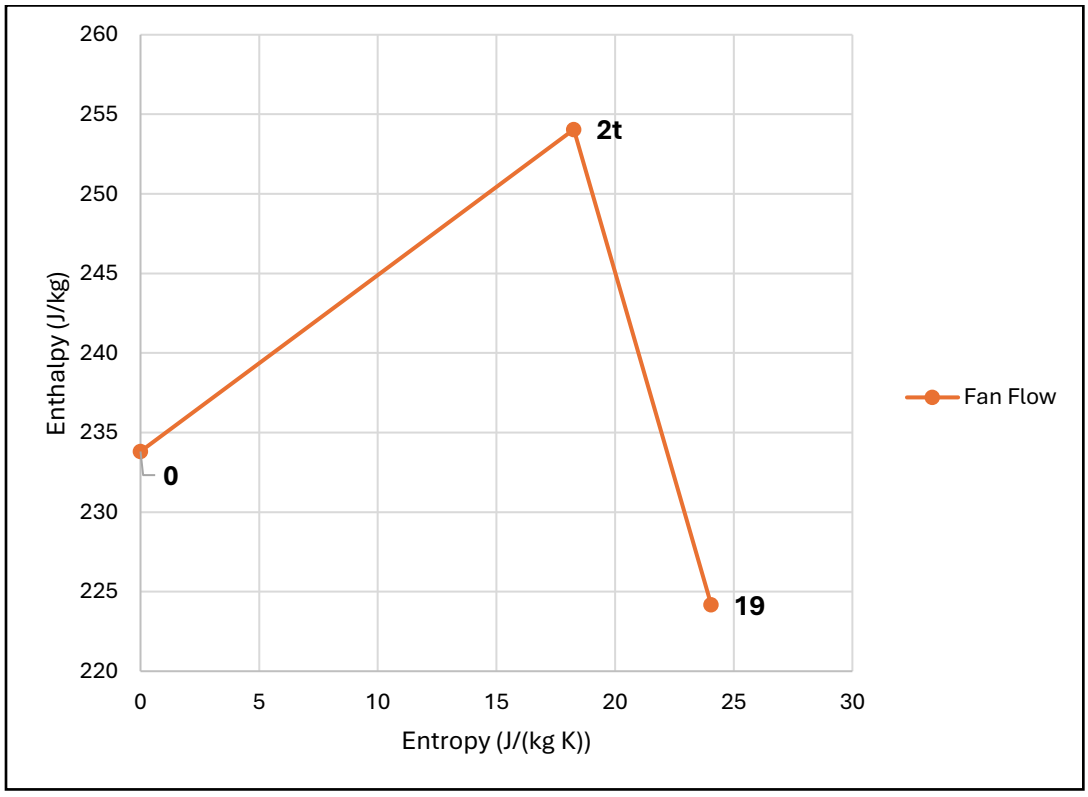

Figure 5: h-s Diagram (Bypass) – Cruise Condition

The h-s diagram provides a clear overview of the thermodynamic processes across the engine. The initial portion represents compression through the fan, LPC, and HPC, where both total and static enthalpy increase with a relatively small rise in entropy, indicating efficient compression.

A significant increase in enthalpy is observed across the combustor, representing heat addition at nearly constant pressure, with a moderate increase in entropy due to combustion losses.

Following this, the expansion through the HPT and LPT shows a decrease in enthalpy as work is extracted to drive the compressors and fan, along with a gradual increase in entropy due to aerodynamic losses.

The nozzle section continues this trend, where the flow expands further, resulting in a drop in static enthalpy as the flow accelerates to produce thrust. The difference between total and static enthalpy highlights the kinetic energy effects within the engine, with larger gaps observed in regions of higher velocity.

Inlet Design

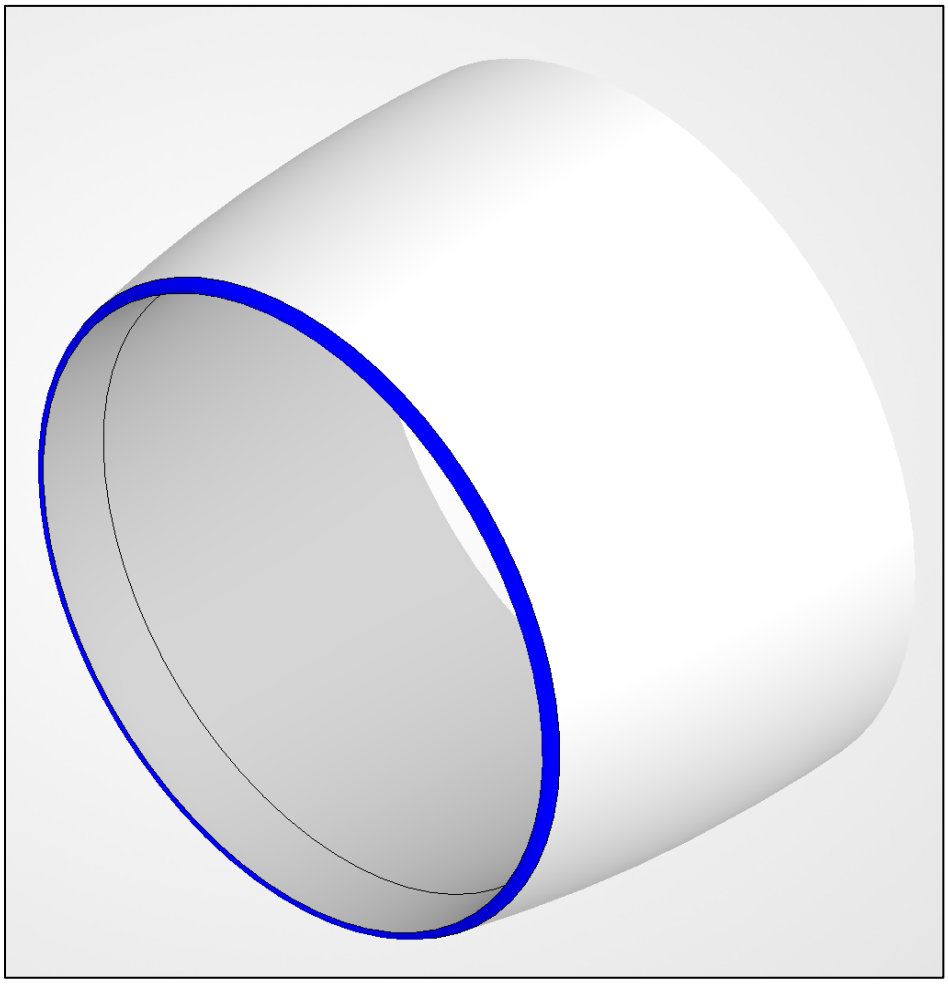

Figure 6: Inlet CAD model

The inlet captures freestream air and delivers it to the fan/low-pressure compressor at the required mass flow rate, Mach number, and total pressure. Its primary objective is to decelerate and condition the flow to a uniform, stable state at the fan face while minimizing total pressure loss. It operates under an adverse pressure gradient which promotes flow separation, stall, and a thick boundary layer. Because the inlet is assumed adiabatic, total temperature remains constant, and performance is governed primarily by how effectively total pressure is preserved.

The key controlled parameters are corrected mass flow, throat Mach number, capture area ratio, diffuser area ratio, and total pressure ratio. Corrected mass flow and throat Mach number determine choking behavior and mass flow compatibility with the engine cycle. Capture area controls spillage and external operability, while diffuser area ratio and nondimensional length govern pressure recovery, evaluated using established diffuser performance maps. The total pressure ratio serves as the dominant performance metric, as losses directly reduce thrust and increase TSFC.

The inlet was designed to satisfy two primary operating conditions: Takeoff (and climb) and Cruise. These conditions represent the two dominant aerodynamic regimes experienced by the inlet:

- Low-speed, high-power operation (Takeoff/Climb)
- High-speed, low-power operation (Cruise)

Designing for these two regimes ensures acceptable performance across the full mission envelope. The following plots summarize the aero-thermo properties at both flight conditions.

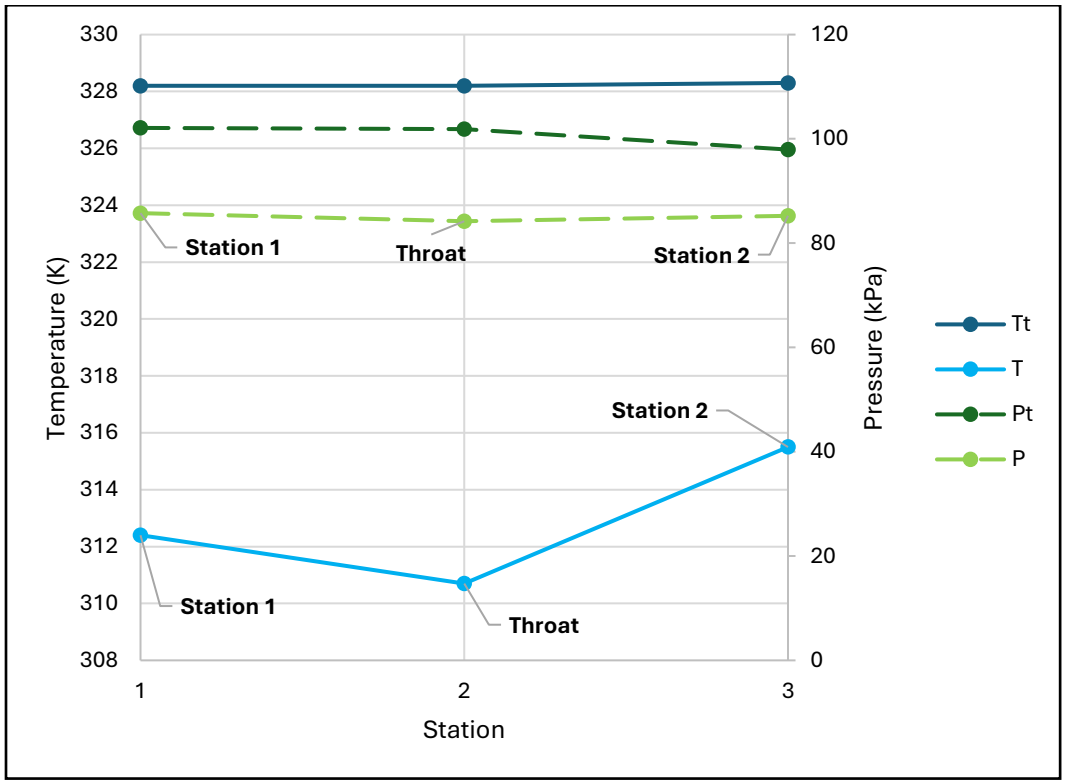

Figure 7: Takeoff Conditions

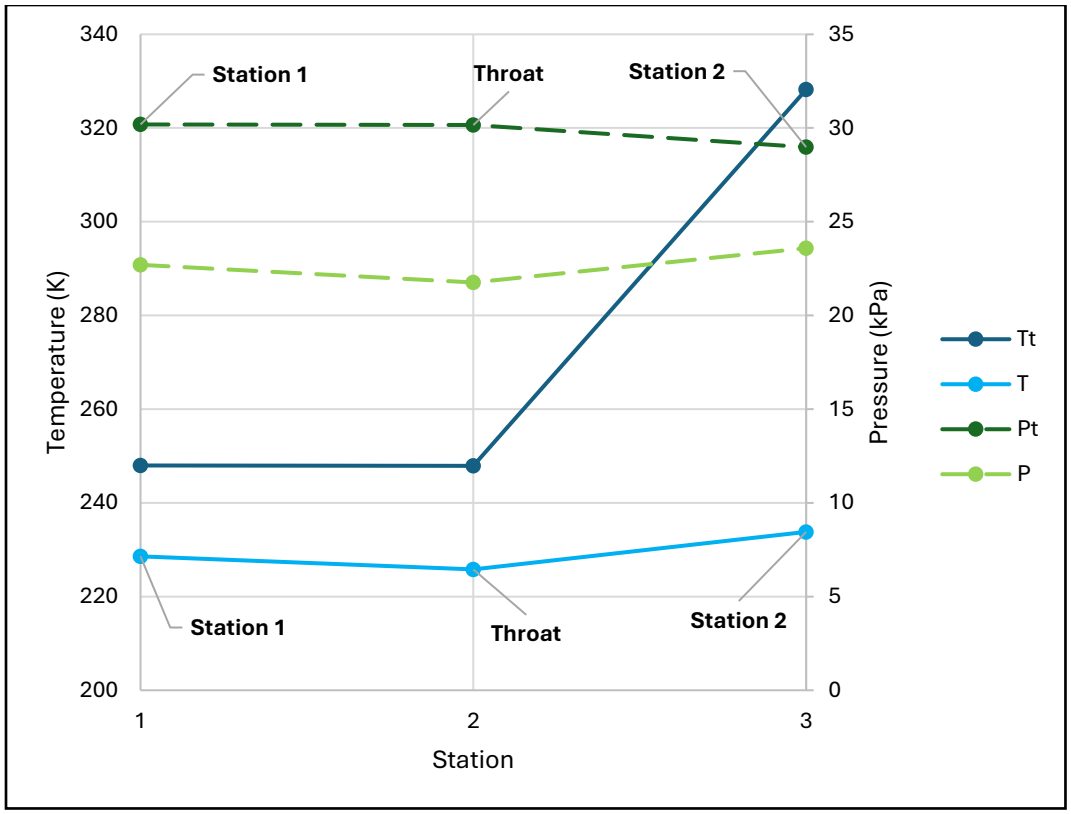

Figure 8: Cruise Conditions

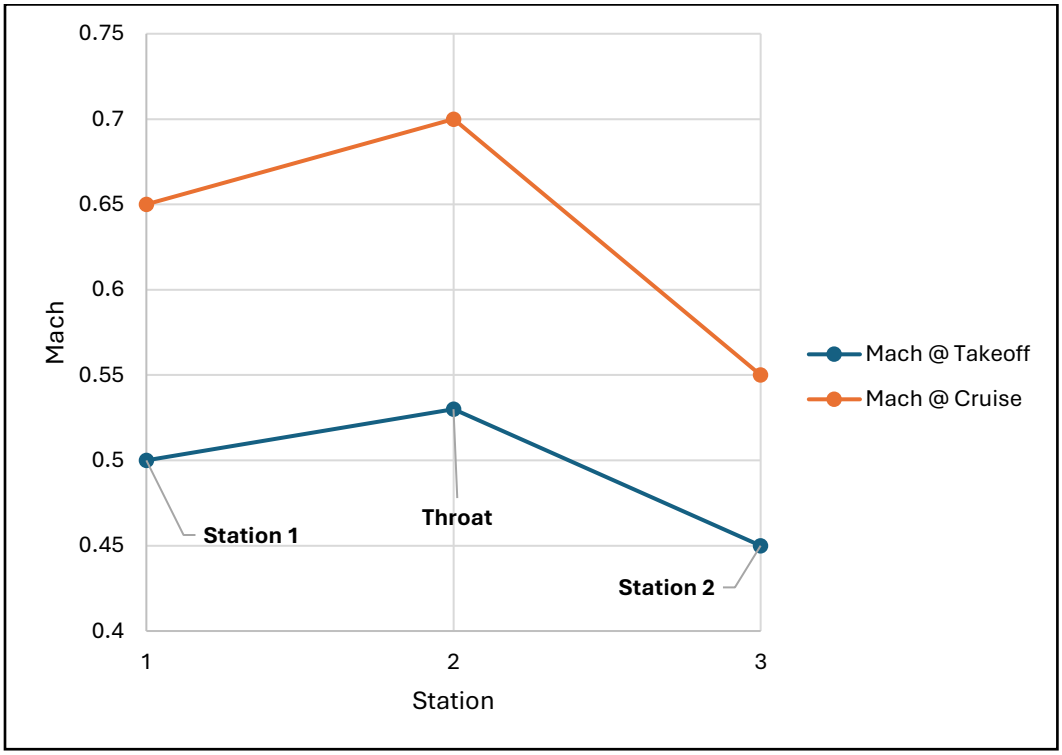

Figure 9: Mach at Takeoff & Cruise

From table 14, the comparison of corrected mass flow rate at station 0 revealed a deviation from conventional expectation. Typically, corrected mass flow at cruise is lower than at takeoff. However, calculations indicated a higher corrected mass flow requirement at cruise. The primary driver was the significant thrust lapse at high altitude, which altered the mass flow demand more than initially anticipated. As a result, the conventional approach of sizing the throat based on takeoff conditions was reconsidered. The throat was instead sized for cruise conditions to prevent choking and ensure compatibility with the required mass flow. The selected diffuser exit Mach number was $M_2 = 0.55$ at cruise, while at takeoff, it was calculated to be $M_2 = 0.45$, providing a balance between diffusion effectiveness and stability across both regimes.

The inlet capture area ratio at subsonic cruise was set to:

$$\frac{A_0}{A_1} = 0.90$$

This assumption ensures consistency with highlight geometry constraints while maintaining an area ratio (A_{max}/A_1) greater than the maximum allowed value determined for the calculated critical pressure coefficient ($C_{p,crit}$).

The maximum Mach number at the throat was initially assumed to be 0.75 and later reduced to 0.70. Since the throat Mach number directly determines the required throat area, several iterations were performed to determine an acceptable $M_{th,max}$ that prevents choking while satisfying mass flow and pressure recovery constraints.

Inlet lip bluntness was evaluated to be:

$$\frac{A_1}{A_{th}} = 1.04$$

This value indicates a fairly mild bluntness, favoring high-speed performance.

The diffuser performance parameters were determined next:

- Pressure recovery coefficient

$$C_{PR} = 0.25$$

- Diffuser area ratio

$$\frac{A_2}{A_{th}} - 1 = 0.19$$

Using the Sovran & Klomp diffuser maps, these values produced a nondimensional diffuser length:

$$\frac{N}{R_1} = 0.95$$

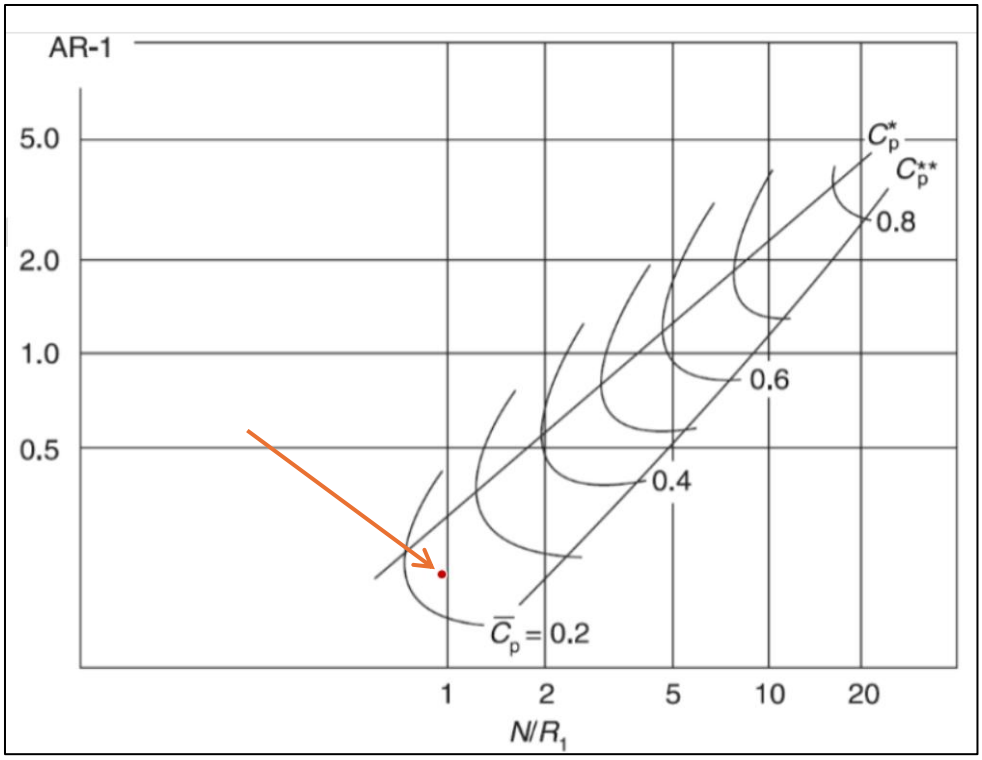

Figure 10: Sovran & Klomp diffuser map (with design point)

Multiple iterations were performed to ensure that the design point remained within the acceptable operating domain of the diffuser maps. The primary variables adjusted during iteration were A_0/A_1, $M_{th,max}$, and M_2.

A significant design compromise involved the diffuser total pressure ratio (π_d). The initial assumed value of 0.998 was reduced to 0.960. This reduction positioned the design point near the maximum C_p for given N while remaining within the stable operating domain of the diffuser performance maps. Although lower than the ideal assumption, this value provides a physically realistic balance between diffusion performance, operability, and geometric constraints.

Table 4 illustrates the impact of the updated π_d value on key performance parameters:

Table 4: Performance Parameters Comparison

	$\pi_d = 0.998$	$\pi_d = 0.960$	% Change
Net Thrust (kN)	217.2	195.9	9.81
Specific Thrust (N/(kg/s))	95.2	85.8	9.87
TSFC (mg/(N·s))	18	20	11.11

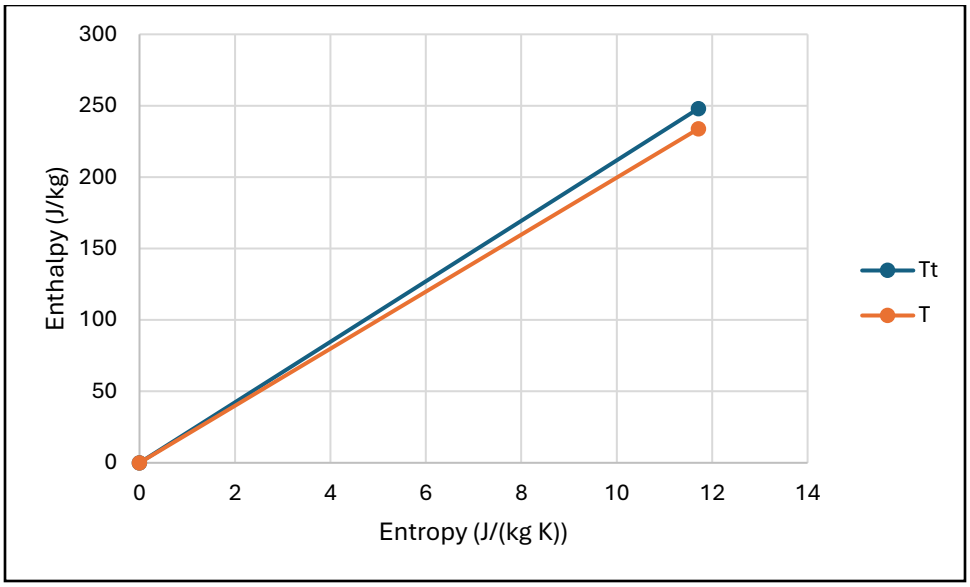

Figure 11: h-s Diagram - Inlet

The following figures display the inlet profile. Excel was used to generate the sketches.

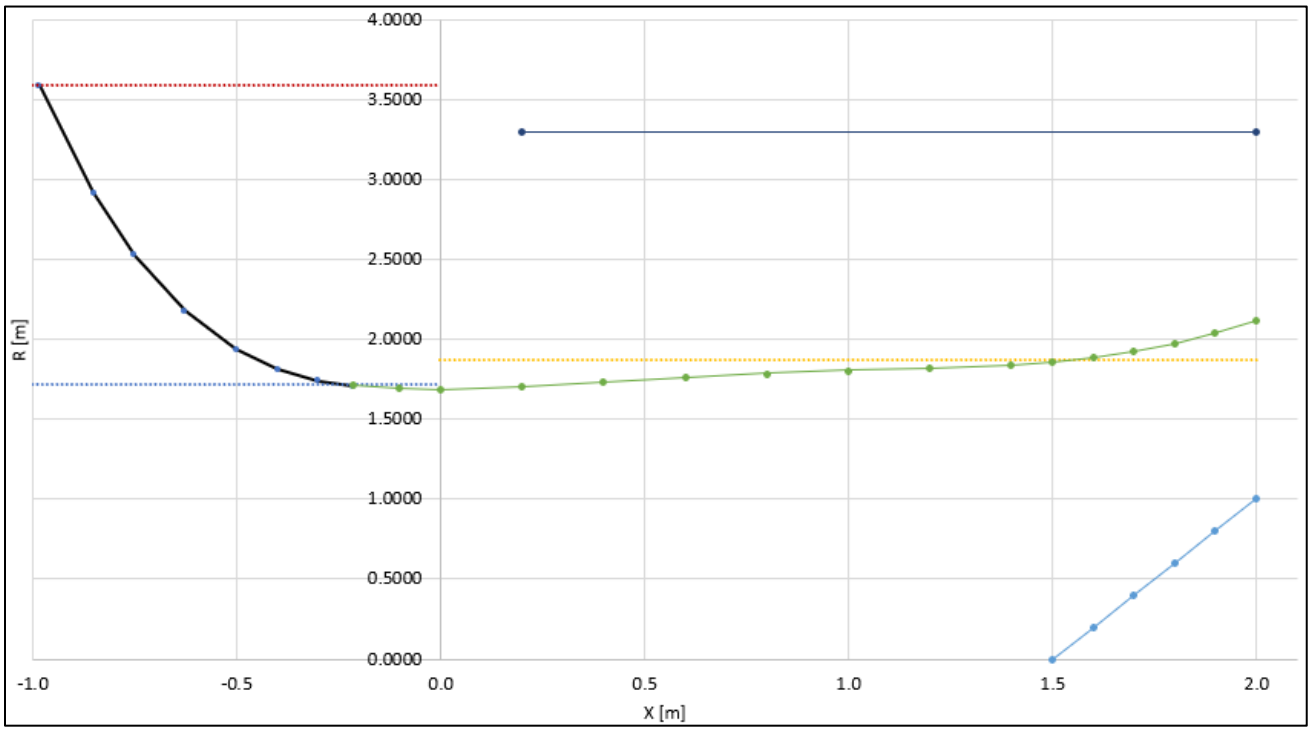

Figure 12: Inlet Radius with Spinner – Smoothed

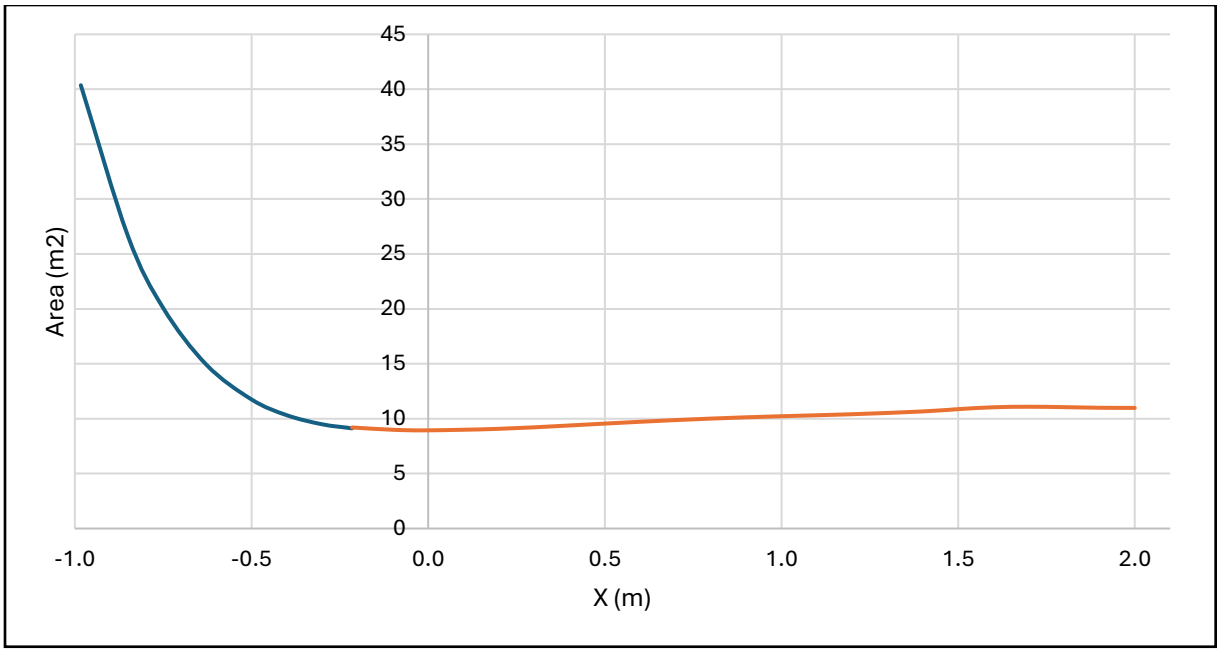

Figure 13: Inlet Smoothed Areas

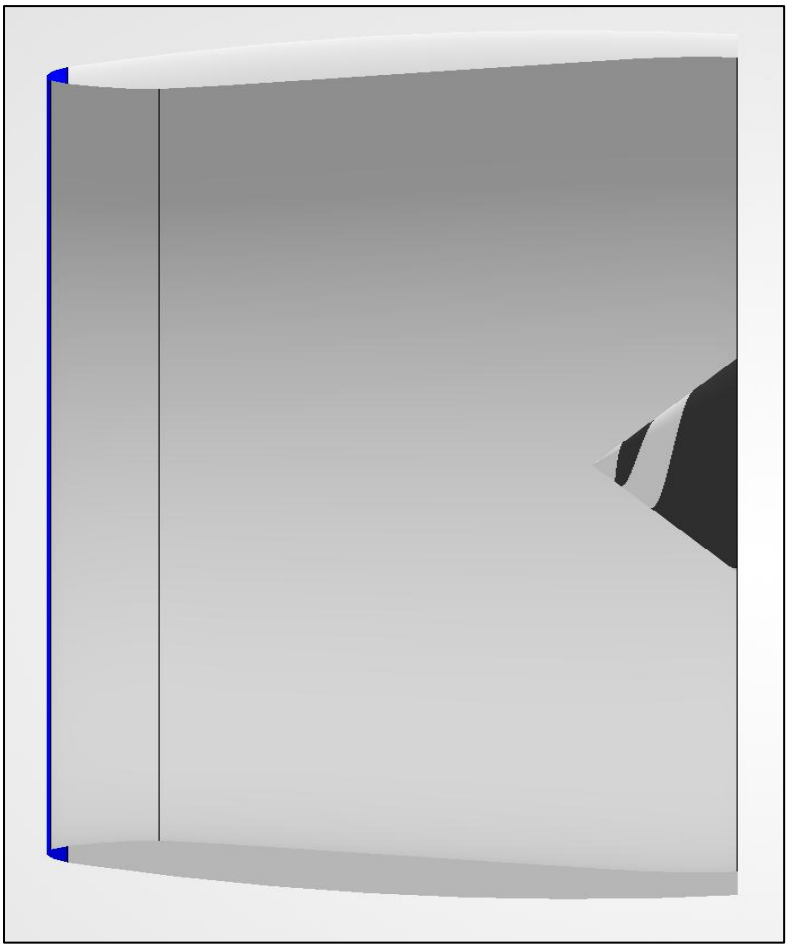

Figure 14: Inlet CAD model

Table 5: Inlet Station Parameters

Parameters	Numerical Value
A_1	9.24 m^2
R_1	1.71 m
A_{th}	8.91 m^2
R_{th}	1.68 m
A_2	11.03 m^2
R_2	1.87 m
N_{diff}	1.61 m
ϕ_W	3.38 deg

The spinner geometry was selected to remain consistent with the established flow and area constraints. A conical spinner was assumed for geometric simplicity and compatibility with the inlet profile. The CFM56 engine was used as a baseline reference due to the availability of sectional views, with particular attention given to the axial placement of the spinner relative to station 2. The primary reference was the relative starting position of the spinner and its spacing from station 2. Following integration of the spinner, the radii at stations 0 through 2 were recalculated to preserve the effective flow areas and maintain geometric and mass flow consistency.

Fan Design

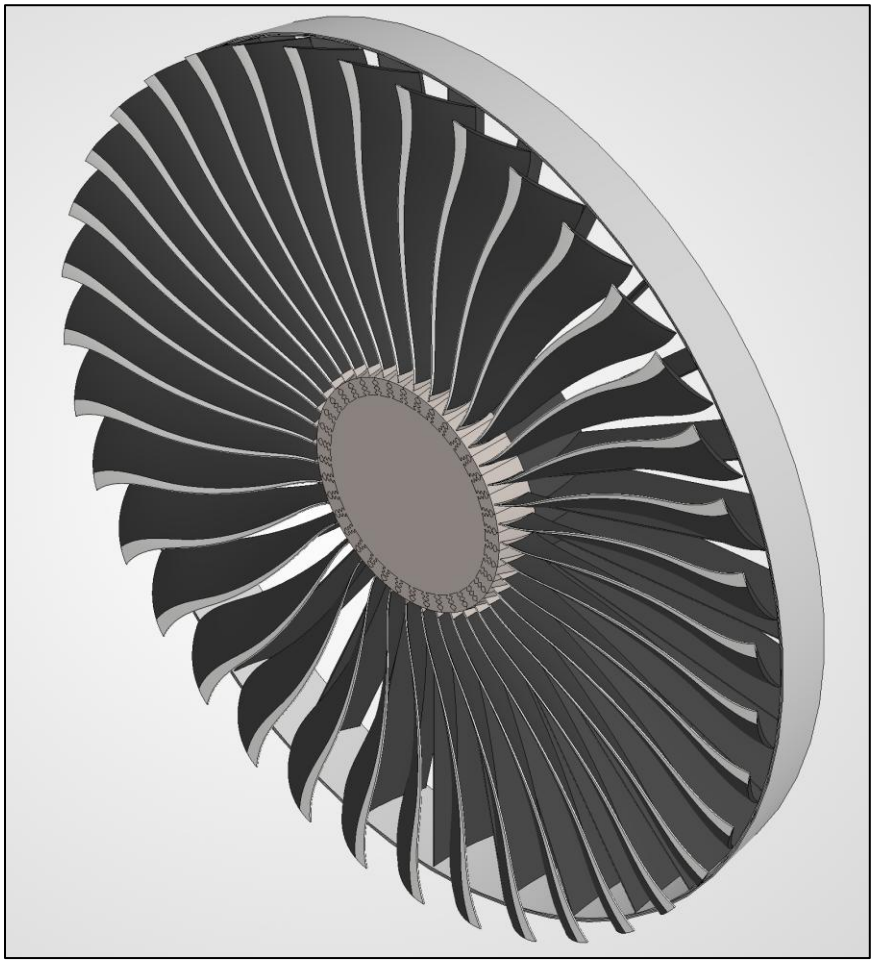

Figure 15: Fan CAD model

The fan is the first turbomachinery component of the engine in the sequential flow path and plays a critical role in setting the aero-thermal properties of the flow and the overall performance of the engine. The configuration of the fan is shown below.

Table 5: Fan Design Configuration

Parameter	Value
Stage	1
RPM	2,200
Blade Number - Rotor	38
Blade Number – Stator	30
$\boldsymbol{\pi_f}$	1.30
$\boldsymbol{\eta_f}$	0.92
$\boldsymbol{\psi}$	-0.30
$\boldsymbol{\phi_1}$	0.63

ϕ_2	0.58
$\dot{W}$	12.3 MW
$\Delta\alpha$	-27.35 deg
$\Delta\beta$	7.23 deg

The primary challenge in designing the fan was maintaining a single-stage configuration while determining an appropriate operating RPM. Since fan efficiency generally improves at lower rotational speeds, a gearbox was introduced between the low-pressure compressor (LPC) and the fan. The LPC operates at approximately 7,000 RPM, while the fan operates at 2,200 RPM, resulting in a gear ratio of approximately 3.2:1. This value is well within current industry capabilities, where gear ratios up to approximately 5 are feasible. Selecting an appropriate RPM also minimized the need for a large transition duct between the fan and LPC, thereby reducing potential total pressure losses.

Another challenge was the relatively high pressure ratio across the fan, which led to consideration of a multi-stage configuration. However, adding additional stages would increase system complexity, weight, and cost, while providing only marginal efficiency improvements. Therefore, a single-stage design was retained, prioritizing reduced weight and complexity at the expense of a slight reduction in efficiency. As a result, certain stage parameters, such as loading and flow coefficients, are slightly outside commonly recommended ranges, but this trade-off provides an overall system-level benefit.

The following plots show the thermodynamic properties of the fan.

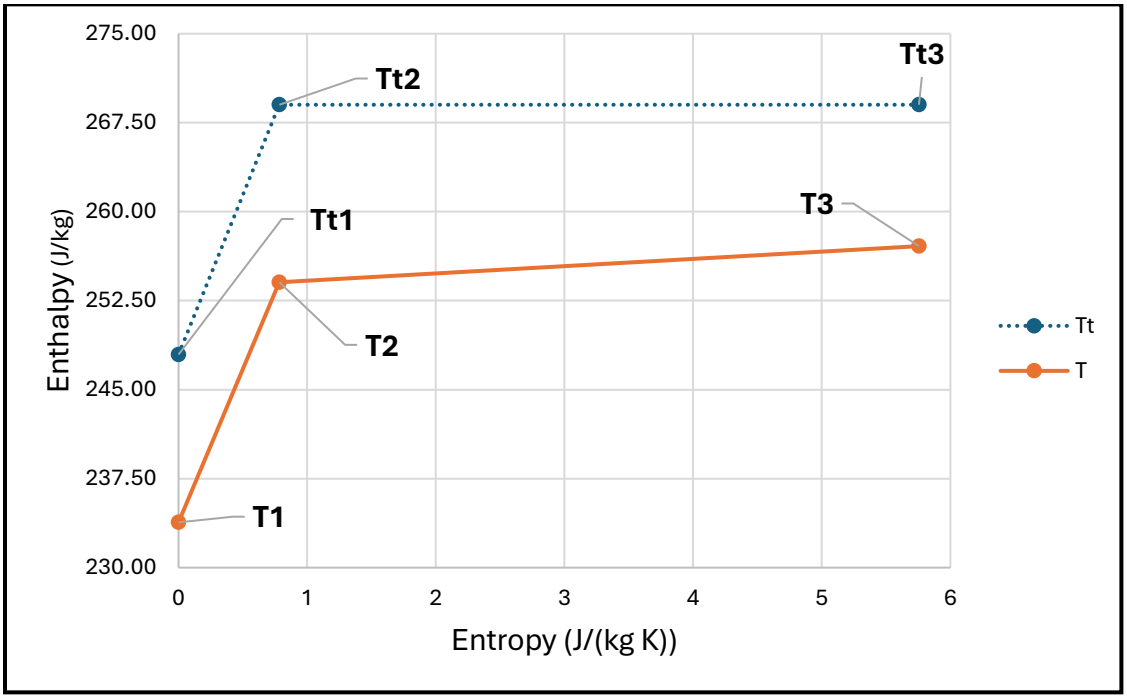

Figure 16: h-s Diagram – Fan

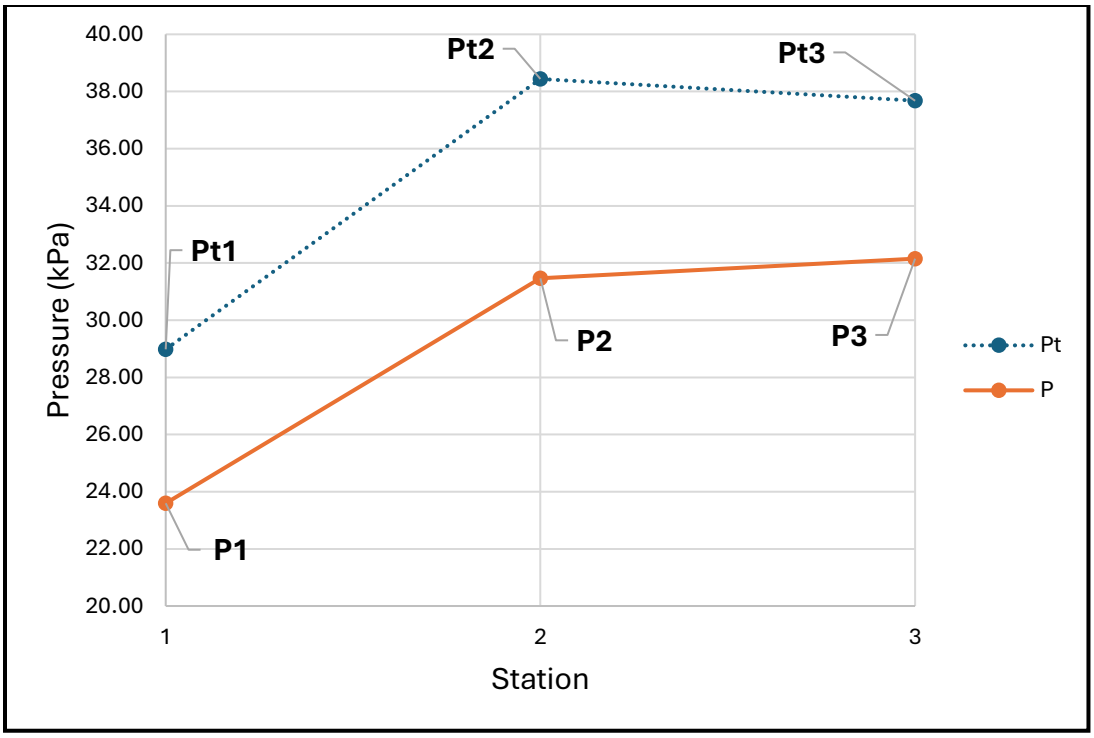

Figure 17: Pressure vs Station – Fan

Care was taken to ensure smooth variation of properties across all stations, avoiding abrupt changes in thermodynamic behavior.

Velocity triangles (cascade view) and the aerodynamic properties are shown in the following plots:

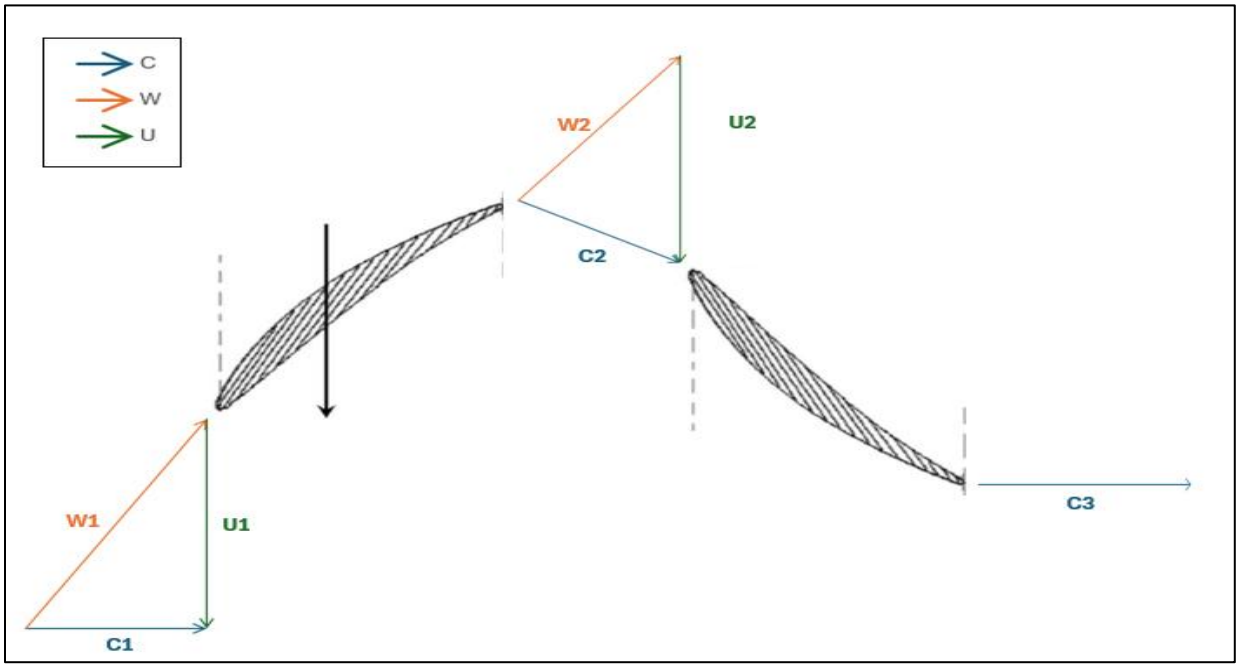

Figure 18: Velocity Triangles – Fan

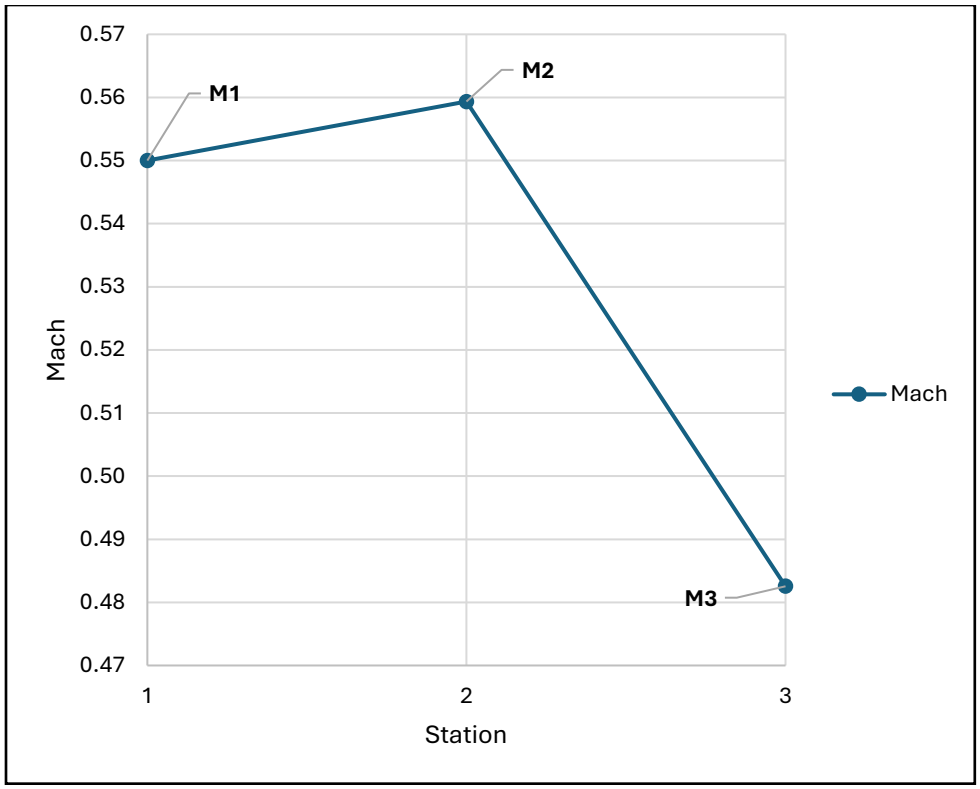

Figure 19: Mach vs Station – Fan

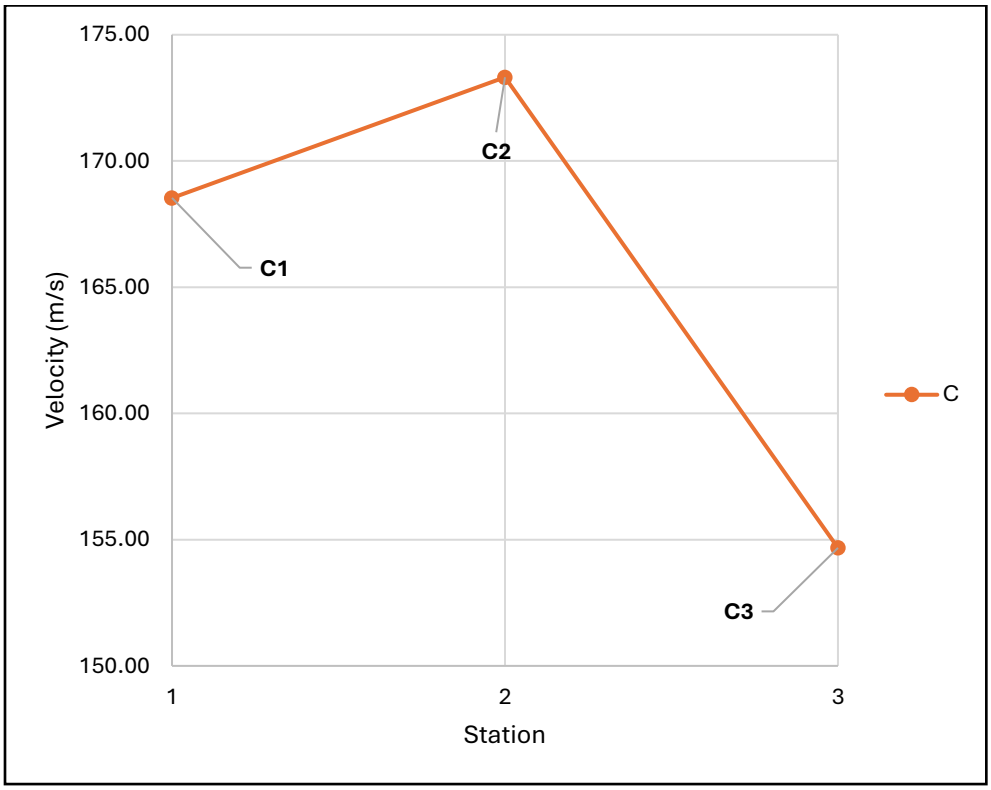

Figure 20: Absolute Velocity vs Station – Fan

These plots demonstrate that the fan follows the expected aerodynamic trends: the absolute velocity increases through the rotor and decreases through the stator, with axial flow at both the inlet and exit (zero swirl). The relative velocity decreases through the rotor, consistent with expected fan behavior.

A smooth geometric profile was also maintained throughout the fan design. The following plot illustrates the meridional view, showing the variation of hub, mean, and tip radii across the stage, along with the rotor and stator blade locations.

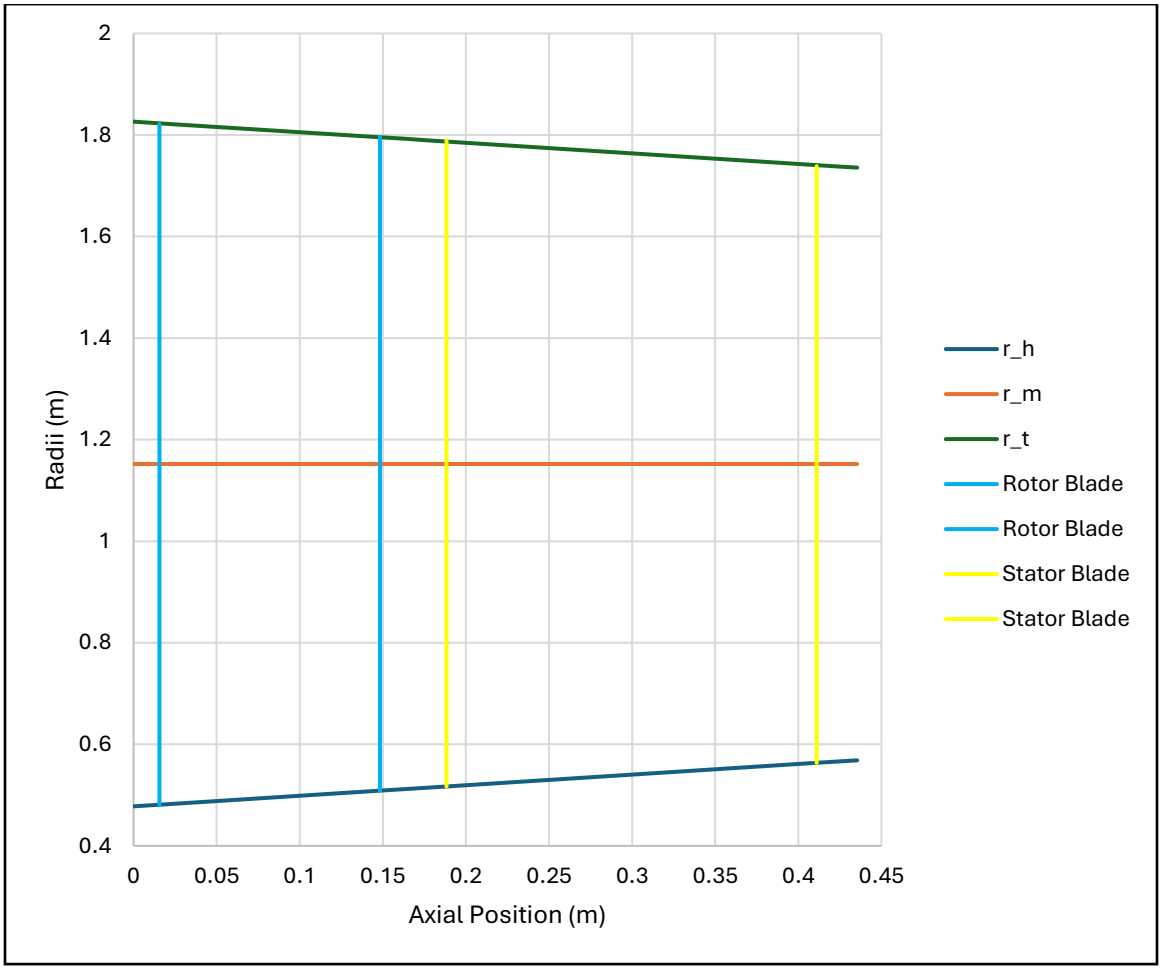

Figure 21: Meridional View – Fan

Health assessments were also conducted to ensure that the fan not only meets the design targets but is also healthy.

Table 6: Airfoil Health

Parameter	Rotor	Stator
DeHaller Number	0.77	0.89
$\overline{\boldsymbol{Diffusion\ Factor}}$	0.03	0.41

The De Haller number for both the rotor and stator was maintained above 0.68, while the average diffusion factor was kept below 0.45. The low value of the diffusion factor for the rotor is influenced by a slightly negative value at the hub. However, since the average rotor diffusion factor remains positive and close to zero, and all other performance and aerodynamic checks are satisfied, no further modifications were made to avoid unnecessary changes to the overall design.

Additional stage characteristics, such as the degree of reaction, were maintained within a range of approximately 0.4 to 0.95 from hub to tip, ensuring effective stage performance. Detailed numerical results are provided in the Appendix.

Low-Pressure Compressor Design

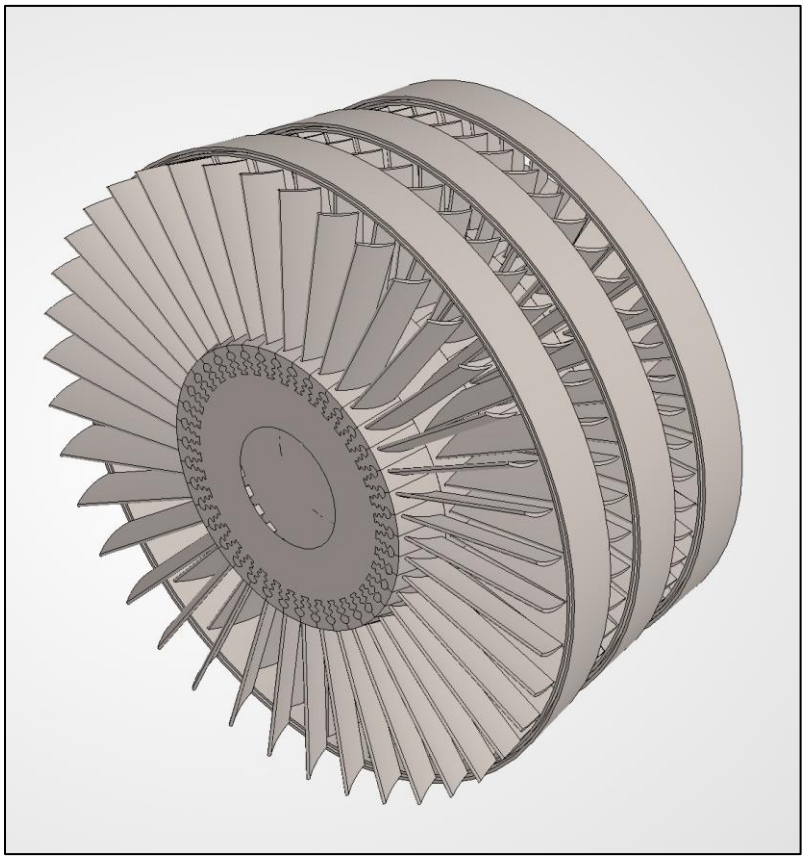

Figure 22: LPC CAD model

The low-pressure compressor (LPC) rotates on the low-pressure spool, which is connected to the low-pressure turbine. Its inlet conditions are obtained from the fan core flow after passing through the transition duct. The LPC is the first component responsible for compressing the incoming flow, increasing the total pressure before it is further compressed by the high-pressure compressor (HPC). Proper LPC performance is critical, as its exit conditions directly influence the effectiveness and efficiency of the downstream HPC. The configuration of the LPC is shown below.

Table 7: LPC Design Configuration

Parameter	Value
Stages	3
RPM	7,000
$\dot{m}$	53 kg/s
π_{cL}	3.5
η_{cL}	0.90
$\dot{W}$ **(Power Input)**	18.9 MW
b_{avg}	24 – 13 cm
$C_{xm,avg}$	5 cm
U_{avg}	275 m/s

The LPC operates at an RPM of 7,000. This value was obtained through an iterative process aimed at achieving stable and effective compressor performance. The selected RPM also influenced the geometric parameters, particularly the mean-line radius. Special attention was given to maintaining a smooth radial profile, as the LPC must interface seamlessly with the high-pressure compressor, as shown in figure 23. As discussed in the fan section, a gearbox was introduced between the fan and the LPC to accommodate the difference in rotational speeds.

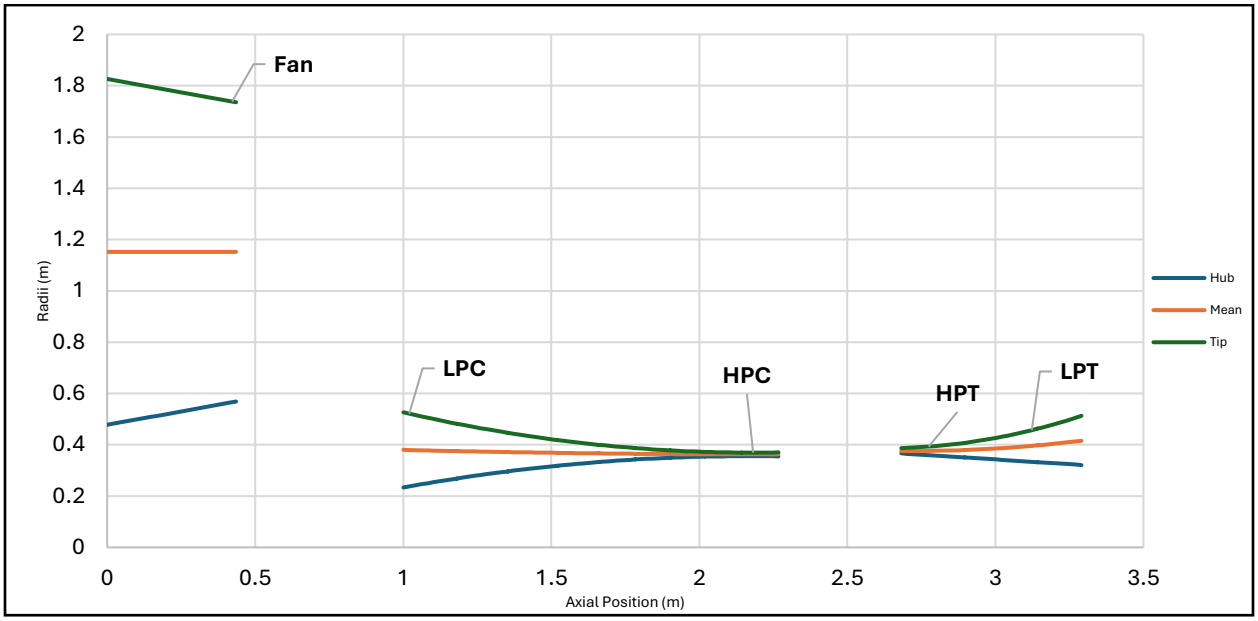

Figure 23: Radii vs Axial Position

The LPC consists of three stages, with blade height varying from approximately 24 cm at the first stage to 13 cm at the third stage, and an average blade thickness of approximately 5 cm. The average blade speed is approximately 275 m/s. The core flow mass flow rate is 53 kg/s, while the bypass flow mass flow rate is 582 kg/s.

The following plots show the thermodynamic properties of the low-pressure compressor.

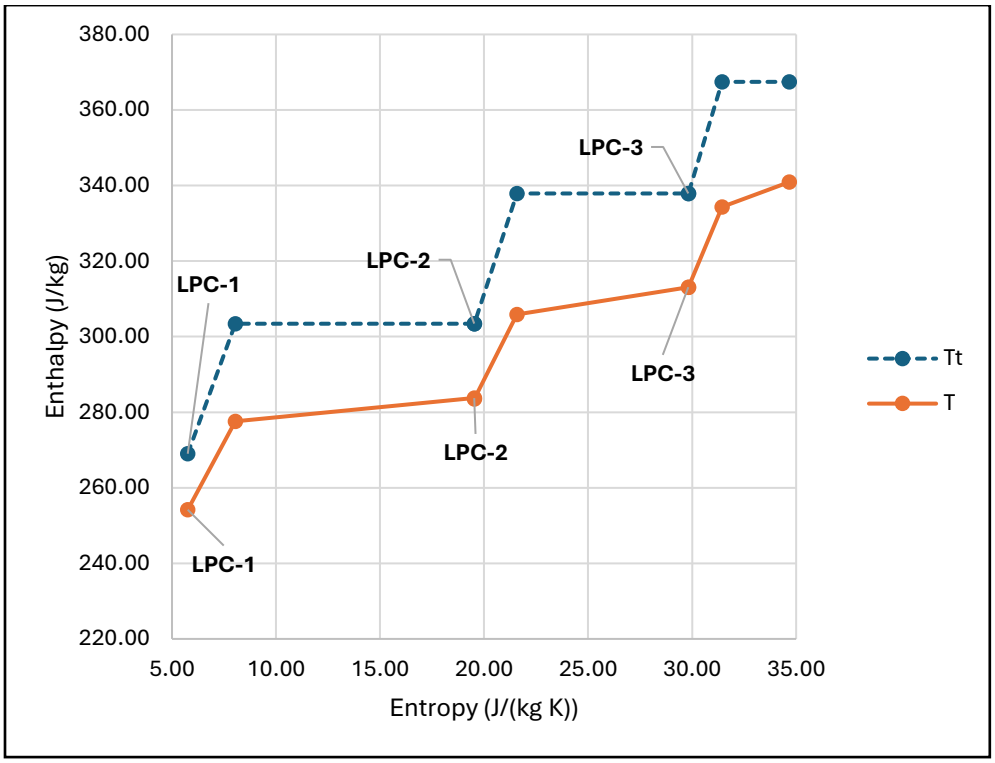

Figure 24: h-s Diagram – LPC

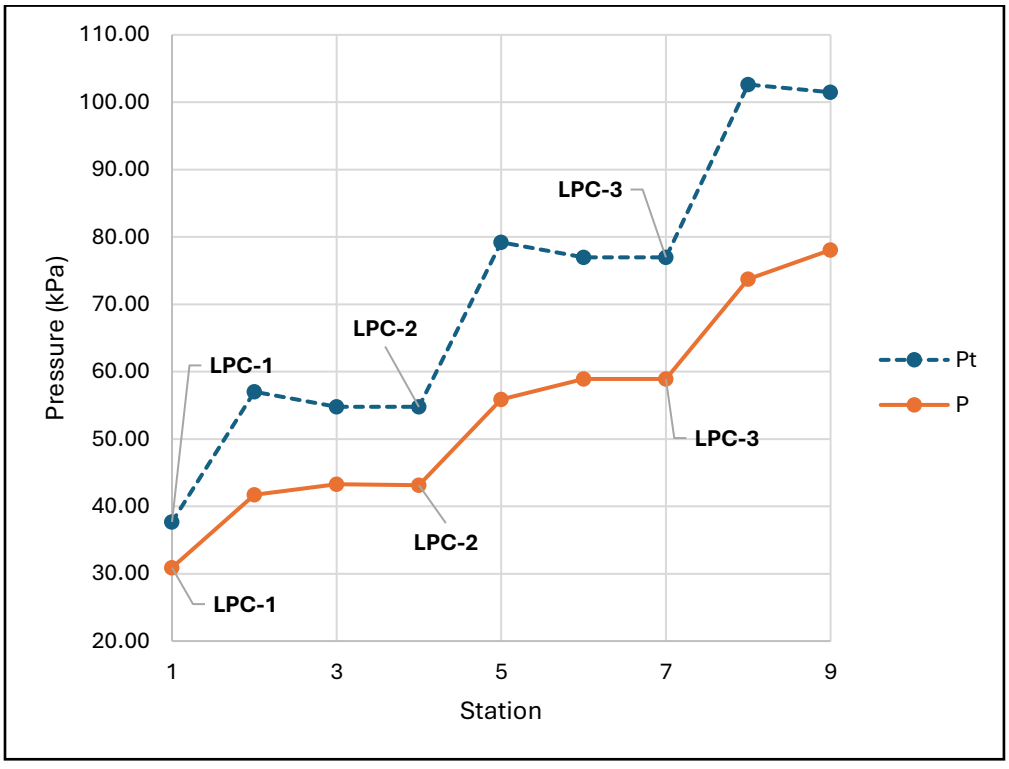

Figure 25: Pressure vs Station – LPC

A smooth pressure rise is observed across the stages, with each stage achieving a pressure ratio of approximately 1.3 to 1.4.

Velocity triangles (cascade view) and aerodynamic properties are shown in the following plots.

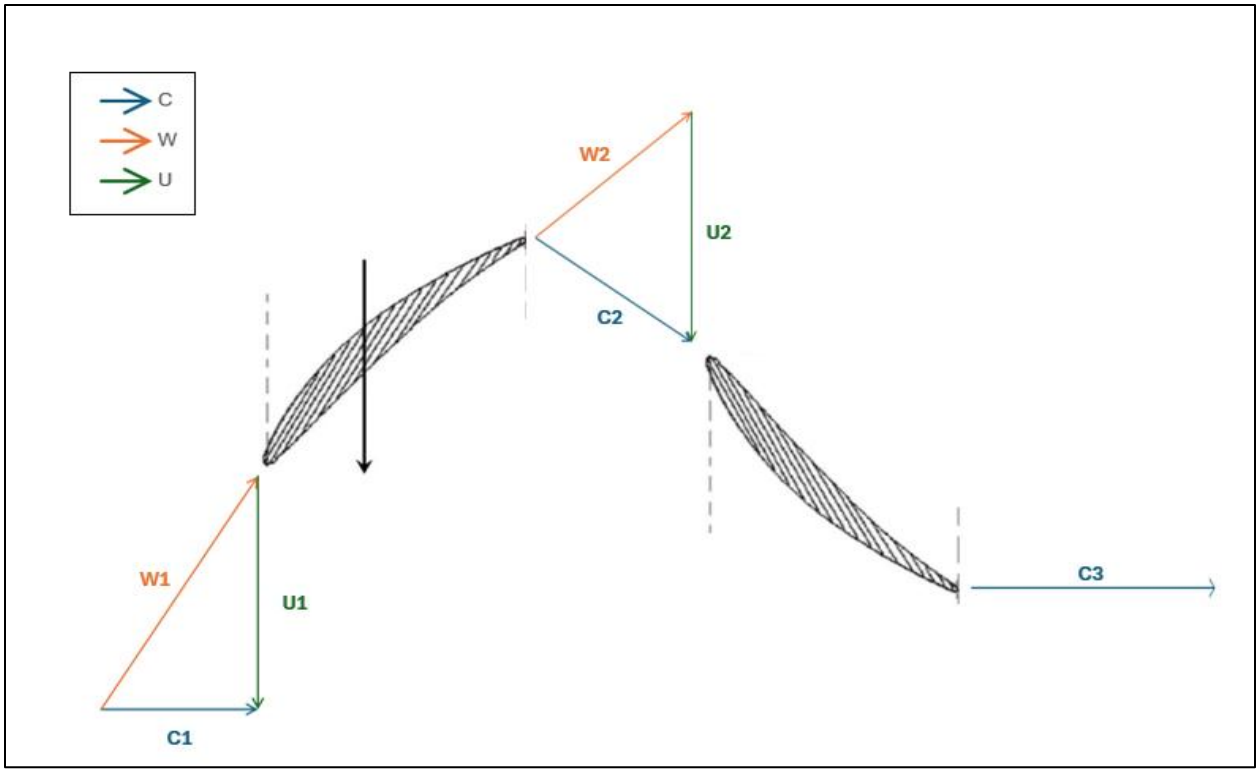

Figure 26: Velocity Triangles (mean-line radius) – LPC 1st stage

The LPC demonstrates consistent velocity triangle behavior across all three stages and at all radial locations (hub, mean, and tip).

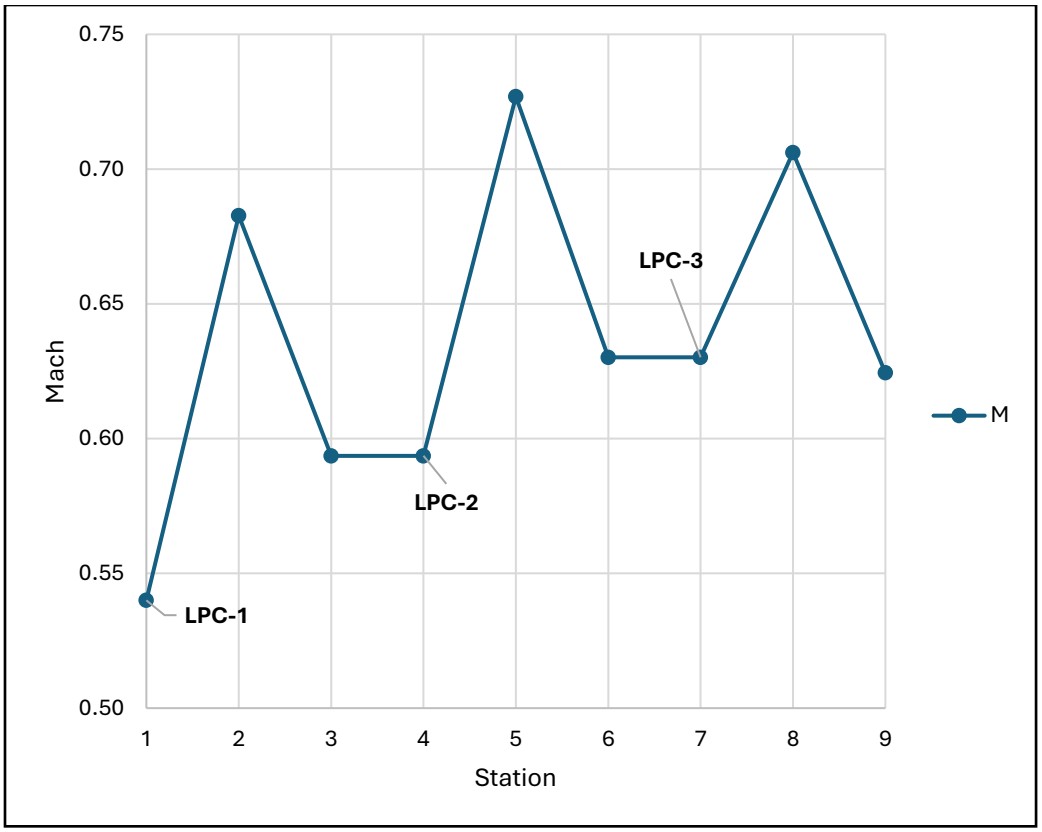

Figure 27: Mach vs Station – LPC

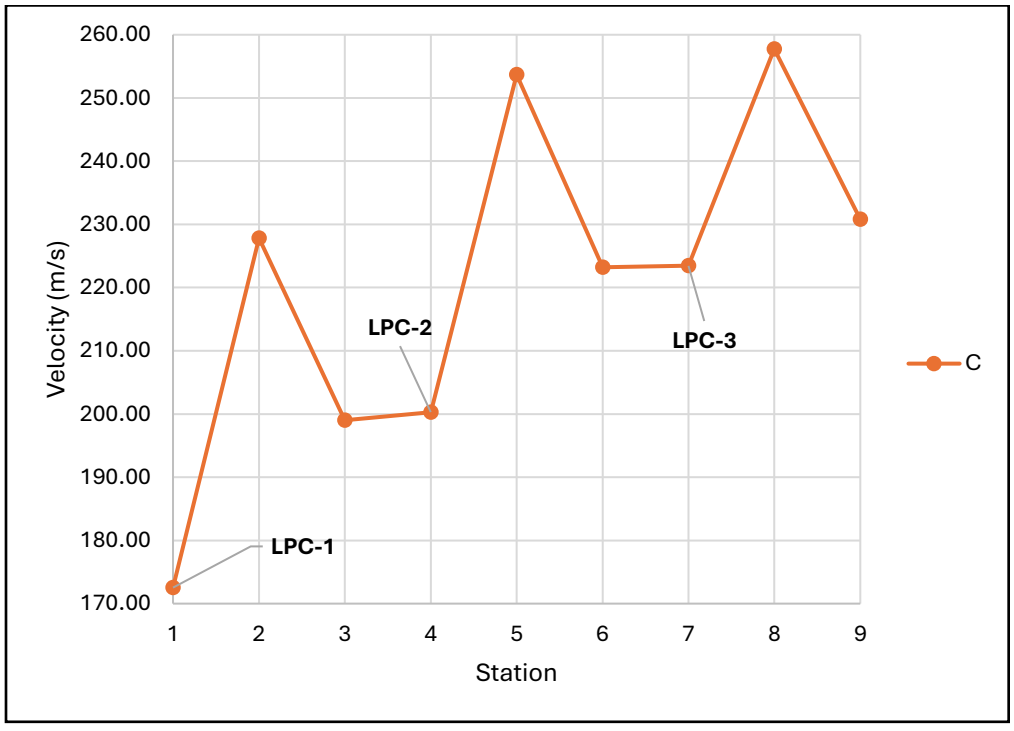

Figure 28: Absolute Velocity vs Station – LPC

The trends follow expected compressor behavior. Additionally, zero exit swirl was maintained at the stator exit for each stage, ensuring axial flow into the subsequent stage and minimizing exit losses. Both absolute and relative Mach numbers remain below 1.4, consistent with recommended compressor design limits.

A smooth geometric profile was maintained throughout the LPC design. The following plot illustrates the meridional view, showing the variation of hub, mean, and tip radii across all three stages, including the rotor-stator pairs.

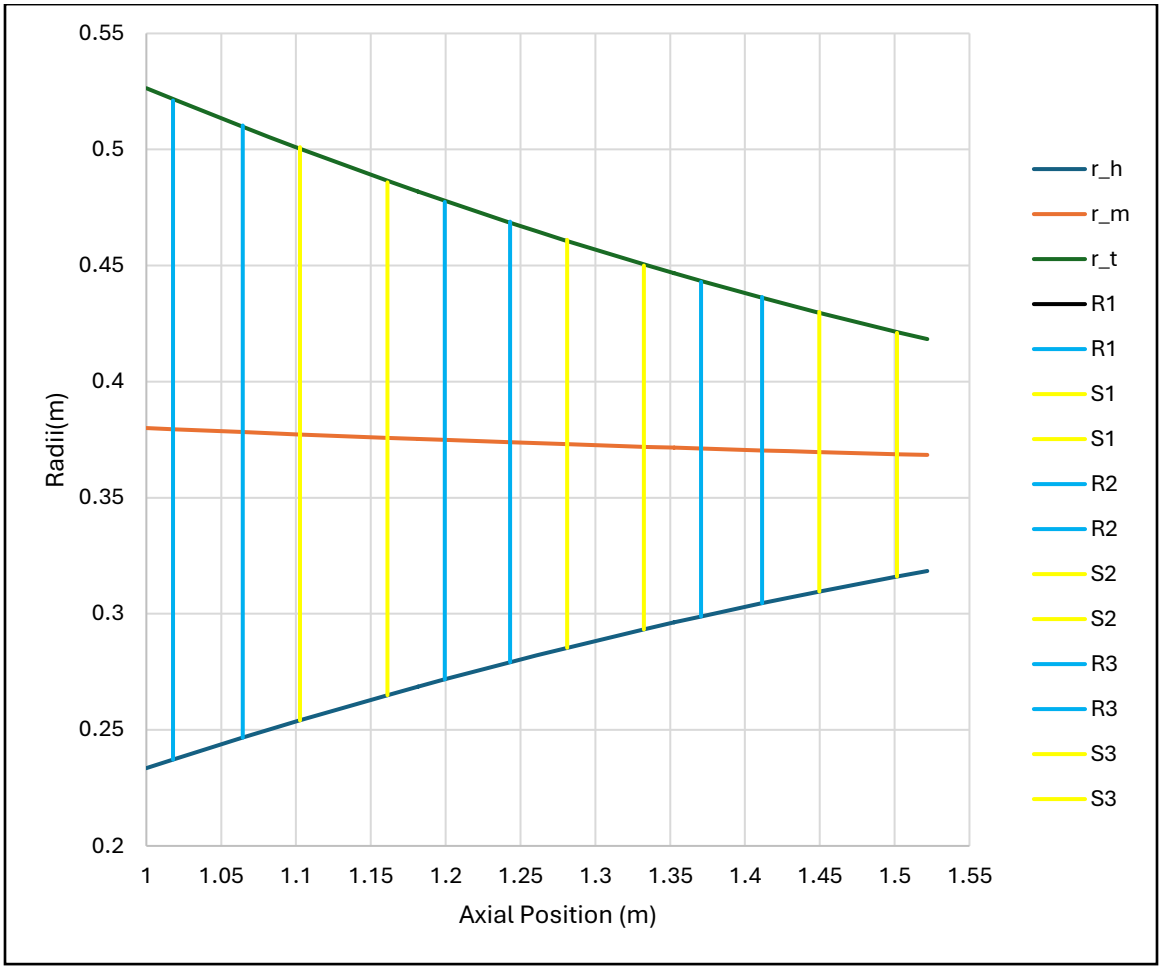

Figure 29: Meridional View – LPC

The following plots demonstrate the stage characteristics and their variation across the three stages.

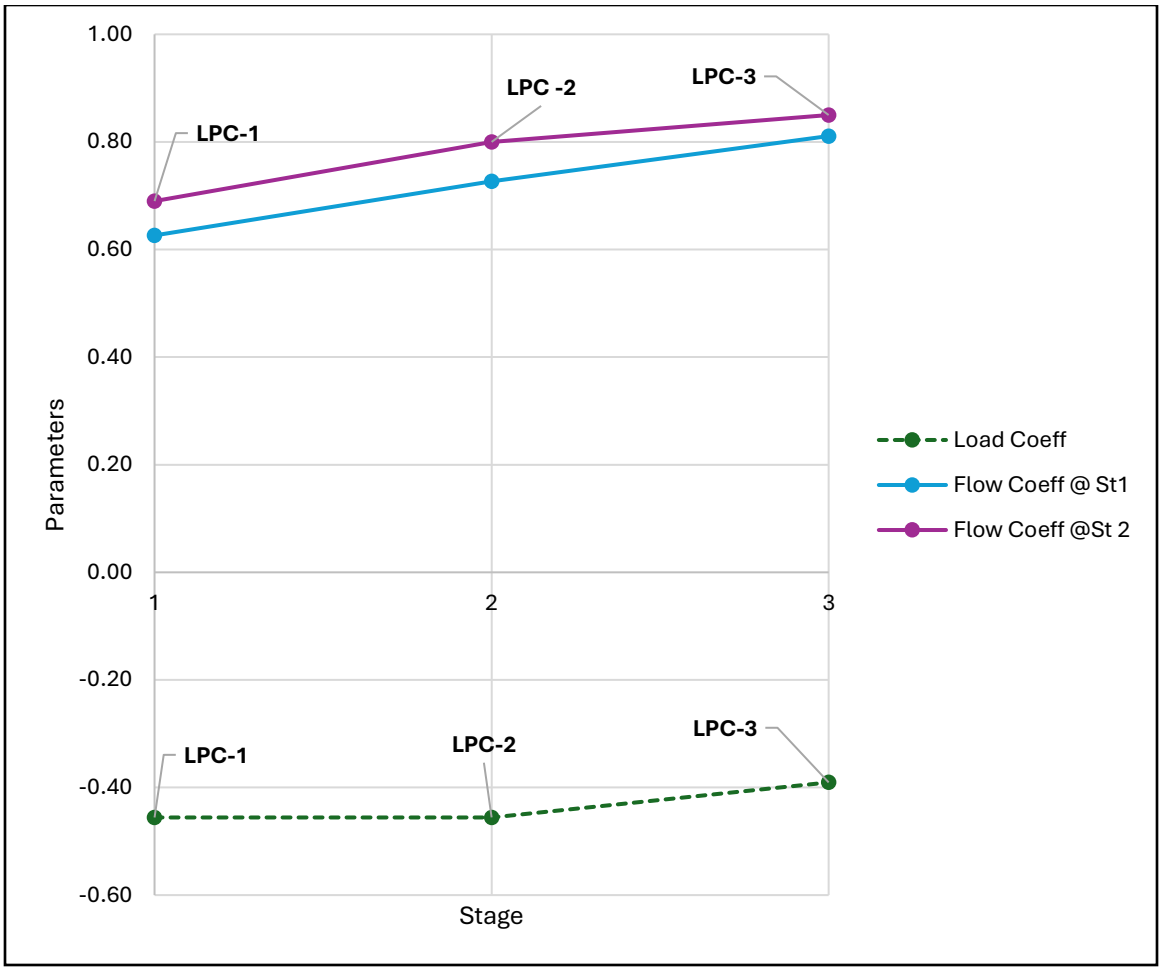

Figure 30: Stage Characteristics – LPC

A key design decision was to minimize the number of stages to reduce overall weight and cost. This resulted in a three-stage LPC configuration. This represents a trade-off between efficiency and complexity, where a slight reduction in efficiency was accepted in favor of fewer stages. As a result, some parameters, such as loading and flow coefficients, slightly deviate from recommended ranges, occasionally falling below 0.4 or exceeding 0.6 in magnitude.

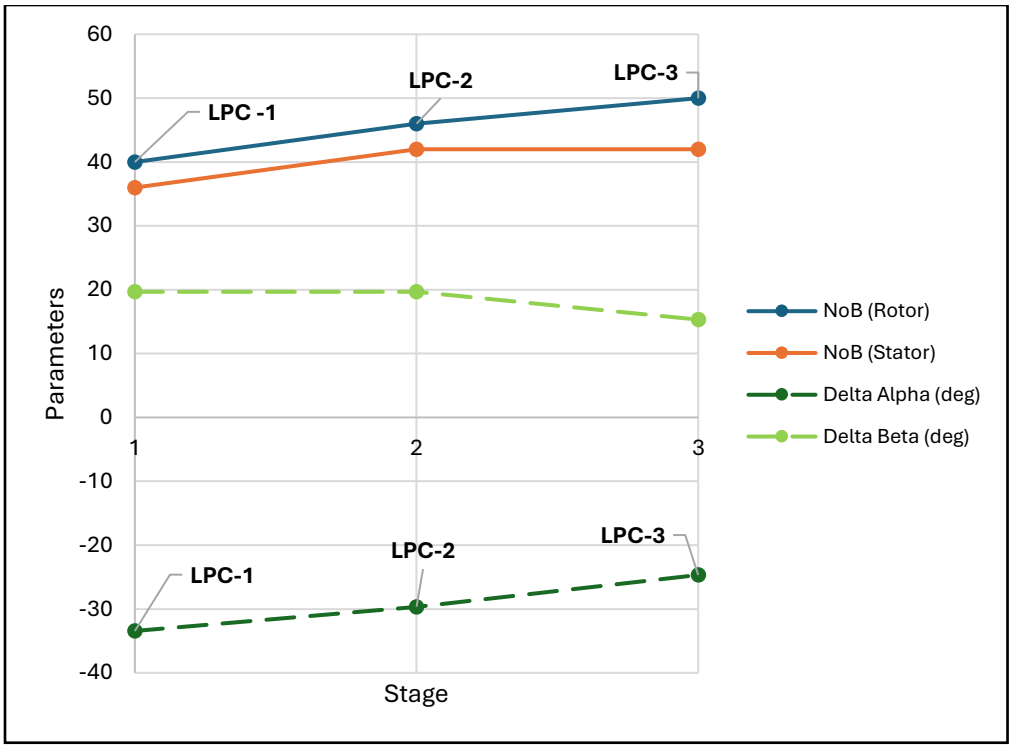

Figure 31: Stage Characteristics – LPC

The number of blades ranges from approximately 35 to 50 per stage, with camber angles maintained below a magnitude of 45 degrees.

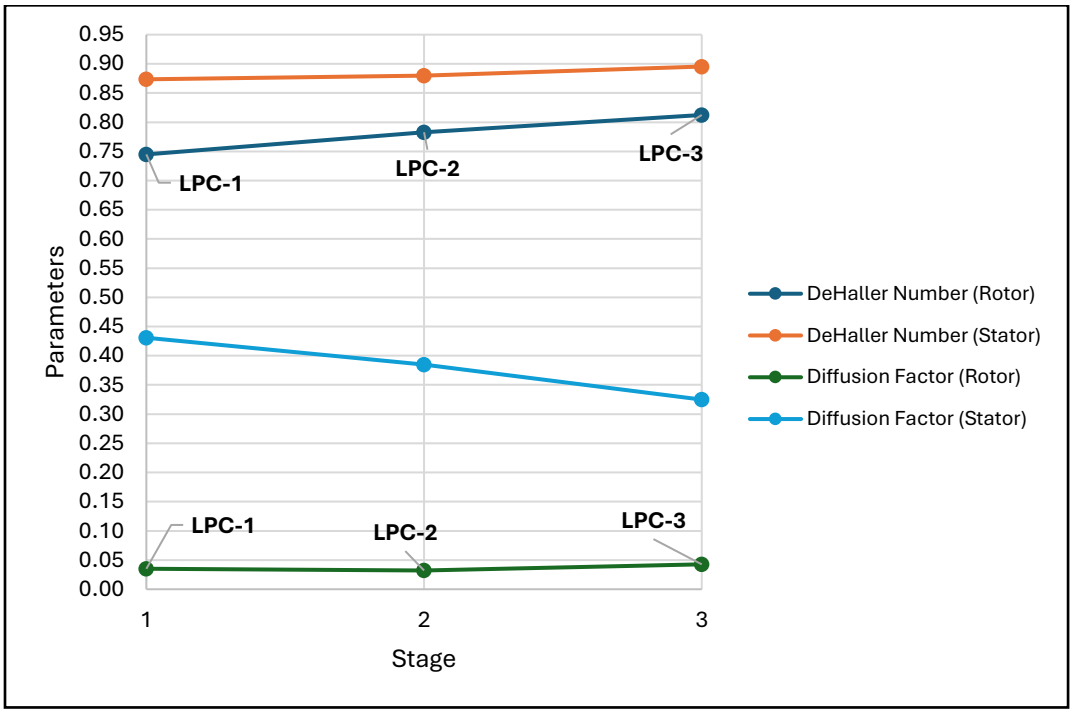

Figure 32: Airfoil Health – LPC

The De Haller number for both rotor and stator across all stages was maintained above 0.68, while the average diffusion factor was kept below 0.45. The rotor diffusion factor values are relatively low compared to the stator, indicating lightly loaded rotor stages. This provides a high margin against flow separation, resulting in improved efficiency, higher stall margin, and a more stable operating range. Therefore, this behavior was retained rather than modifying the overall LPC design.

Other stage characteristics, such as the degree of reaction, were maintained between approximately 0.5 and 0.9 from hub to tip, ensuring effective compressor performance. Detailed numerical results are provided in the Appendix.

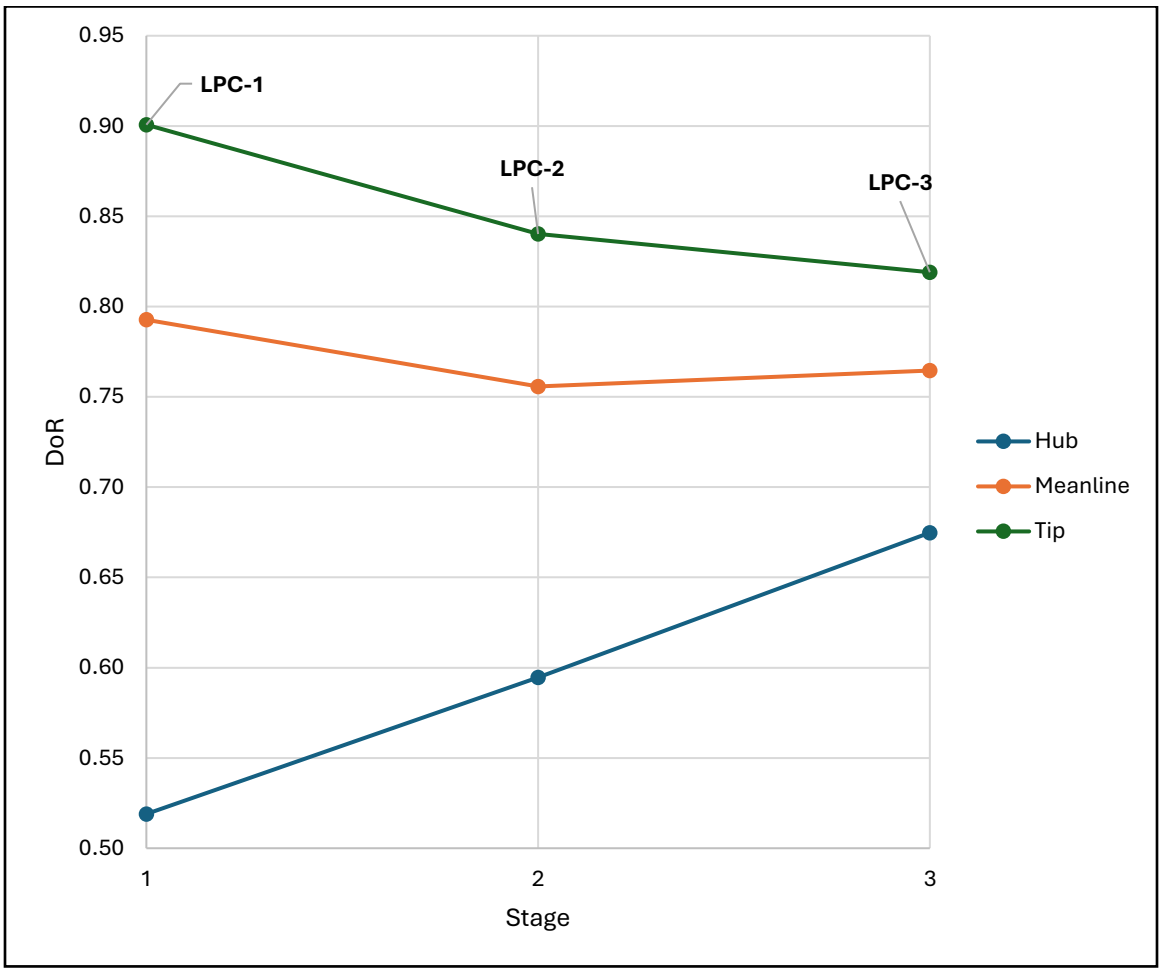

Figure 33: Degree of Reaction vs Stage

High-Pressure Compressor Design

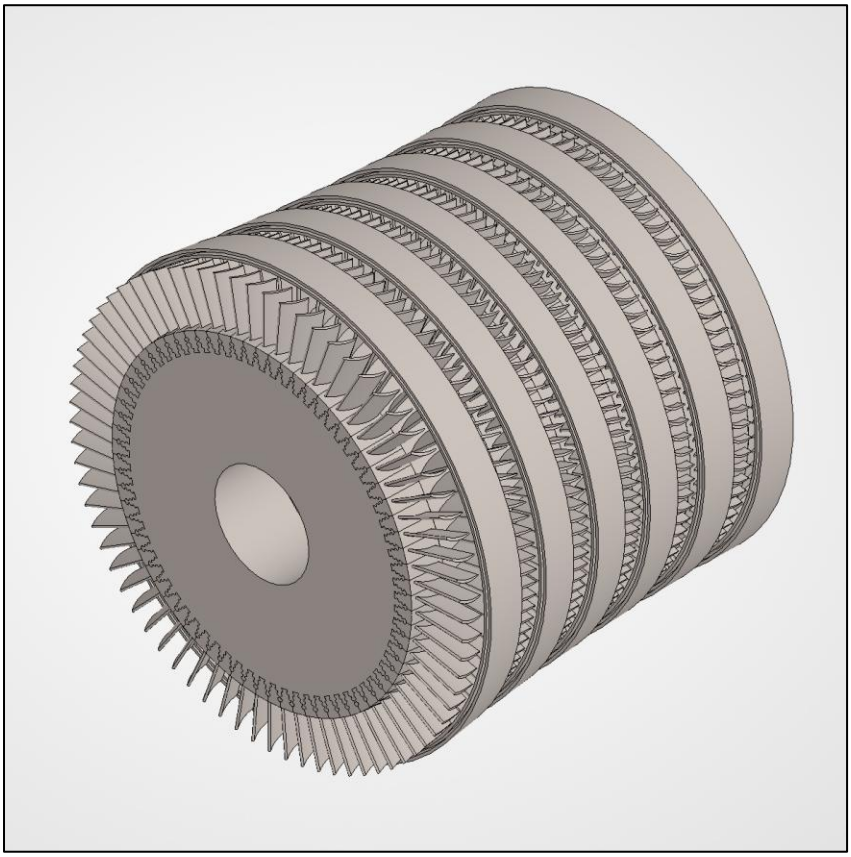

Figure 34: HPC CAD model

The high-pressure compressor (HPC) rotates on the high-pressure spool, which is connected to the high-pressure turbine. Its inlet conditions are obtained from the LPC. The HPC performs the primary compression, significantly increasing the total pressure required for efficient combustion. The configuration of the high-pressure compressor is shown below.

Table 8: HPC Design Configuration

Parameter	Value
Stages	6
RPM	13,000
$\dot{m}$	53 kg/s
π_{cH}	15.7
η_{cL}	0.89
$\dot{W}$ **(Power Input)**	26.8 MW
b_{avg}	8 – 1 cm
$C_{xm,avg}$	3 – 1 cm
U_{avg}	495 m/s

The HPC operates at a higher rotational speed of approximately 13,000 RPM, at which it demonstrated the most effective performance. This RPM also influenced the geometric parameters, particularly the mean line radius. Special attention was given to maintaining a smooth radial profile and aligning the mean line radius as consistently as possible between the compressor and turbine components, as shown in figure 23.

The HPC consists of six stages, with blade height decreasing from approximately 8 cm at the first stage to 1 cm at the sixth stage. Blade thickness ranges from approximately 3 cm to 1 cm across the stages. The average blade speed is 495 m/s.

The following plots show the thermodynamic properties of the high-pressure compressor:

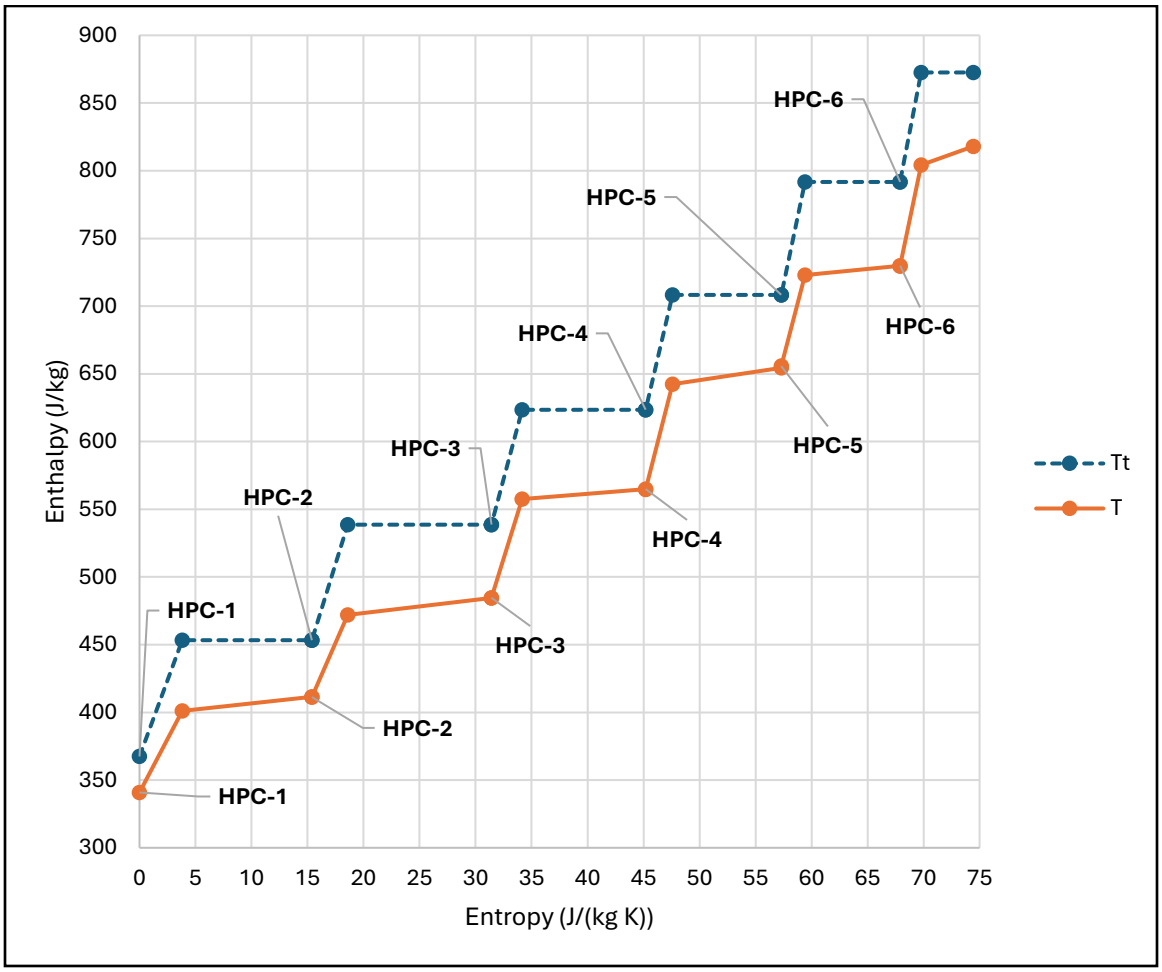

Figure 35: h-s Diagram – HPC

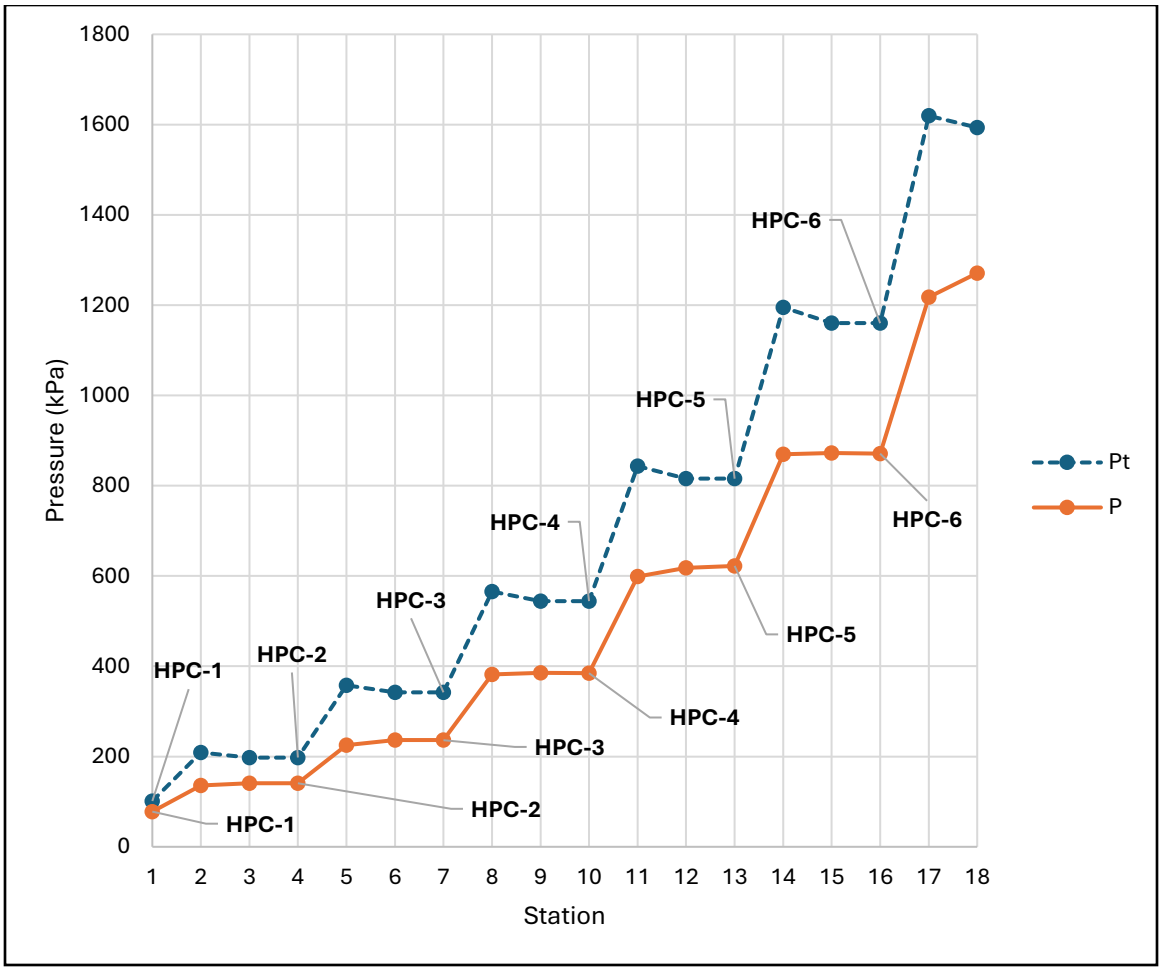

Figure 36: Pressure vs Station – HPC

A smooth pressure rise is observed across the stages. A key design decision was to achieve a higher pressure ratio in the initial stages. The first stage operates at a pressure ratio of approximately 1.95, while subsequent stages experience progressively lower pressure ratios ranging from approximately 1.7 to 1.4, with the final stage at approximately 1.37. Although relatively high values for the initial stages considering the adverse pressure gradient in compressors, they remain within limits suggested in academic literature, where stage pressure ratios up to approximately 2 are considered acceptable.

This approach, combined with slight deviations from recommended ranges for loading and flow coefficients (discussed later in the report), enabled the design of a six-stage HPC. This results in a total of nine compressor stages for the entire engine (LPC + HPC).

A sanity check was performed against existing engines (see table 3), where the GE90 and GE9X utilize approximately 13 and 14 compressor stages, respectively, compared to the nine-stage compressor system in the proposed design.

Velocity triangles (cascade view) and the aerodynamic properties are shown in the following plots:

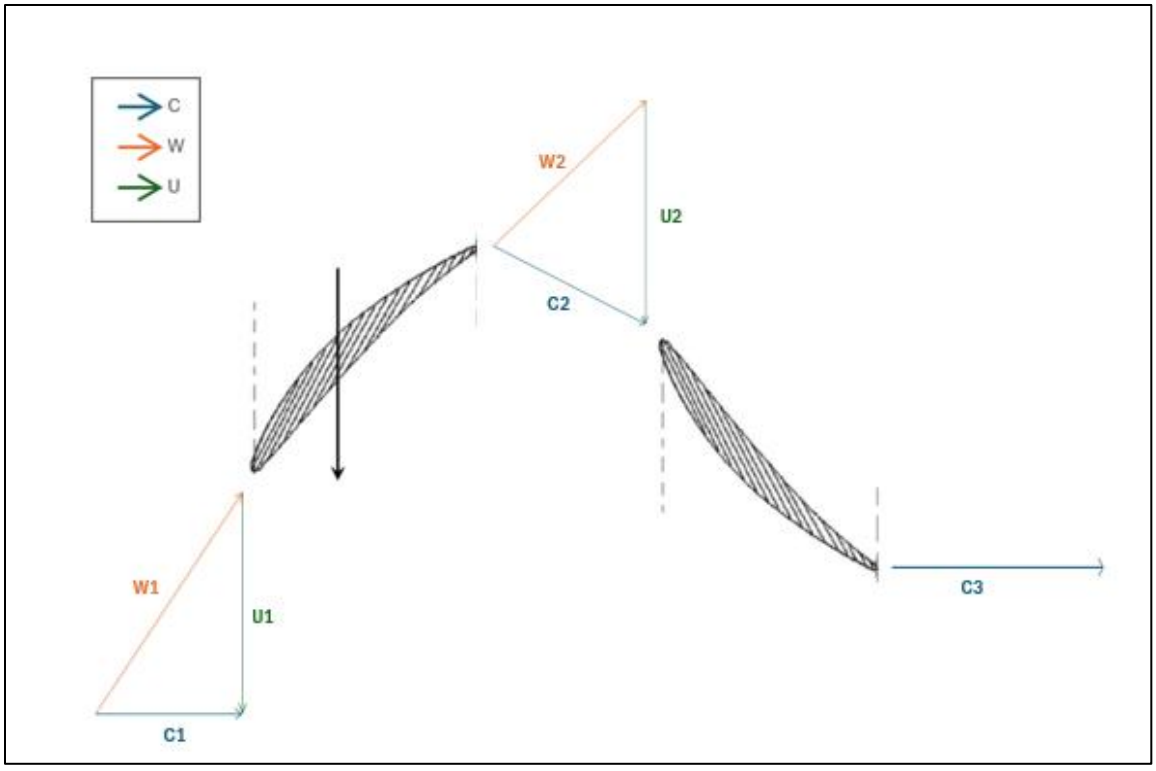

Figure 37: Velocity Triangles (mean-line radius) – HPC 1st stage

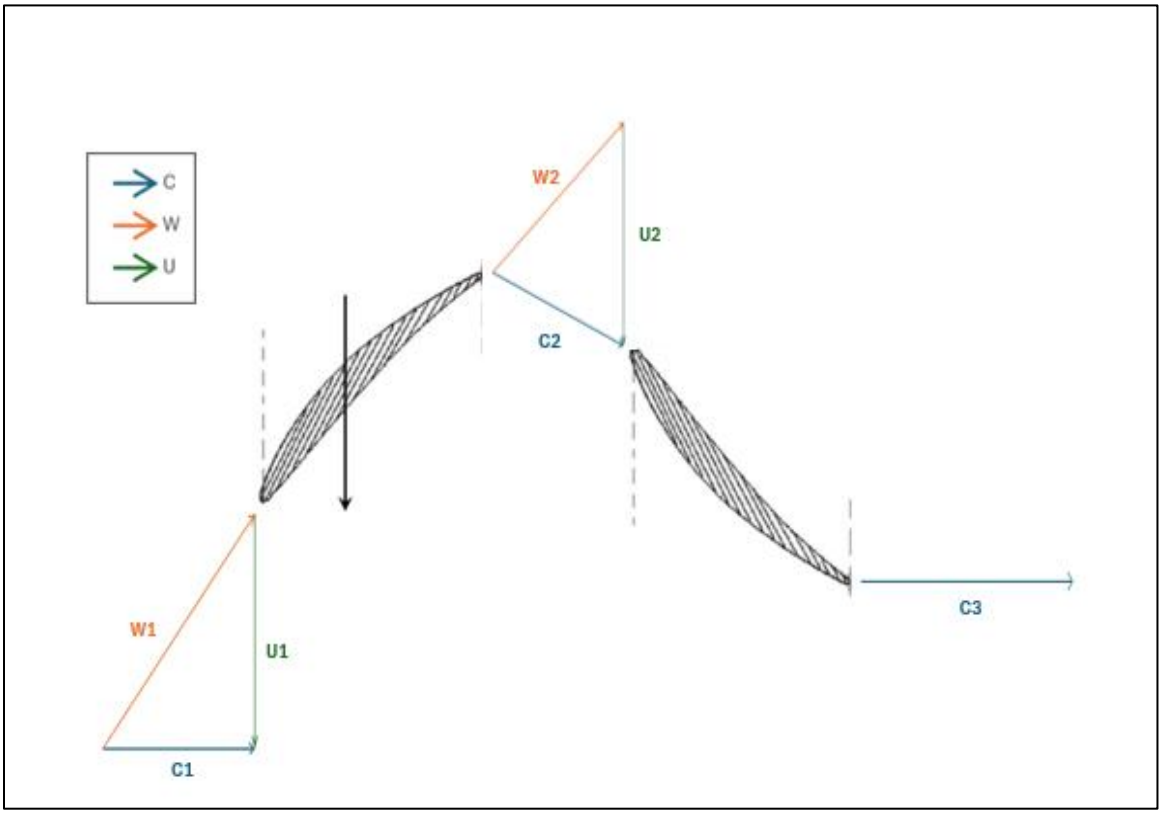

Figure 38: Velocity Triangles (mean-line radius) – HPC 6th stage

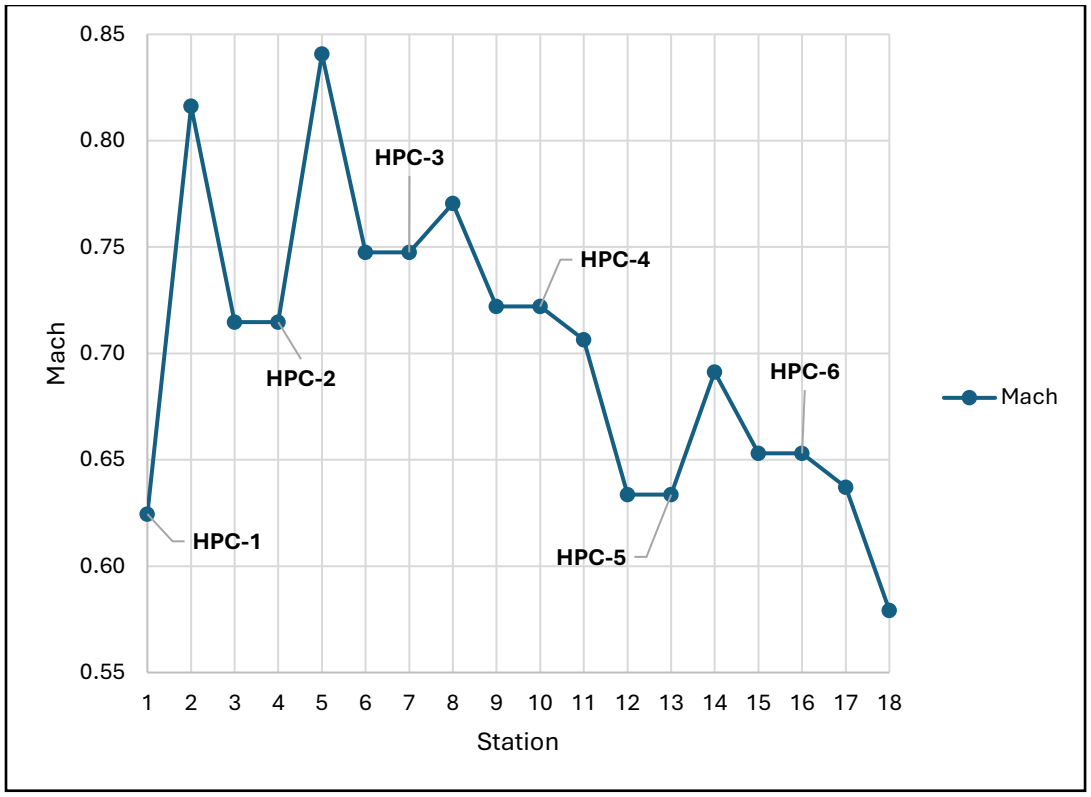

Figure 39: Mach vs Station – HPC

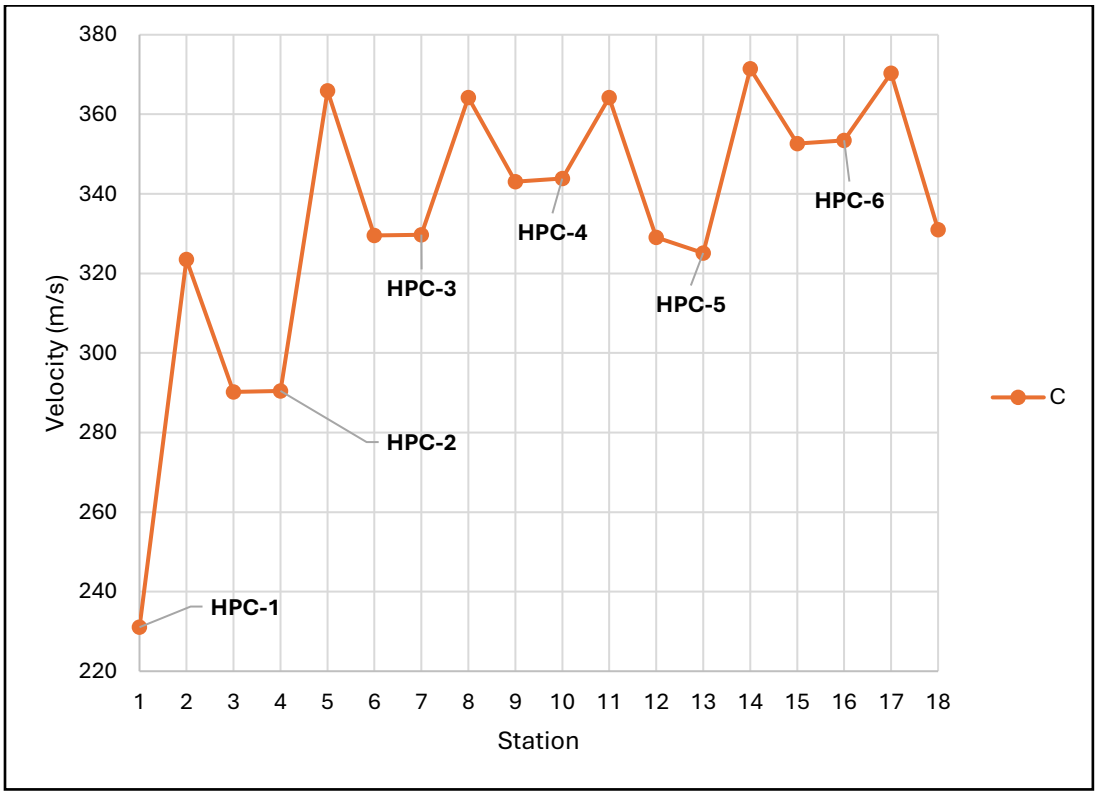

Figure 40: Absolute Velocity vs Station – HPC

The HPC demonstrates consistent velocity triangle behavior across all six stages and at all radial locations (hub, mean, and tip). The trends align with expected compressor behavior. Zero exit swirl was maintained at the stator exit for each stage, ensuring axial flow into subsequent stages and minimizing losses. Both absolute and relative Mach numbers remain well below 1.4.

A smooth geometric profile was maintained throughout the HPC design. The following plot illustrates the meridional view, showing the variation of hub, mean, and tip radii across all six stages, including the rotor-stator pairs.

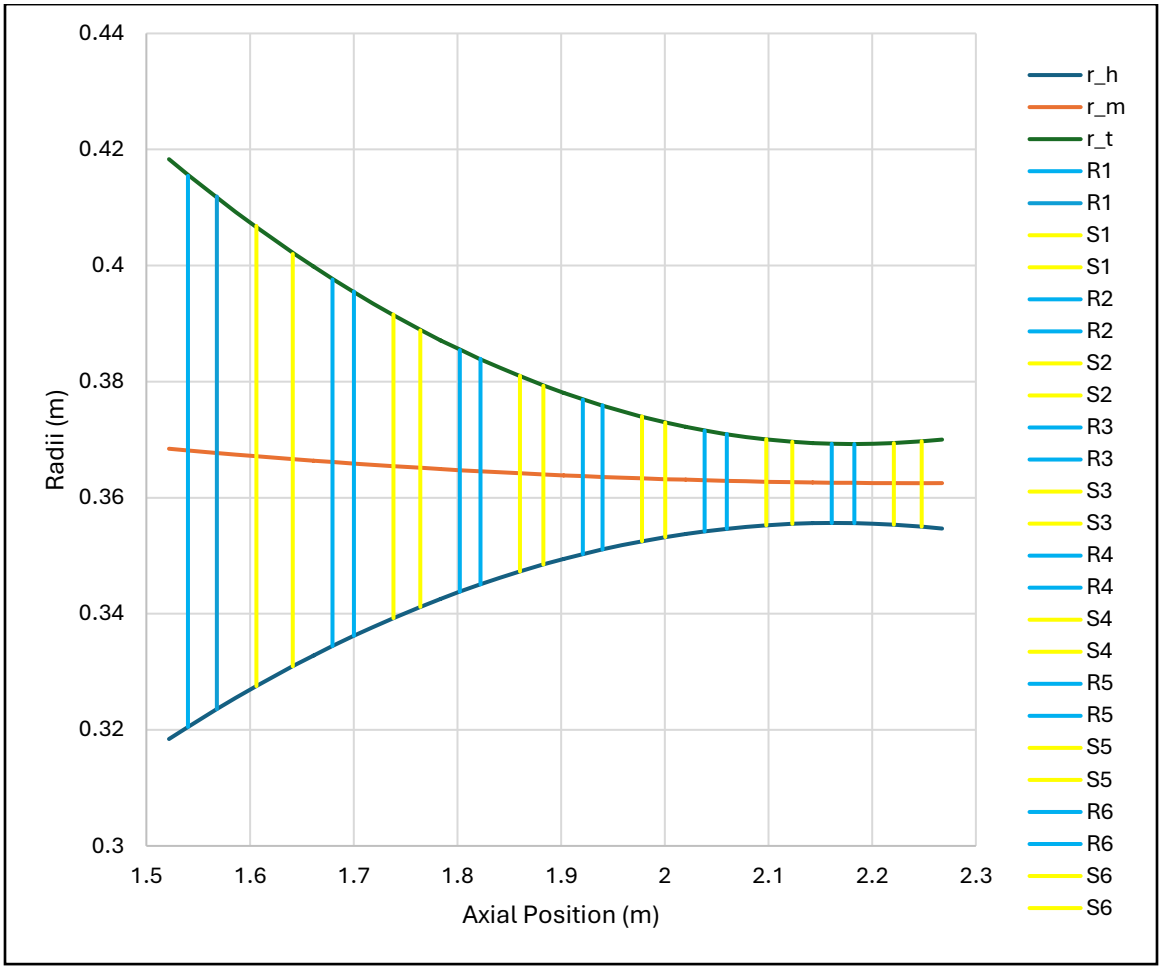

Figure 41: Meridional View – HPC

The following plots demonstrate stage characteristics and their trends across the six stages.

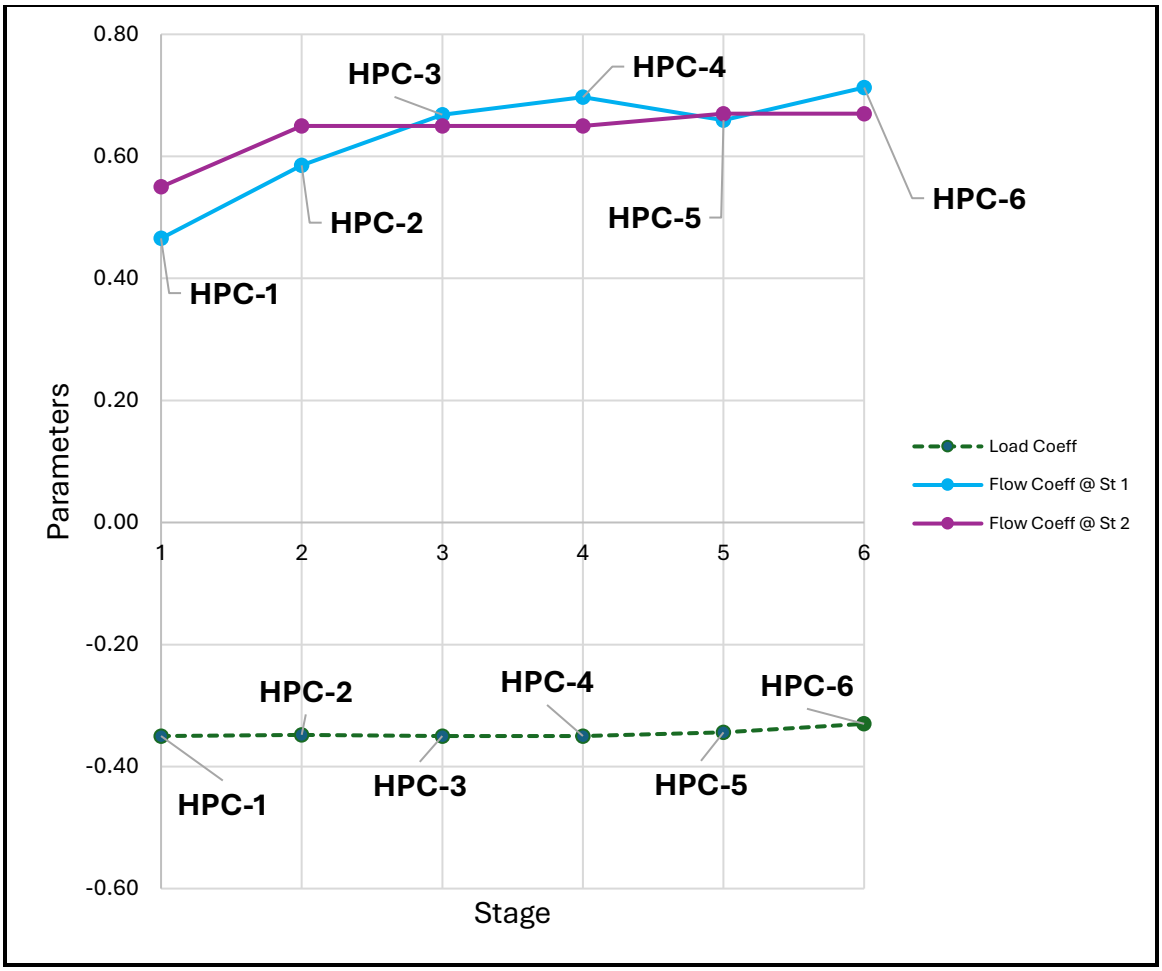

Figure 42: Stage Characteristics – HPC

As discussed earlier, a key design philosophy was to minimize the number of stages to reduce weight and cost. This resulted in a six-stage HPC configuration, representing a trade-off between efficiency and complexity. While efficiency experiences a slight reduction, the overall system benefits from a reduced stage count. This approach led to occasional deviations from recommended ranges for loading and flow coefficients, including values slightly below 0.4 or above 0.6 in magnitude.

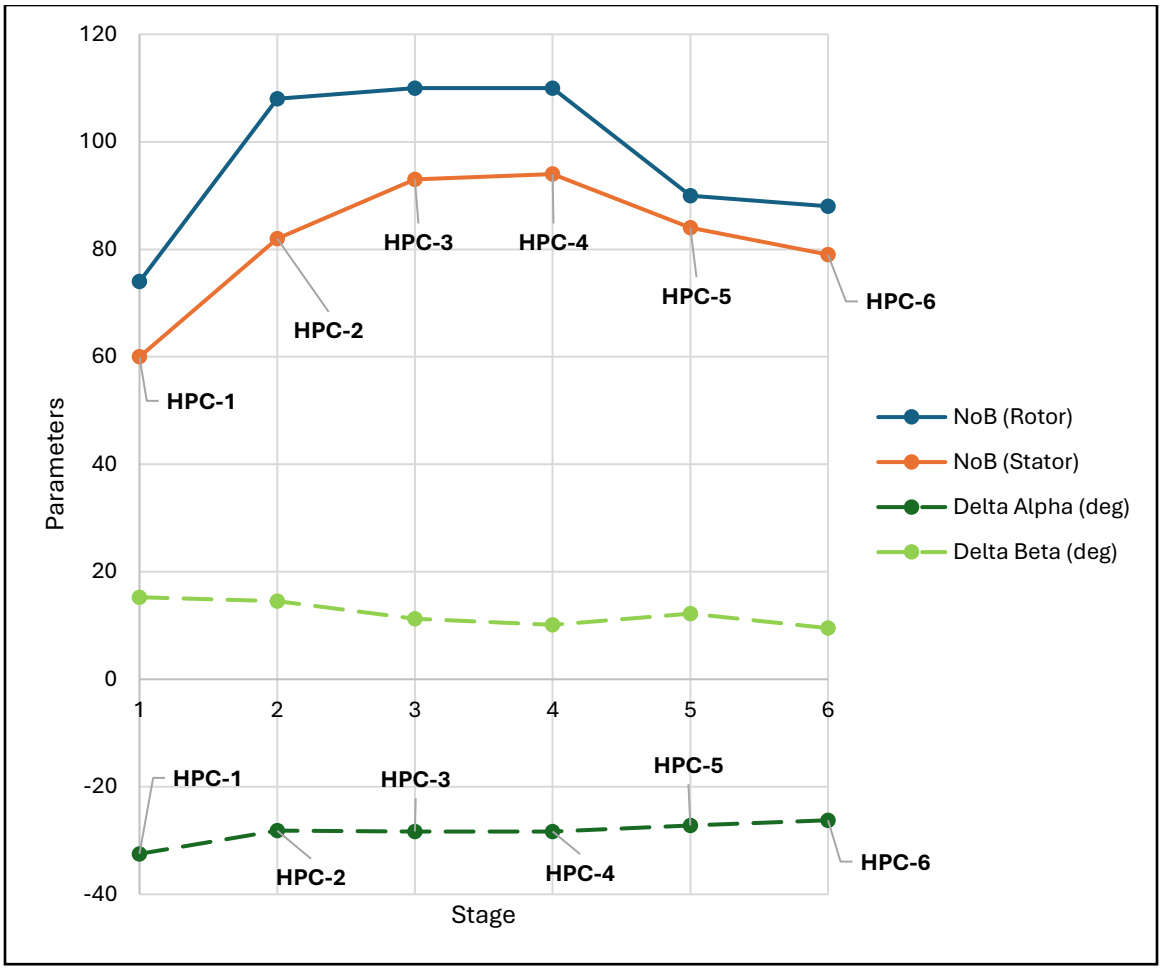

Figure 43: Stage Characteristics – HPC

The number of blades ranges from approximately 60 to 110 per stage, with camber angles maintained below a magnitude of 45 degrees.

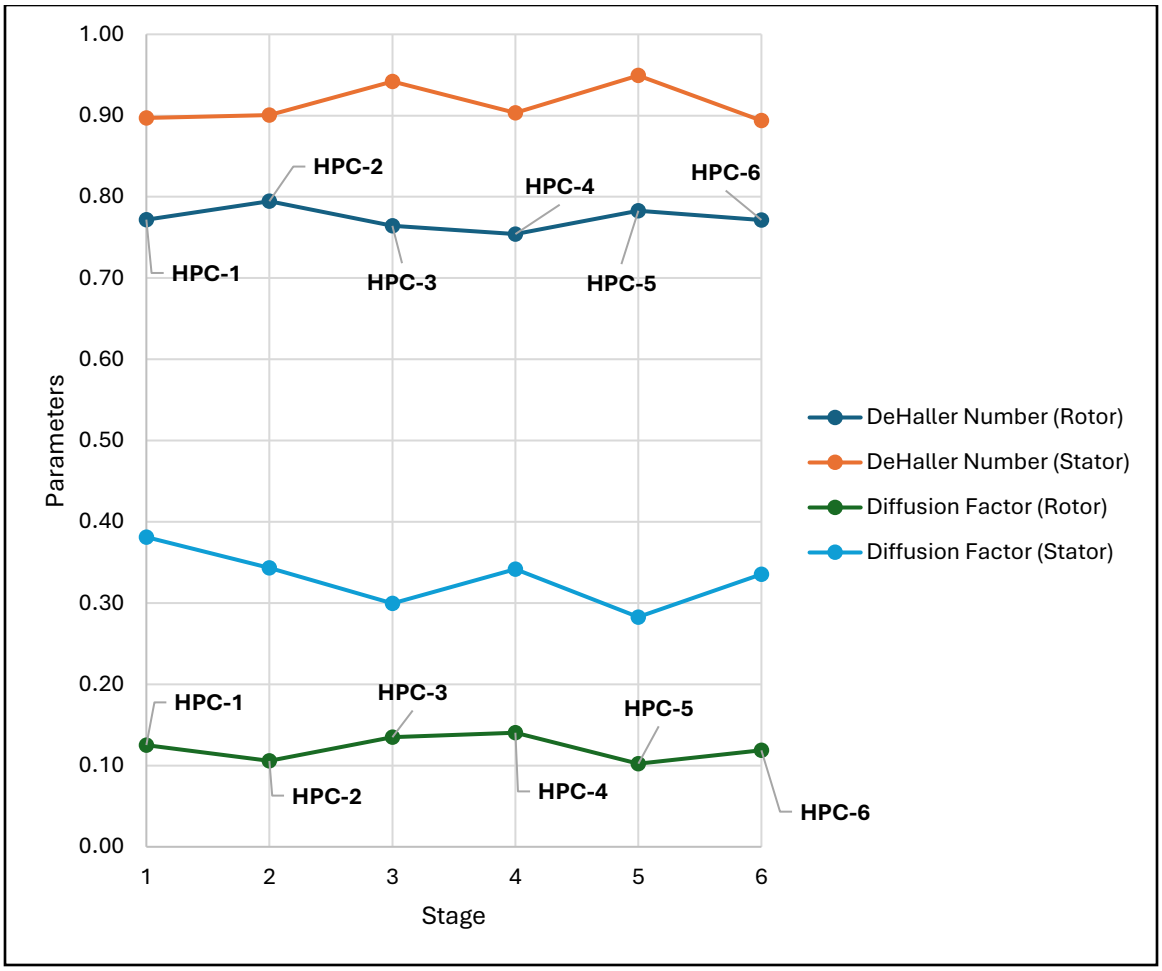

Figure 44: Airfoil Health – HPC

The De Haller number for both rotor and stator across all stages was maintained above 0.68, while the average diffusion factor was kept below 0.45. Slightly lower diffusion factor values in the rotor indicate lightly loaded stages, which reduces the risk of flow separation and improves efficiency, resulting in higher stall margins and a more stable operating range.

Other stage characteristics, such as the degree of reaction, were maintained between approximately 0.8 and 0.92 from hub to tip, ensuring effective compressor performance. Detailed numerical results are provided in the Appendix.

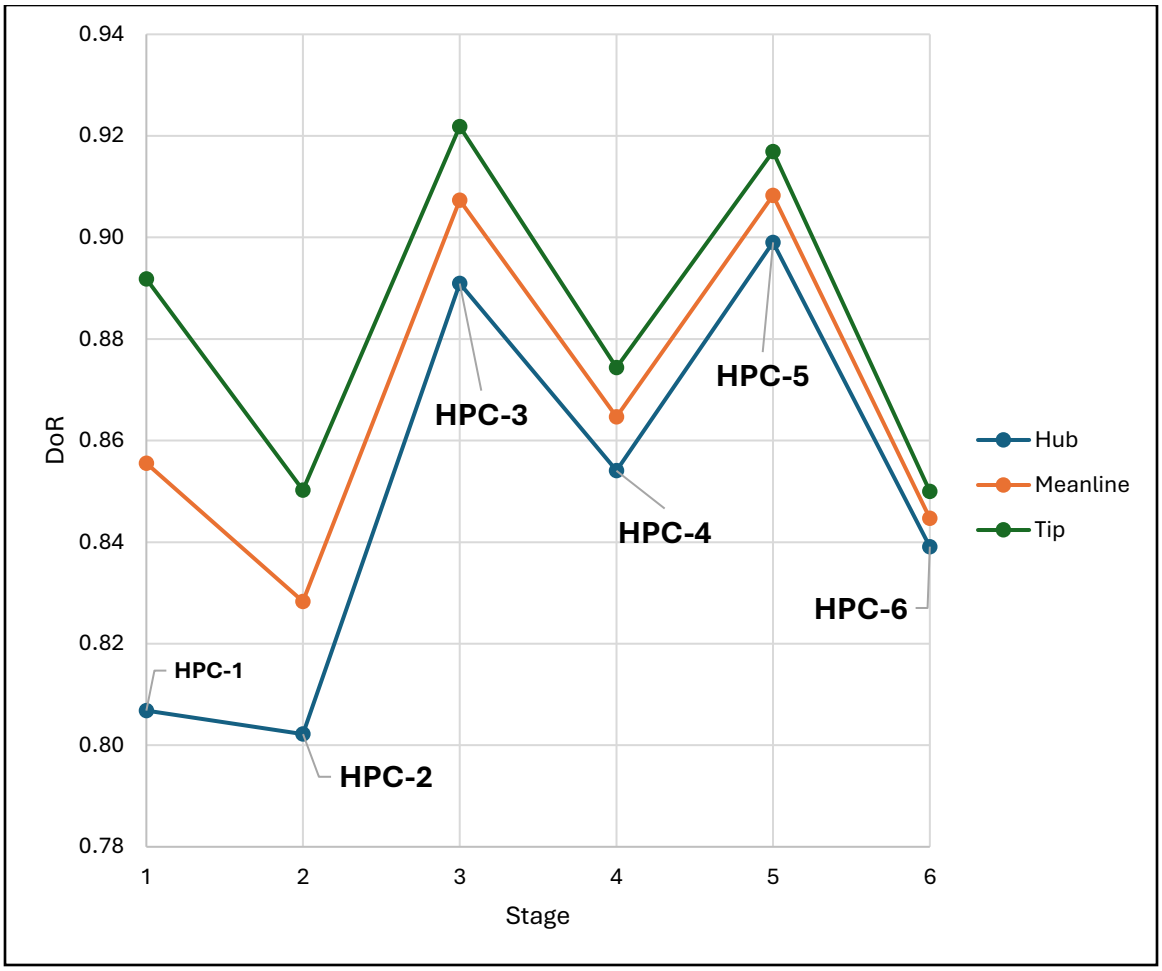

Figure 45: Degree of Reaction vs Stage

Combustor Design

Figure 46: Combustor CAD model

The purpose of the combustor is to mix high-pressure air with fuel to add thermal energy to the flow, which is then used to drive the turbine. A well-designed combustor should have low pressure loss, high combustion efficiency, and stable operation over a wide range of conditions. It is also critical to ensure that the exit temperature remains within allowable limits so that the downstream turbine components are not exposed to excessive thermal loading.

The combustor design was based on the inlet and outlet thermodynamic conditions obtained from the cycle analysis. These values were used to determine the internal flow conditions required to achieve the desired performance. The turbine inlet temperature was selected as a key design parameter to ensure that the flow entering the turbine remains consistent with the turbomachinery design.

Table 9: Thermodynamic Conditions for Combustor

Parameter	Station 3	Station 4
Total Pressure (kPa)	1593	1530
Static Pressure (kPa)	1271	1340
Total Temperature (K)	873	1778
Static Temperature (K)	818	1721

The pressure drop across the combustor is relatively small, indicating that pressure losses have been kept within acceptable limits while still allowing for effective mixing and combustion.

Once the internal conditions were established, the combustor geometry was determined using a scaling approach based on the TF39 annular combustor. This provided a realistic reference for airflow distribution, mixing characteristics, and overall geometry. The airflow distribution within the combustor is illustrated below, representing a typical modern combustor design.

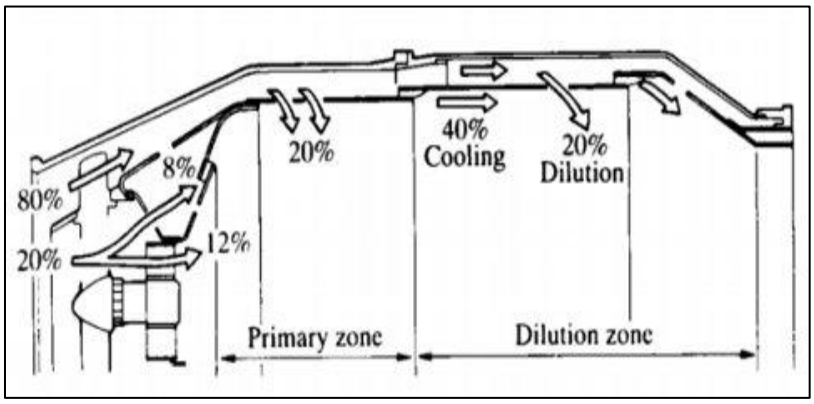

Figure 47: Airflow Distribution

The combustor follows an annular configuration, which allows for compact geometry, efficient mixing, and uniform temperature distribution at the exit. The design incorporates primary, secondary, and dilution zones to ensure proper combustion and temperature control before the flow enters the turbine.

The scaled combustor was then integrated into the overall engine design. The final dimensions are summarized below.

Table 10: Combustor Dimensions

Parameter	Value
Length	0.41 m
Diameter	0.67 m
L/D	0.62
$\boldsymbol{t_{res}}$	0.01 s

The selected dimensions provide sufficient residence time for combustion while maintaining a compact design. The relatively low L/D ratio reflects a design that prioritizes reduced size and weight while still meeting combustion and flow requirements.

Overall, the combustor design meets the primary objectives of maintaining low pressure loss, achieving the required temperature rise, and providing stable operation with adequate residence time. The resulting configuration is consistent with modern annular combustor designs and integrates effectively with the upstream compressor and downstream turbine components.

Turbine (High-Pressure & Low-Pressure) Design

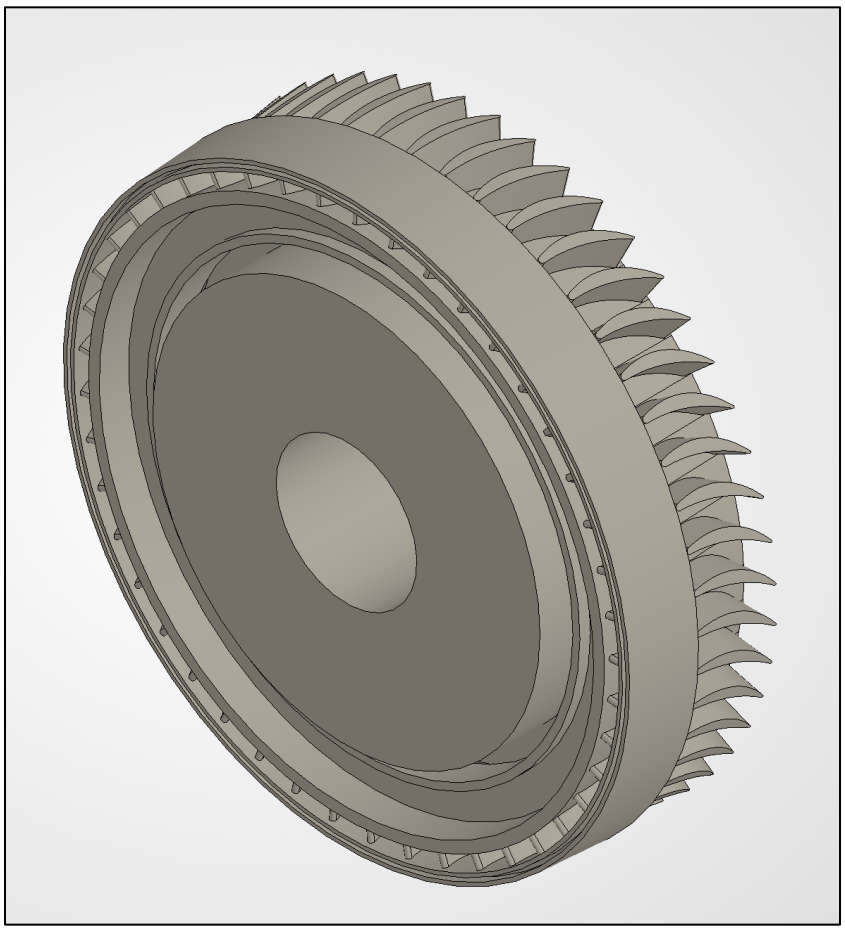

Figure 48: HPT CAD model

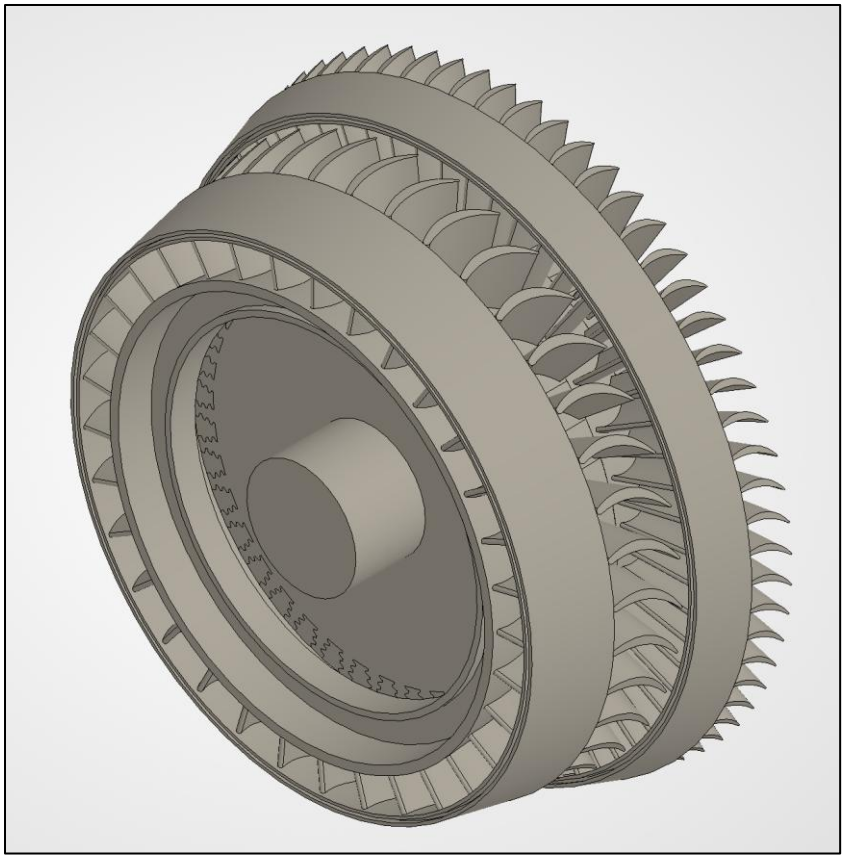

Figure 49: LPT CAD model

Since the high-pressure turbine (HPT) and low-pressure turbine (LPT) consist of a relatively small number of stages, they are presented together as a single component in this report.

The HPT operates under the most severe flow conditions, receiving high-temperature, high-energy flow directly from the combustion chamber. It is mounted on the high-pressure spool and is responsible for driving the high-pressure compressor (HPC). Downstream of the HPT, the LPT operates under comparatively less extreme conditions and is mounted on the low-pressure spool, where it powers both the LPC and the fan. The configurations of the HPT and LPT are shown below.

Table 11: HPT Design Configuration

Parameter	Value
Stages	1
RPM	13,000
$\dot{m}$	53 kg/s
T_{t4}	1778 K
η_{tH}	0.96
$\dot{W}$ **(Power Output)**	26.8 MW
b_{avg}	4 cm

$C_{xm,avg}$	7 cm
U_{avg}	515 m/s

Table 12: LPT Design Configuration

Parameter	Value
Stages	2
RPM	7,000
$\dot{m}$	53 kg/s
$T_{t4.4}$	1344 K
η_{tL}	0.92
$\dot{W}$ $(Power\ Output)$	18.9 MW
b_{avg}	9 – 15 cm
$C_{xm,avg}$	9 – 4 cm
U_{avg}	300 m/s

The HPT operates at approximately 13,000 RPM, while the LPT operates at approximately 7,000 RPM. These values were determined through an iterative design process aimed at achieving effective performance while maintaining realistic and consistent geometric scaling across the engine, particularly in terms of mean-line radii, as illustrated in figure 23.

The HPT consists of a single stage with a blade height of 4 cm and a blade thickness of 7 cm. The LPT consists of two stages, with blade height varying from approximately 9 cm to 15 cm across stages, and blade thickness ranging from approximately 9 cm to 4 cm.

A sanity check was performed against existing engines (see table 3), where both the GE90 and GE9X utilize approximately eight turbine stages. In comparison, the proposed engine uses a total of three turbine stages, reflecting a design choice to minimize complexity.

The following plots show the thermodynamic properties of the turbine.

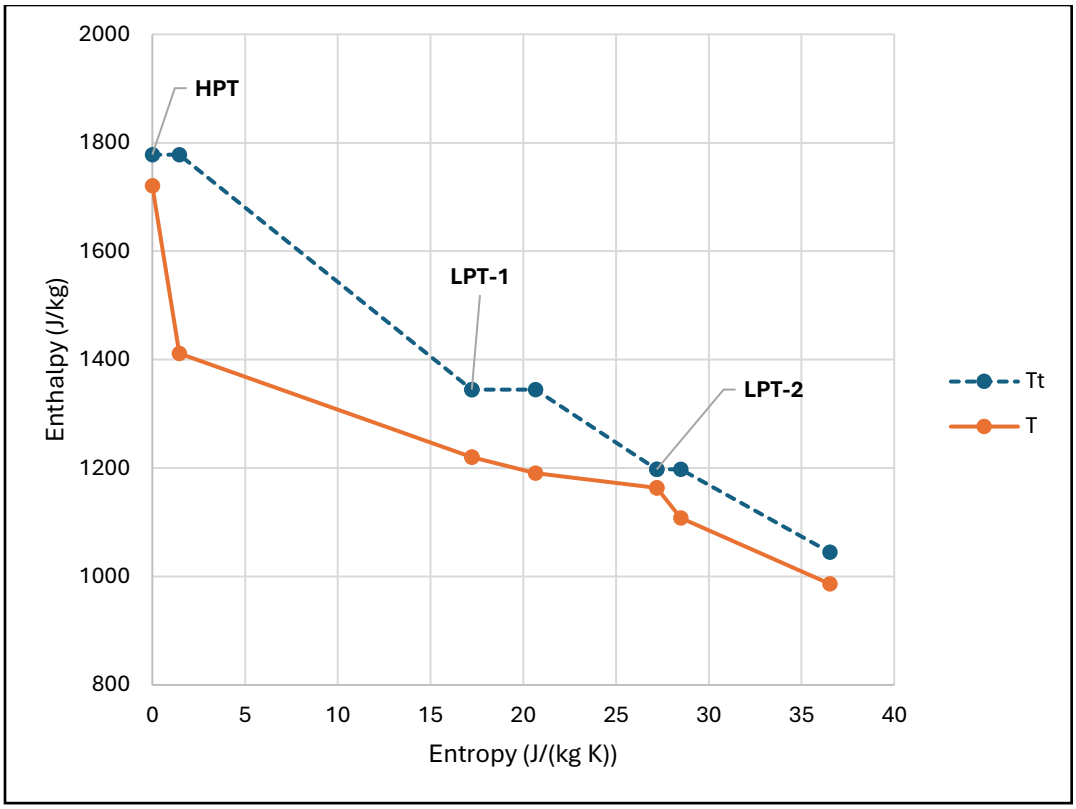

Figure 50: h-s Diagram – HPT & LPT

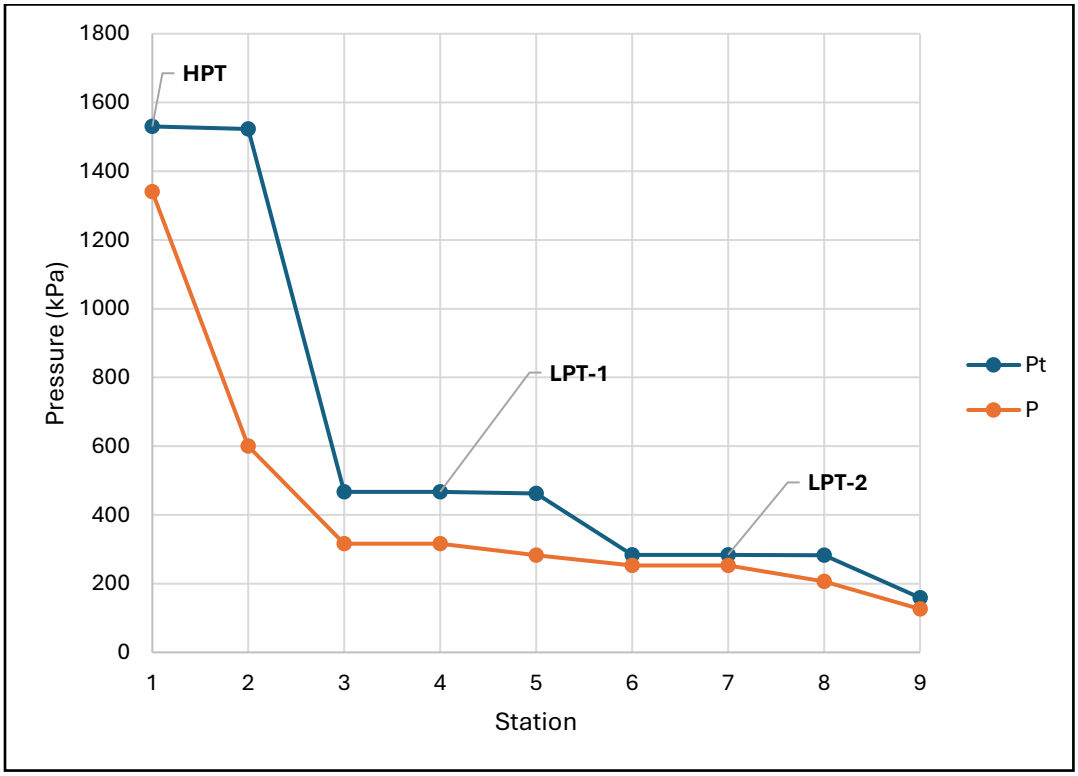

Figure 51: Pressure vs Station – HPT & LPT

A smooth decrease in pressure and enthalpy was maintained across the stages, avoiding abrupt variations in thermodynamic behavior. The HPT experiences a significantly larger enthalpy drop compared to the LPT due to the high-energy flow entering from the combustor and extracting significant energy to power the HPC.

Velocity triangles (cascade view) and aerodynamic properties are shown in the following plots.

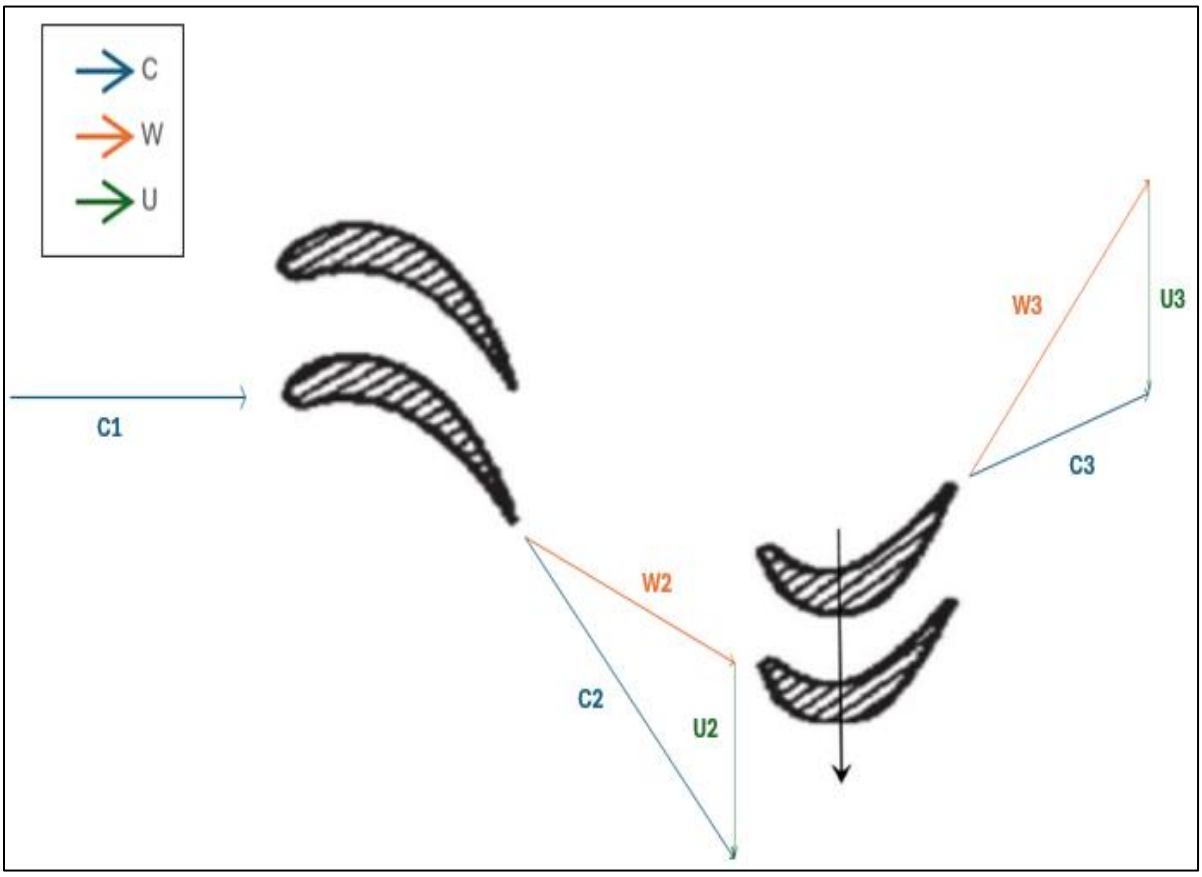

Figure 52: Velocity Triangles (mean-line radius) – HPT

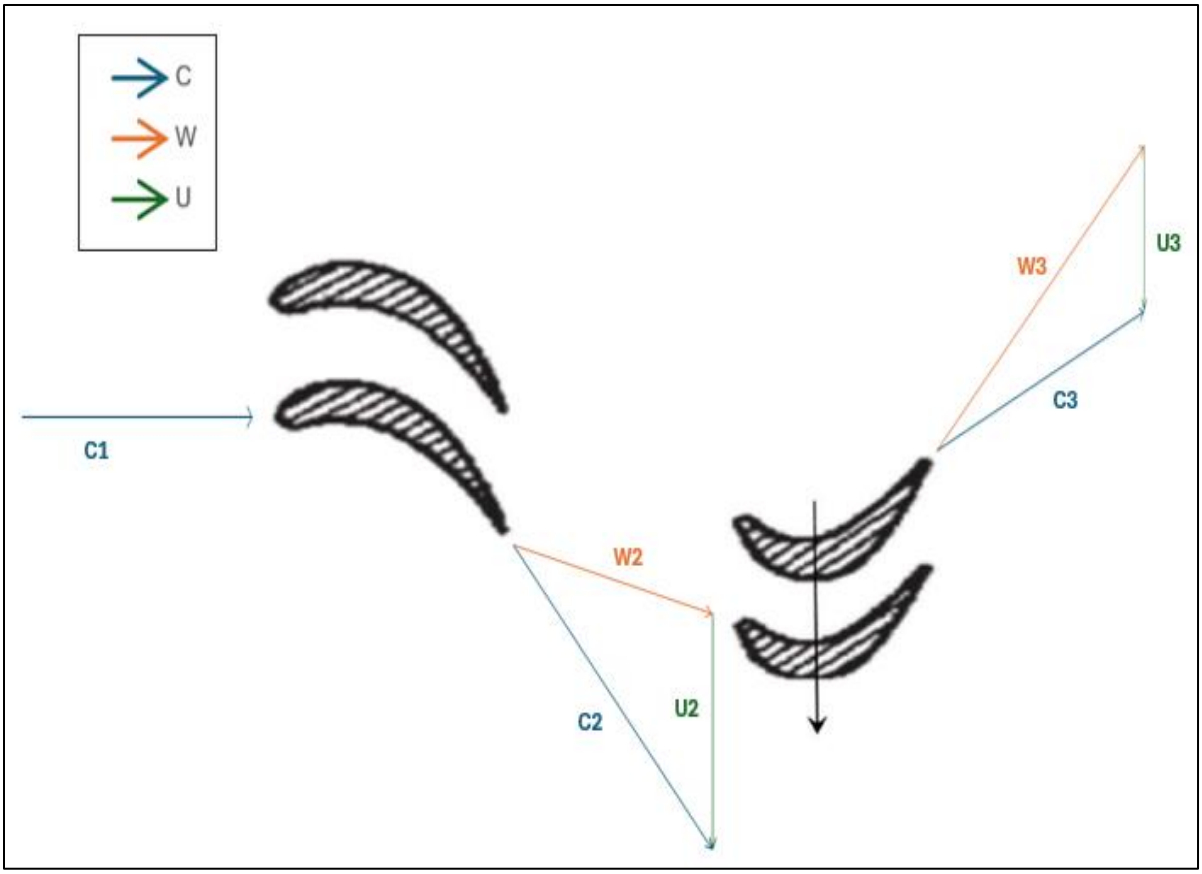

Figure 53: Velocity Triangles (mean-line radius) – LPT 2nd stage

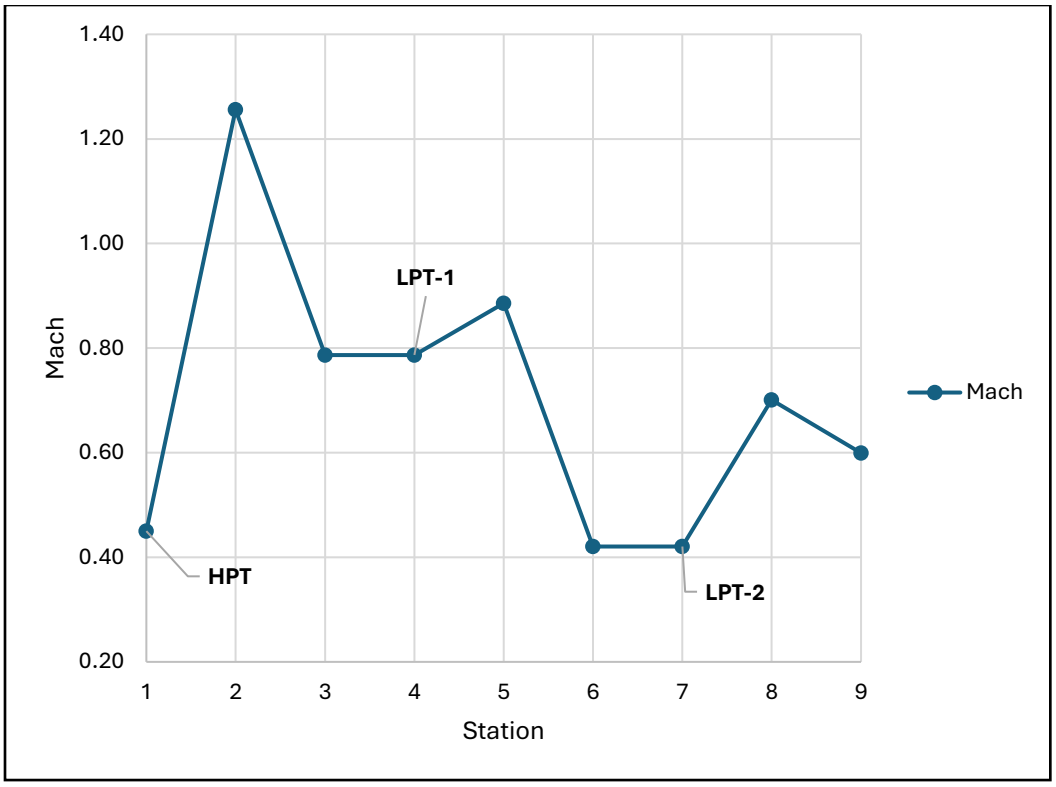

Figure 54: Mach vs Station – Turbine

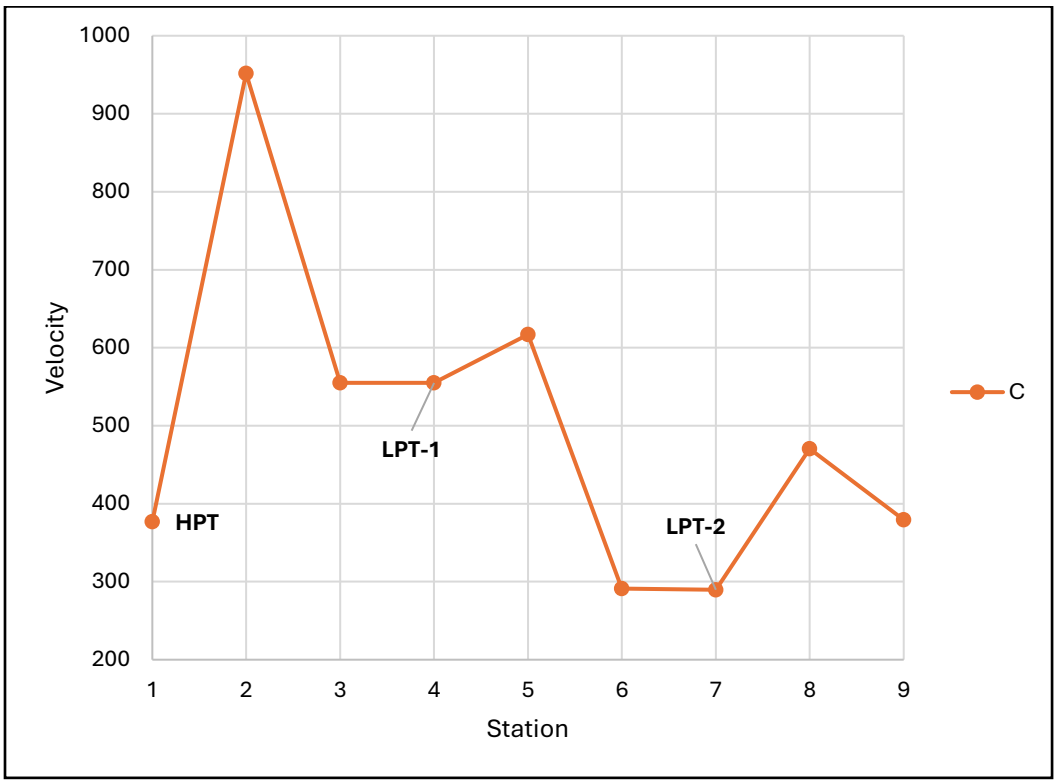

Figure 55: Absolute Velocity vs Station – Turbine

The turbine exhibits consistent velocity triangle behavior across all stages and radial locations (hub, mean, and tip). The expected trends are observed, with appropriate variation of absolute and relative velocities across each stage. Additionally, zero exit swirl was maintained at each stage, ensuring axial flow into downstream components and minimizing exit losses. Both absolute and relative Mach numbers remain below 1.3.

A smooth geometric profile was maintained across the turbine. The following plot illustrates the meridional view, showing hub, mean, and tip radii across all stages, along with rotor-stator pairs.

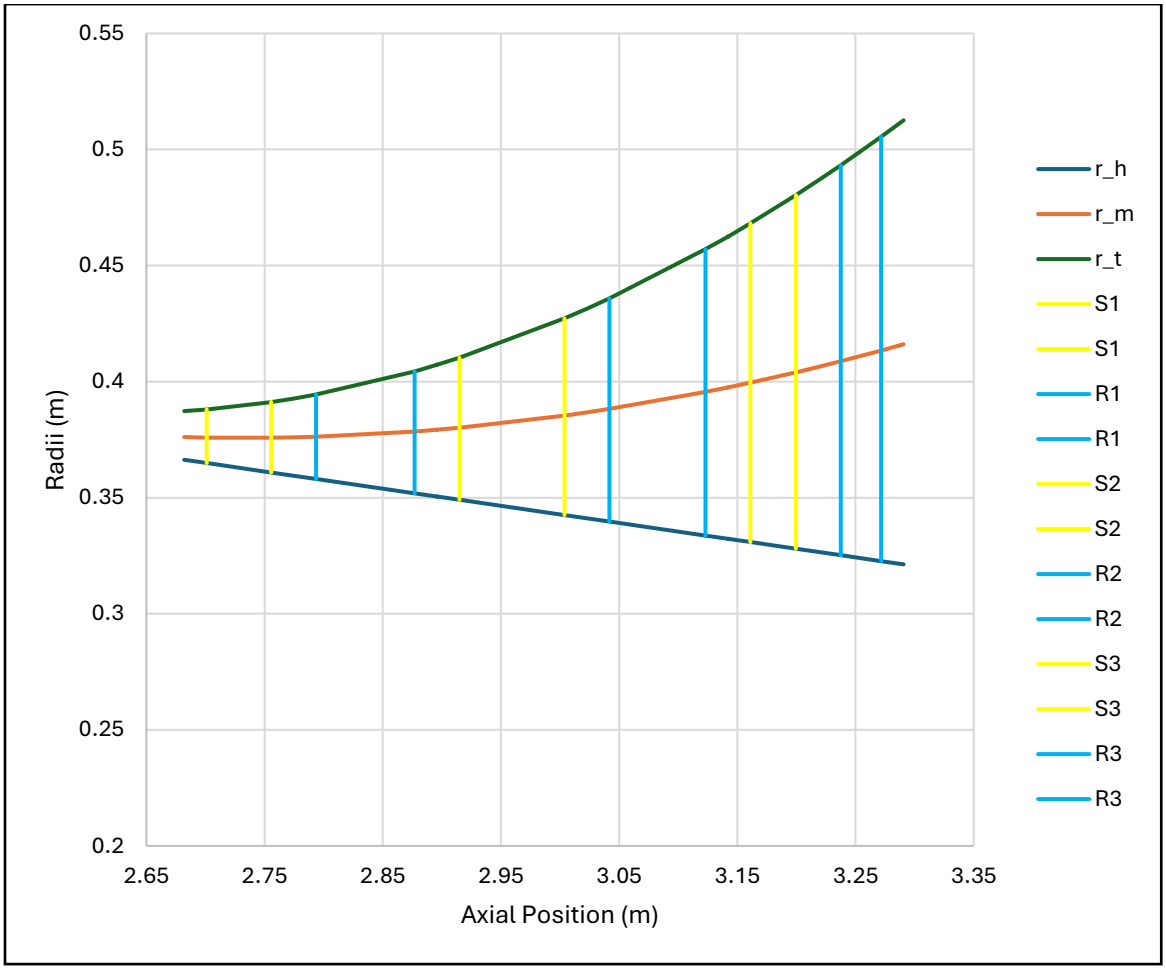

Figure 56: Meridional View – Turbine

The following plots demonstrate stage characteristics and their variation across all turbine stages.

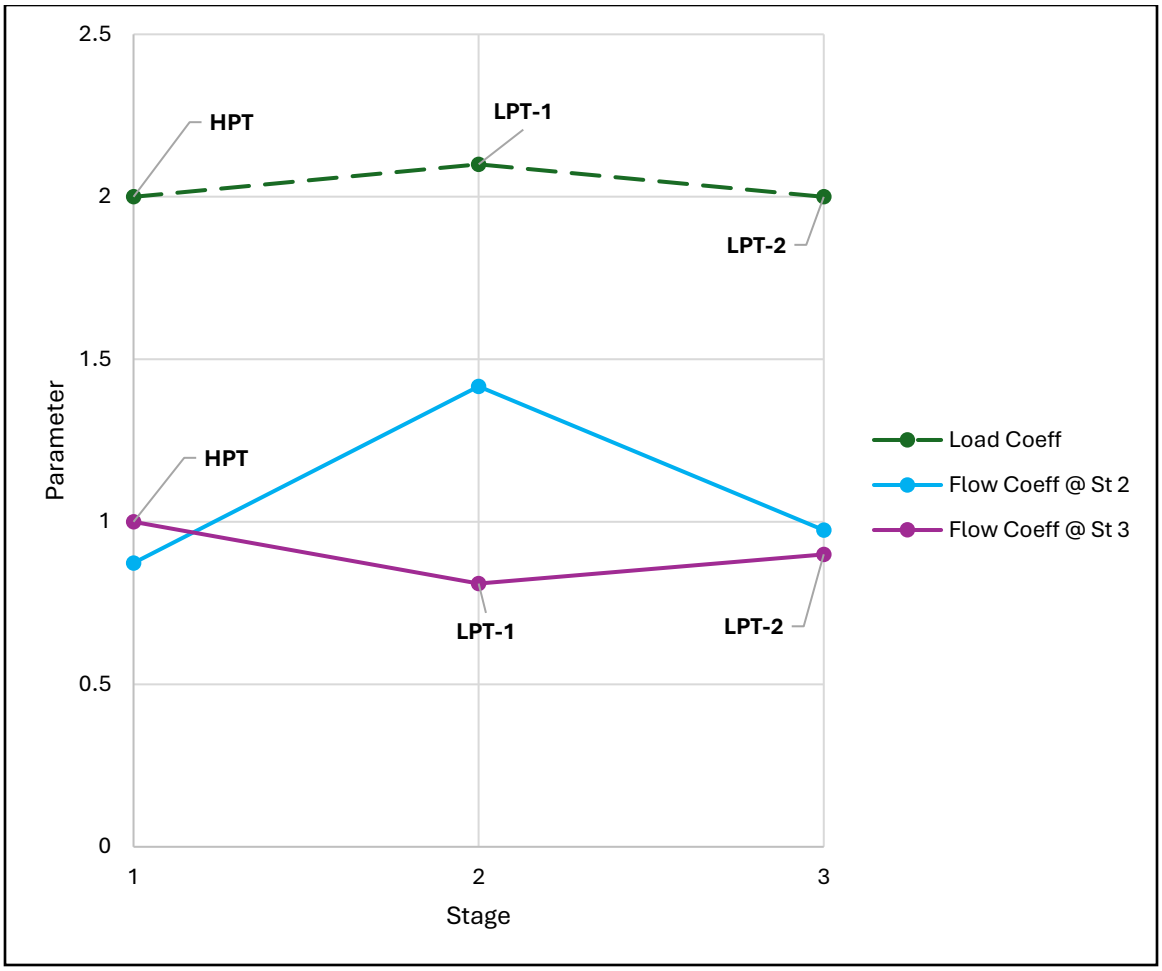

Figure 57: Stage Characteristics – Turbine

Consistent with the compressor design approach, a key design objective was to minimize the number of stages to reduce weight and cost. This resulted in a configuration consisting of one HPT stage and two LPT stages. This approach introduces a trade-off, where a slight reduction in efficiency is accepted in exchange for lower system complexity. As a result, some parameters, such as loading and flow coefficients, may slightly deviate from recommended ranges, occasionally falling below 0.4 or exceeding 0.6 in magnitude.

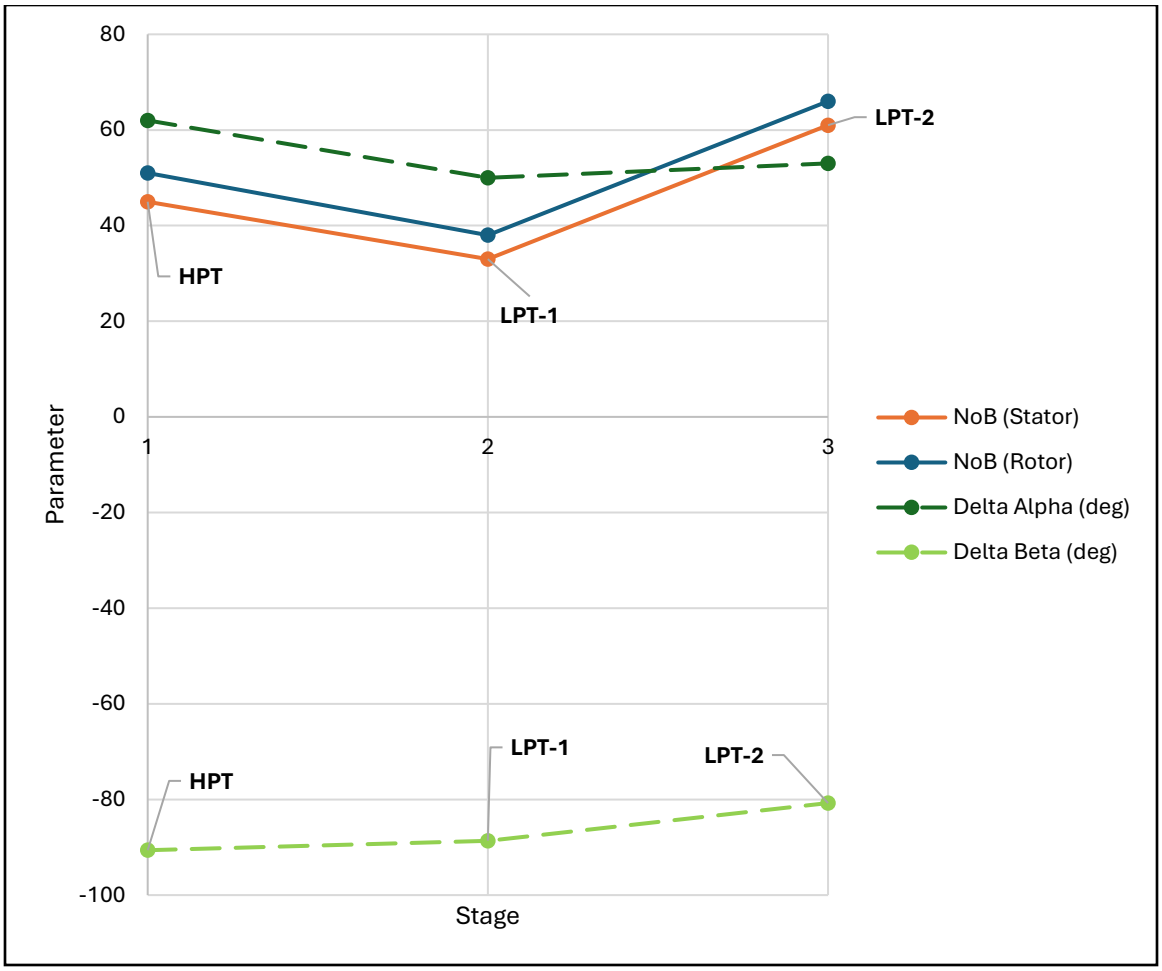

Figure 58: Stage Characteristics – Turbine

The number of blades ranges from approximately 30 to 70 per stage, with camber angles maintained below a magnitude of 120 degrees.

Other stage characteristics, such as the degree of reaction, were maintained within a range of approximately 0.1 to 0.76 from hub to tip, ensuring effective work extraction across the turbine. Detailed numerical results are provided in the Appendix.

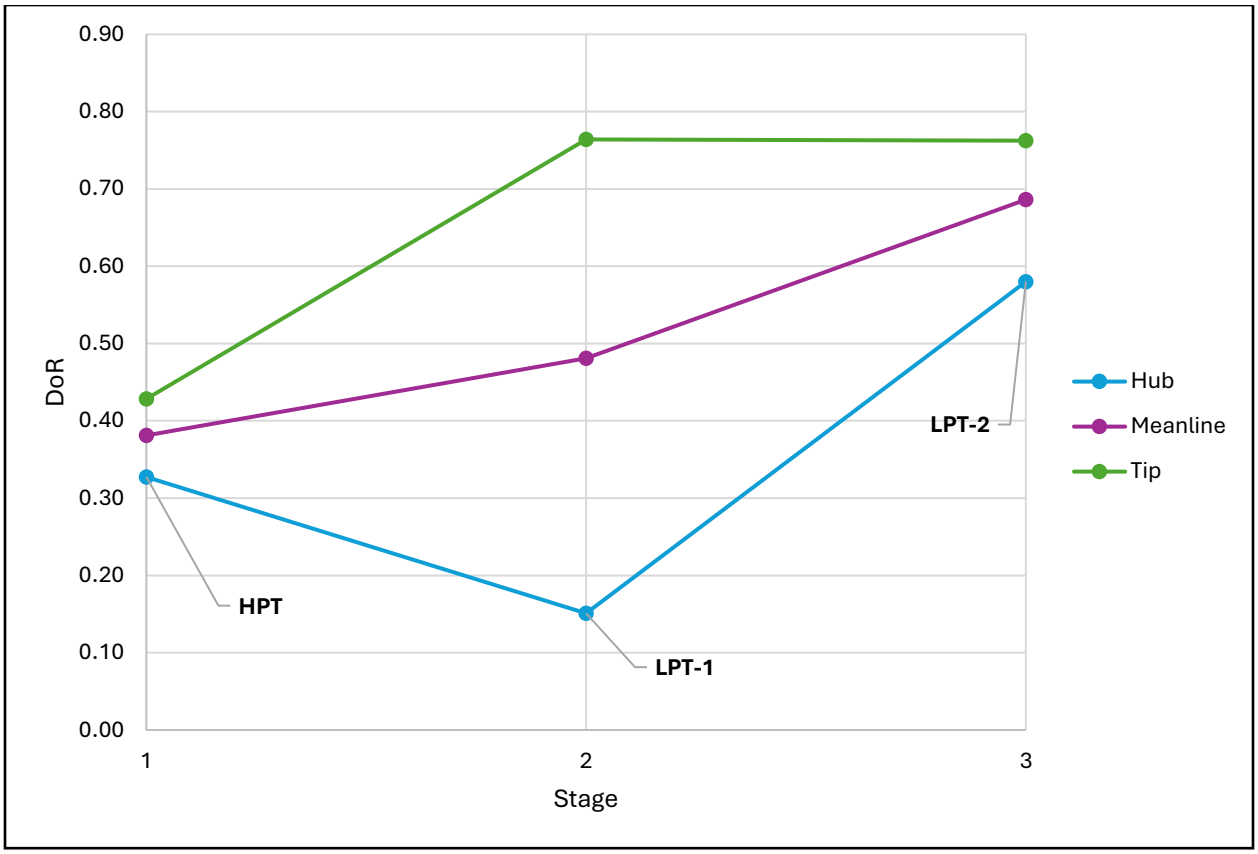

Figure 59: Degree of Reaction vs Stage

Nozzle Design

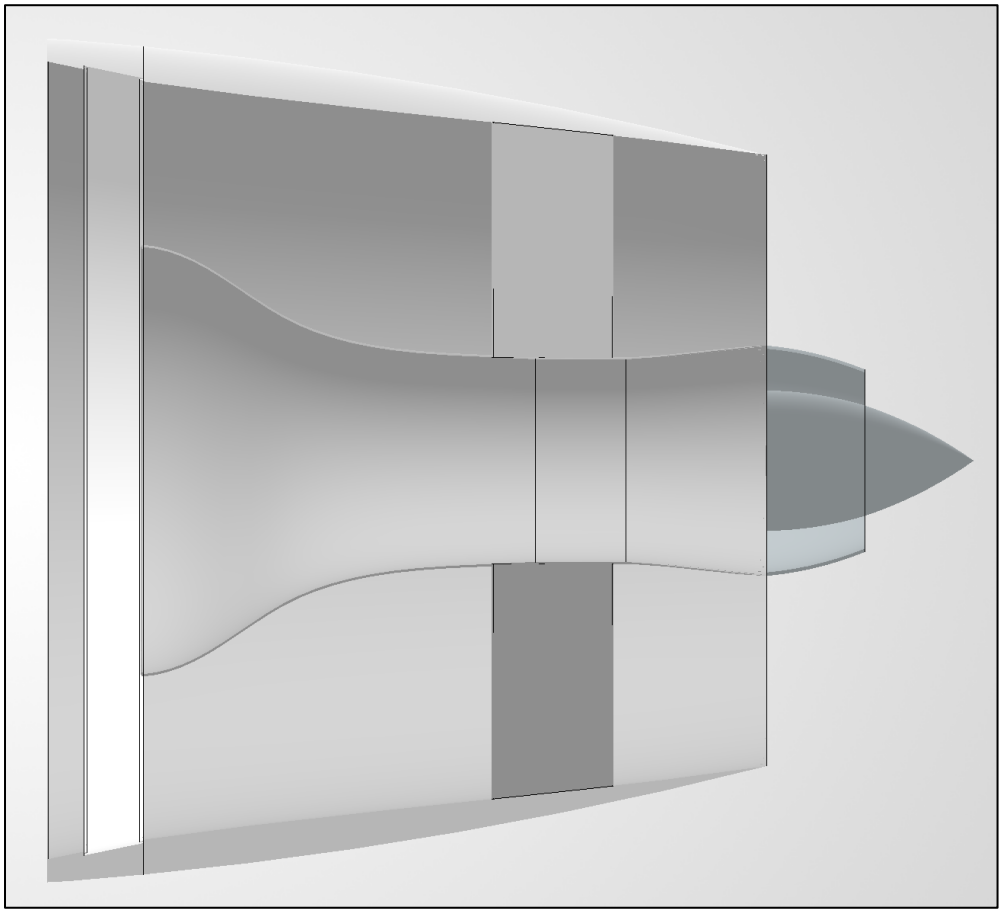

Figure 60 – Nozzle CAD model

The nozzle serves as the final stage of the engine cycle. It is responsible for converting the high-internal energy of the core and bypass streams into kinetic energy to produce thrust. The goal of the nozzle is to maximize the energy conversion while maintaining a lightweight, low installation, efficient gas expansion, and low noise.

The flight condition at which the nozzle was designed is cruise, where $M_{0R} = 0.85$, $h_{0R} = 12{,}192\ m$, $P_{0R} = 18.823\ kPa$, and $T_{0R} = 216.65\ K$. Following the baseline configuration of a high-bypass turbofan, a separate exhaust, non-afterburning configuration was selected. This decision also comes from the preliminary design analysis. The inlet conditions for the nozzle were derived from the cycle analysis. For the core nozzle, the inlet total conditions at Station 7 were taken from the LPT exit (Station 5), assuming adiabatic flow through the exhaust duct. Therefore $T_{t7} = T_{t5} = 1044.56\ K$ and $P_{t7} = P_{t5} = 158.89\ kPa$. An inlet Mach number of $M_7 = 0.6$ was selected which is consistent with the LPT 2nd stage exit from the turbomachinery design. For the bypass nozzle, the inlet total conditions correspond to the fan exit, where $T_{t17} = 269.01\ K$, $P_{t17} =$

37.67 kPa and $M_{17} = 0.55$. The total pressure losses through the nozzle ducts are captured by $\pi_n = 0.997$ for the core and $\pi_{nf} = 0.98$ for the bypass.

The core nozzle throat area is $A_9 = 0.264\ m^2$, converging from an inlet area of $A_7 = 0.501\ m^2$, while keeping the hub-to-tip ratio of 0.627 from the LPT 2nd stage exit geometry. The bypass nozzle converges from an inlet area of $A_{17} = 7.87\ m^2$ to a throat of $A_{19} = 6.40\ m^2$. Both nozzles are choked at cruise, where the core nozzle pressure ratio $NPR = 8.441$ far exceeds the critical value of 1.838. The bypass $NPR = 2.0$, is a little bigger than the critical value of 1.932.

Table 13 summarizes the key nozzle performance parameters at the cruise design point. The nozzle adiabatic efficiencies confirm almost ideal performance for both core and bypass. The gross thrust values are also consistent with the cycle predicted net thrust of 67 kN, which was verified by the equation below:

$$F_{net} = F_{g,core} + F_{g,fan} - F_{ram} = 47.52 + 179.11 - 159.30 = 67.33\ kN$$

Table 13: Nozzle measures of performance

	Core Nozzle	Bypass Nozzle
$\boldsymbol{\pi_n}$	0.997	0. 98
$\boldsymbol{\eta_n}$	0.995	0.972
$\boldsymbol{NPR}$	8.441	2.00
$\boldsymbol{NPR_{crit}}$	1.838	1.932
$\boldsymbol{F_g}$ **(kN)**	47.52	179.11
$\boldsymbol{A_7/A_{17}(m^2)}$	0.501	7.87
$\boldsymbol{A_9/A_{19}(m^2)}$	0.264	6.40

A trade study was conducted to determine if a Convergent-Divergent (CD) nozzle was justified over a simpler convergent-only design. The core nozzle operates at a Nozzle Pressure Ratio (NPR) of 8.44. As shown in Figure 61, the theoretical thrust gain from adding a diverging section at this pressure ratio is about 7.7%. This gain is above the 5% plateau threshold, which is typically required to justify the added weight and complexity of a CD nozzle. However, with a bypass ratio of 11, the core produces only 21% of total gross thrust, which reduces the effective total engine thrust gain from the CD core nozzle to approximately $7.7\% \times 21\% \approx 1.6\%$, which is insufficient to justify the added weight, length, and complexity.

The bypass nozzle design point at $NPR = 2.00$ has a thrust ratio of approximately 1.00, shown in Figure 60, confirming that there is no thrust benefit from adding a diverging section. The exit static pressure ratio $P_{19}/P_0 = 1.036$ at cruise implies that the fan nozzle is nearly perfectly expanded, therefore, no CD trade study is required for the bypass nozzle.

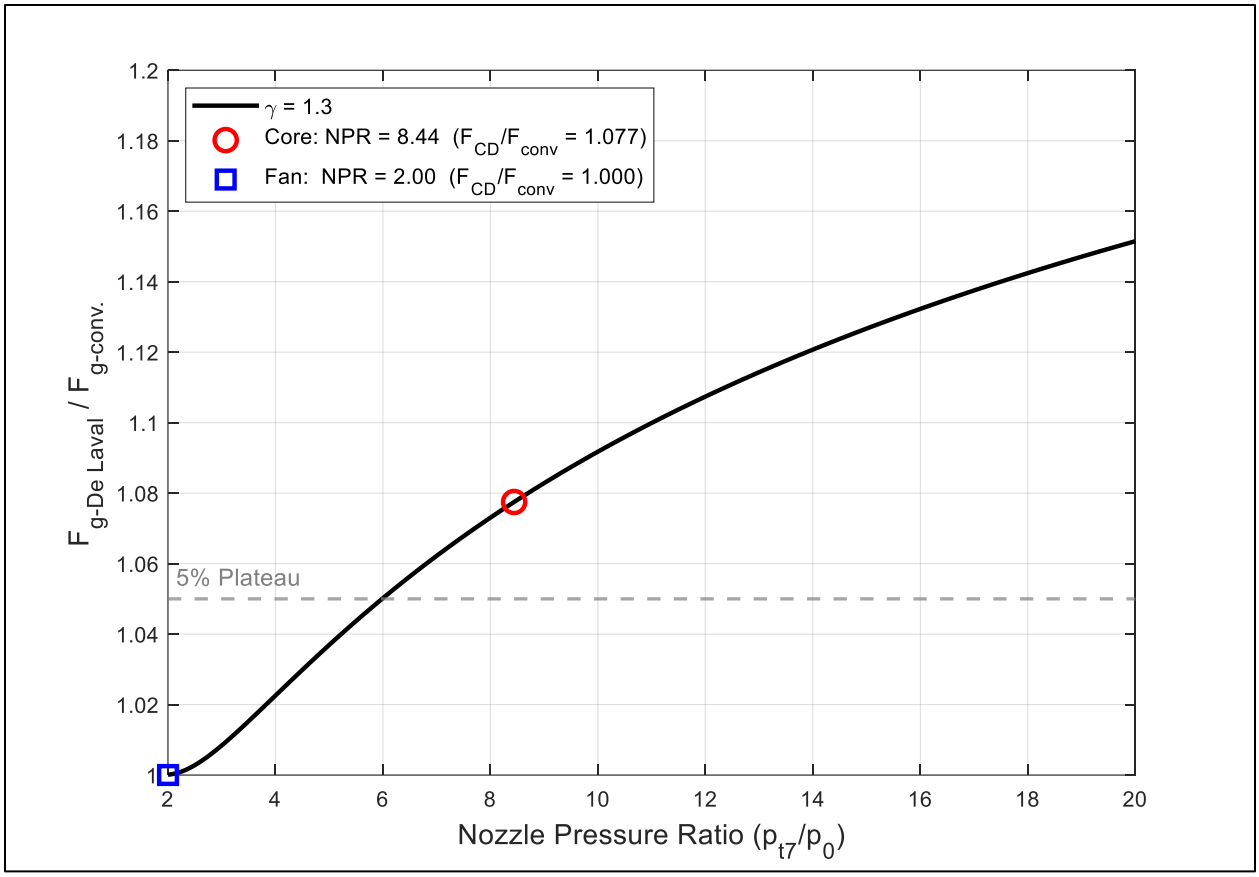

Figure 61: Thrust ratio of ideal CD nozzle to convergent nozzle vs nozzle pressure ratio

Figure 62 shows the core gross thrust versus core diverging section length for a conical nozzle with a 15-degree half-angle. At the diverging length of approximately 0.5 m, the maximum gross thrust of 50.47 kN was reached, where the exit pressure is equal to ambient pressure. While the thrust gain of approximately 3 kN over the convergent-only thrust is visible, the required half-meter diverging section and narrow total engine benefit confirm the convergent-only selection.

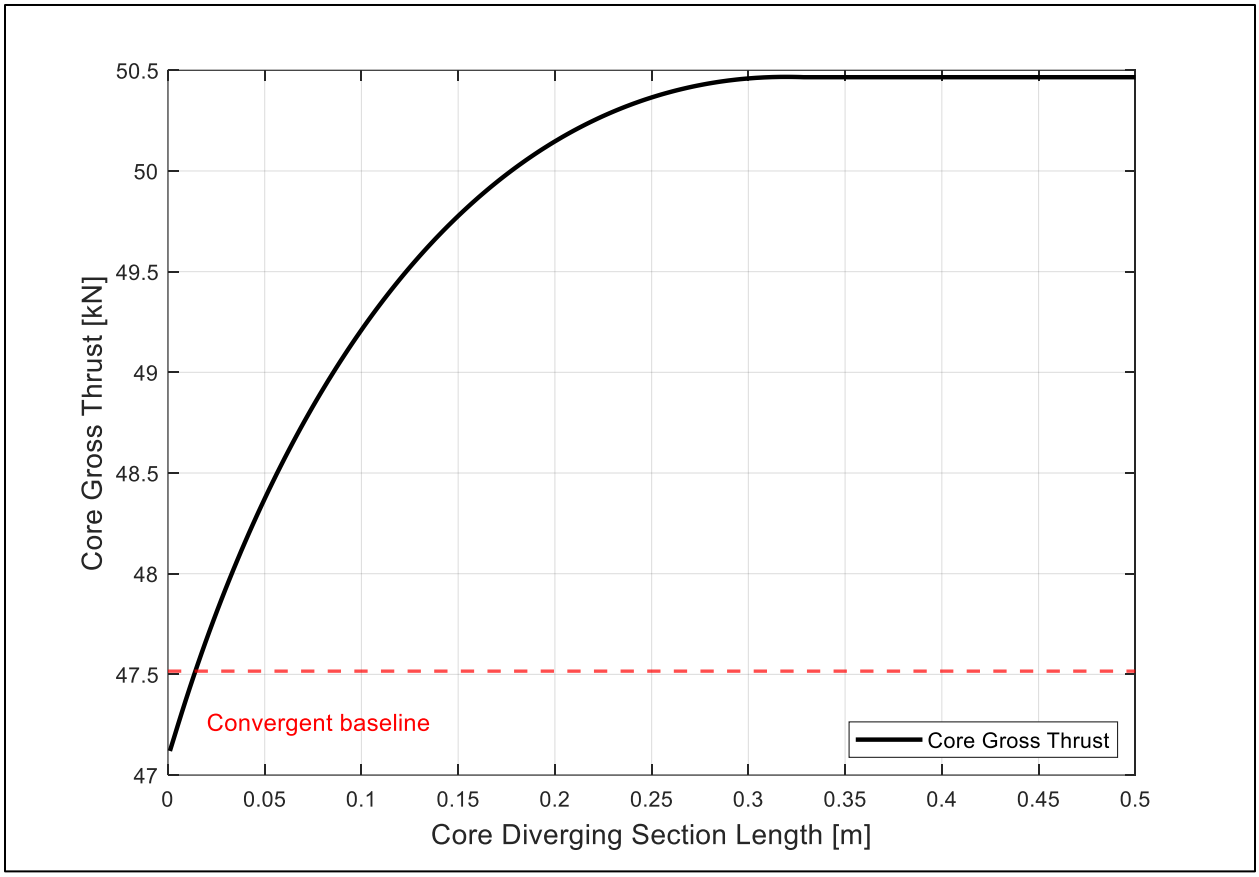

Figure 62: Core nozzle gross thrust vs diverging section length for a conical nozzle with 15-degree half-angle.

Figures 63 and 64 summarize the parameters at nozzle stations 7, 8, 9 (core) and stations 17, 18, and 19 (bypass). They detail the Areas, Flow Velocities, Mach Numbers, Total and Static pressures, and temperatures at each station. For the convergent nozzle, stations 8 and 18 are coincident with the exit stations 9 and 19. The core nozzle accelerates the flow from $M_7 = 0.6$ and $V_7 = 364\ m/s$ at the inlet to a choked exit velocity of $V_9 = 580\ m/s$. The static temperature dropped from 991 K to 908 K as thermal energy is converted to kinetic energy. The total temperature remains constant at $1044.56\ K$ across all core stations, confirming adiabatic assumption. The core exit static pressure $P_9 = 86.45\ kPa$ is more than $P_0 = 18.82\ kPa$, showing the underexpanded condition natural to a convergent nozzle at this NPR. The bypass nozzle accelerates from $M_7 = 0.55$ to a choked exit at $V_{19} = 300\ m/s$ with total temperature 269.01 K.

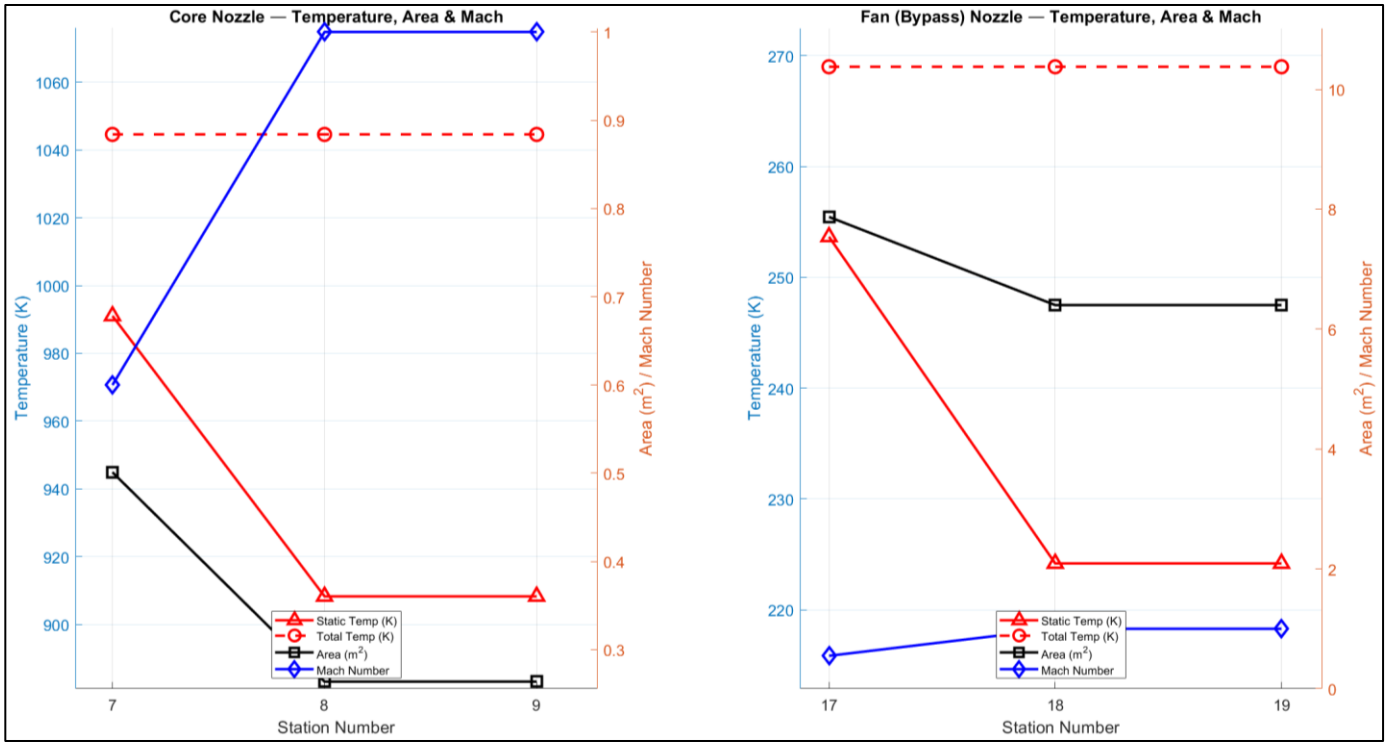

Figure 63: Static and Total Temperature, Area, and Much Number vs Station Number

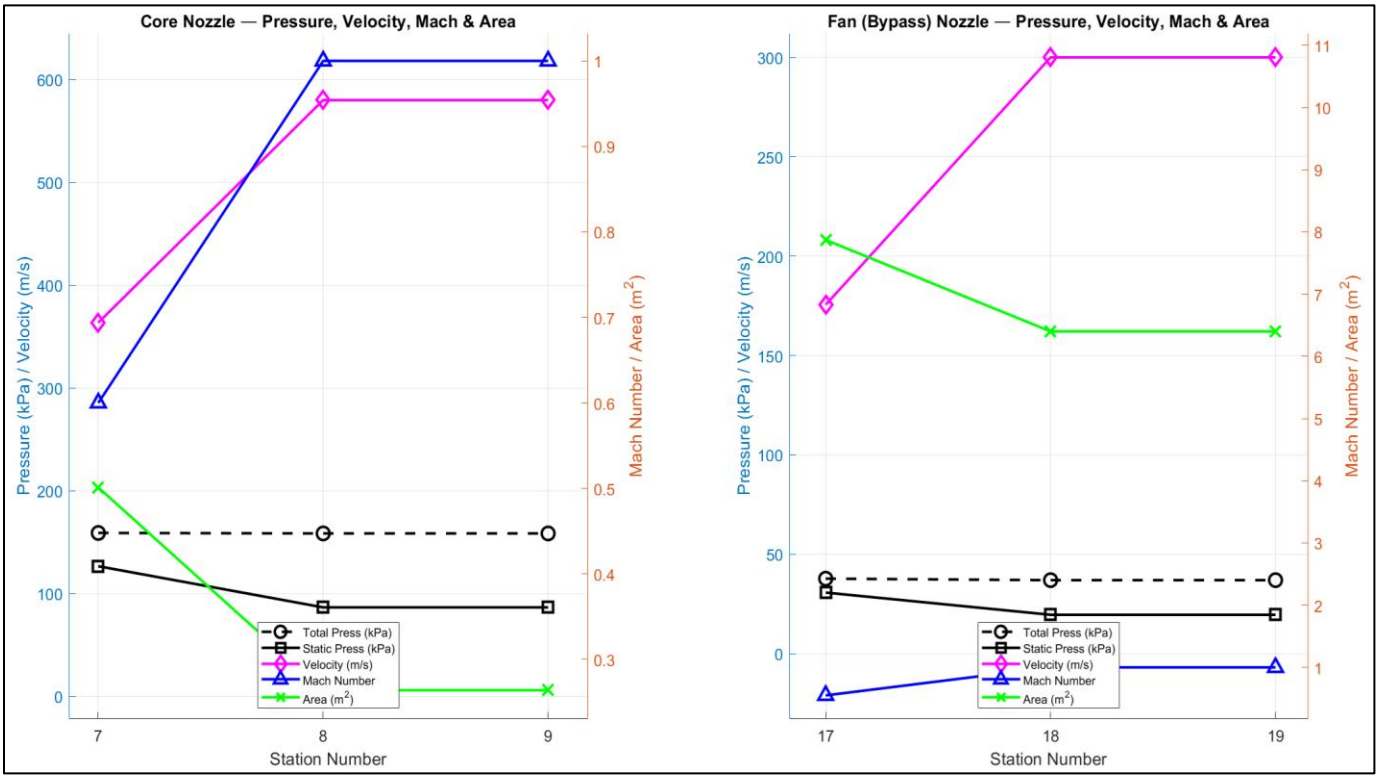

Figure 64: Static & Total Temperature, Flow Velocity, Area, and Mach Number vs Station

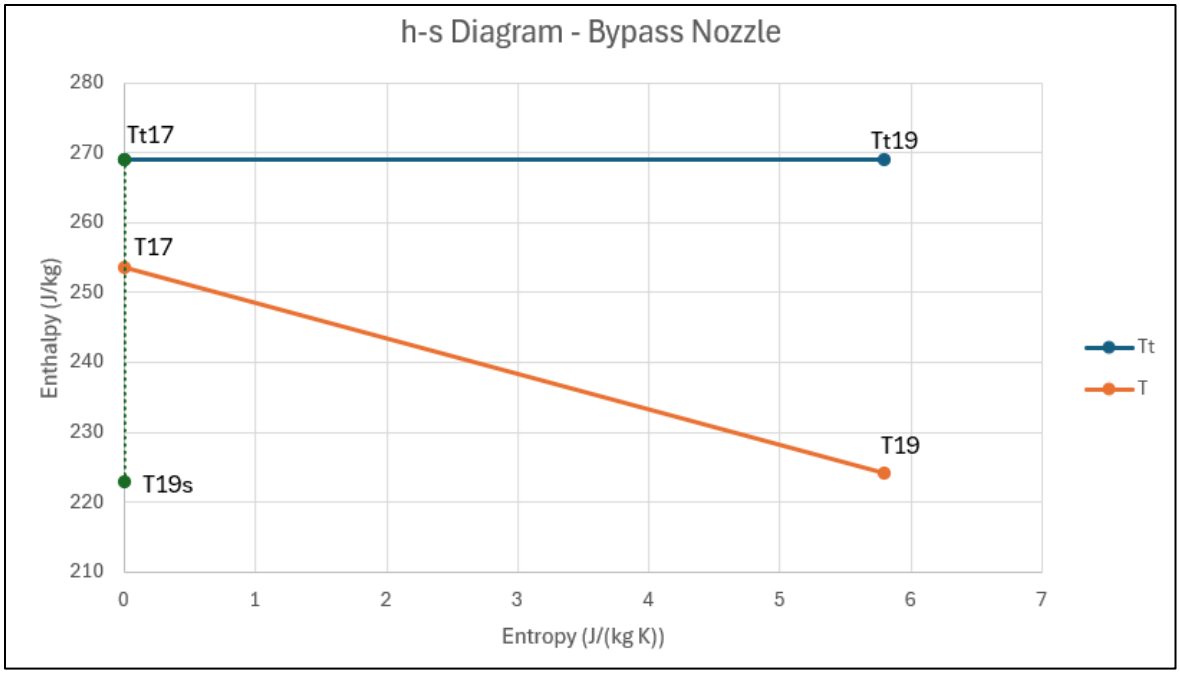

Figure 65: h-s diagram for the bypass nozzle

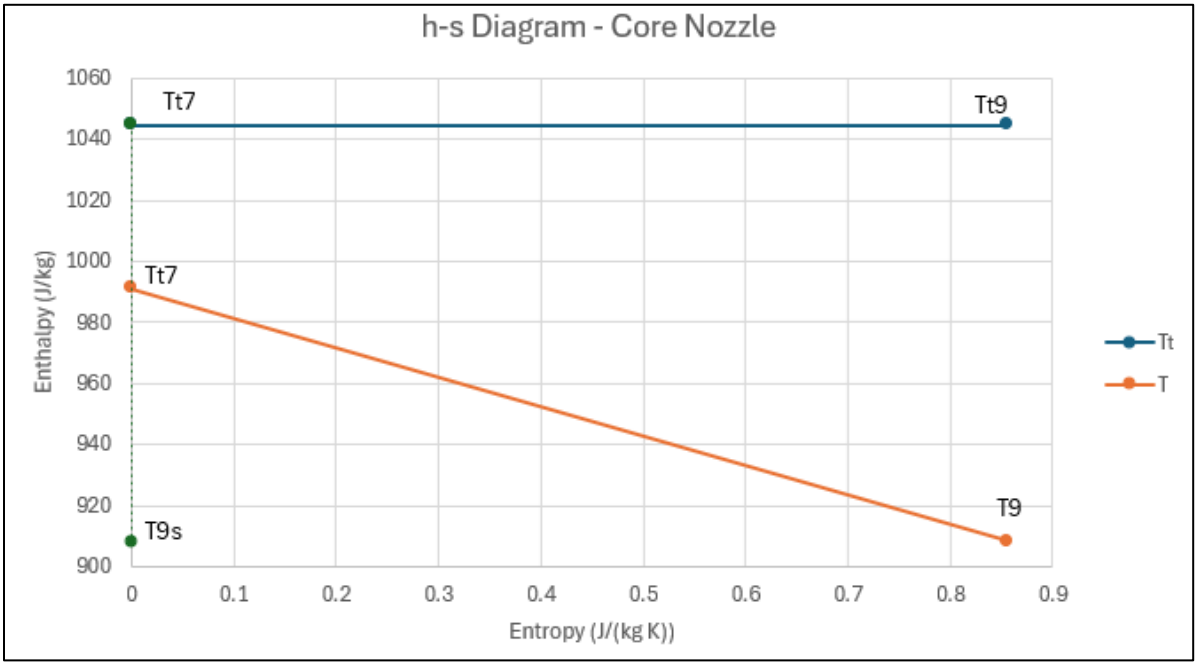

Figure 66: h-s diagram for the core nozzle

Figures 65 and 66 show the h-s diagrams for the core and bypass nozzles and follow the expected trend.

Appendix A: Engineering Ethics

The design of the ER-18 high-bypass turbofan engine has significant impacts on public health, safety, and welfare. Public health and safety are paramount, which is why the ER-18 propulsion system is designed with conservative performance modeling and structural integrity in mind. By making conservative assumptions and validating performance, operators have a better understanding of the limits of the engine, which can be used to determine One Engine Inoperative (OEI) reliability. This reduces the chance that a bird-strike or blade-out scenario causes harm to operators of the aircraft as well as the general public. From an environmental standpoint, the ER-18 propulsion system minimizes its carbon footprint through its efficient design. The engine design implements a high-bypass ratio, maximum pressure ratios, and minimum turbine inlet temperature in an effort to reduce fuel consumption. These design choices reduce the amount of pollution and emissions from the propulsion system. This also brings additional benefits such as reducing operational costs.

There are many ethical implications that must be considered with the design of the ER-18 propulsion system. From a global perspective, the ER-18 engine is designed to support military operations, specifically performing heavy airlifts, delivering supplies, and transporting troops. However, this global reach carries the ethical weight of ensuring the system is versatile enough for humanitarian aid and disaster relief. This is where the engine's reliability and performance are especially important since the aircraft may need to land and take off from suboptimal runways to provide aid. From an environmental perspective, the ER-18 propulsion system must balance technical performance along with environmental stewardship. The ER-18 engine does this by maximizing its efficiency with the previously mentioned design choices. From a societal perspective, the design impacts the safety and welfare of both the crew and the population over which it flies. This necessitates a commitment to providing accurate performance data of the engine. To conclude, the ER-18 propulsion system shouldn't only fulfill its contracted mission, but also ethical commitments that impact society and the environment.

Appendix B: Engineering Standards

As engineers, it is important to adhere to engineering standards during the design process. Early incorporation of engineering standards ensures that the propulsion system is inherently safe, certifiable, and reliable before significant money is invested in manufacturing the engine. The primary challenge in this is the balance of meeting performance targets and aircraft propulsion design standards. An example of this is reducing turbine inlet temperature to improve lifetime of the hot section, but reducing engine performance as a consequence.

1. §33.62 Stress Analysis

   Under standard §33.62, a comprehensive stress analysis must be performed on all high-stress components, such as the compressor and turbine blades. During the detailed design, this involves validating that no component exceeds its yield strength under high-stress operating

conditions like overspeed or extreme temperatures. Specifically, stress analysis can determine the type of materials needed to manufacture certain components, like using nickel-titanium alloys for the extreme temperatures experienced by the turbine blades.

2. §33.65 Surge and Stall

Standard §33.65 requires that the engine remains free of surge and stall throughout its entire operating envelope, including the rapid accelerations required for tactical airlifts. To comply with this, the ER-18 propulsion system may require variable stators and bleed valves to optimize the airflow and reduce stall. However, this solution adds complexities to the engine which increases operational costs.

3. §33.70 Life- Limit on Parts

Under standard §33.70 (a), the design must establish a mandatory life-time limit for critical rotating components, based on the number of flight cycles or operating hours. This is determined through fatigue analysis and testing. In the case of the ER-18 propulsion system, it may require de-rating the engine's performance or increasing the material thickness to meet the life-time requirements.

Appendix C: Teamwork / Self-Reflection

Anuranan Bharadwaj

Attendance and preparation were important for this project since a lot of the design decisions were interconnected, especially between the cycle, turbomachinery, and other components. Missing even a single discussion could lead to inconsistencies later in the design. I made sure to attend all meetings and stay prepared before discussions so I could contribute meaningfully. This helped keep the workflow smooth and avoided rework. Based on this, I would rate my attendance and preparation as 5/5.

Having a collaborative and inclusive environment was important since different parts of the engine design depended on each other. Throughout the project, we made sure to keep communication open and discuss major design choices together rather than working in isolation. I tried to keep everyone aligned with the overall direction of the engine, especially when changes in one component affected others.

Leadership in this project mainly came from driving the overall design direction and making key decisions when needed. My role was focused on leading the engine design, especially for the inlet and turbomachinery components, which were the most critical parts of the system. I was responsible for making many of the design choices and ensuring that everything stayed consistent with the cycle requirements. I also helped troubleshoot issues when things were not working. At the same time, I made sure to support the team by explaining design decisions and keeping the overall approach clear.

Planning was important since this project involved multiple components that had to work together. Instead of trying to design everything at once, we followed a step-by-step approach starting with the cycle, then moving to inlet, turbomachinery, and finally the combustor. We divided work based on components but kept checking in regularly to make sure everything was still aligned. This approach helped us stay on track and gradually refine the design without losing consistency.

Nicholas Pradilla

Being involved in a project requires someone to be present and prepared. Coordination between team members begins with consistent meetings with preparation to give updates on calculations and design decisions. I would rank myself for attendance and preparation at a 4/5. I tried to stay updated on assigned tasks and review before meetings, but I missed attendance on some meetings.

Ensuring that each team member is included in discussions and decisions regarding the design of the engine is important when feedback is needed. Our team was comfortable raising concerns to each other and team members often asked for feedback when it was needed. By doing this our team was able to prevent communication gaps that may have affected our design.

Being a leader was important to stay organized and on task. As the leader of certain sections of the project, I asked my team to have their calculations and models in a designated folder on OneDrive to ensure that everyone had access to each other's files.

For this project planning was essential and required everyone to understand the outcome of each individual goal. By breaking down the project into smaller goals we were able to effectively distribute responsibilities and meet deadlines. We tracked each other's progress through Teams Chat and gave frequent updates for the pacing of our work. This made us meet objectives smoothly and allowed for feedback from teammates often.

Kalkamanali Satvaldy

Attendance and preparation are both very important for working in any team environment, missing any group meetings can possibly delay certain tasks which not only leave you behind in tasks but the team members as well. I would rate myself 4/5 for this aspect as I didn't attend all the lectures due to being away from university in favor of site visits and tour, as well as attending research conferences. But all those times that I missed any of the team meetings, I would make up by both notifying the team about an absence and contacting the team for an update to catch up.

Having and maintaining a collaborative and inclusive environment in a team is also very important because good relationships within the team members lead to better results in the tasks the team is working on. It is important to allow everyone in the team to express their thoughts and opinions without diminishing or belittling them. For our team specifically, the approach was to have an open communication in the aspect of the engine design and collaborate for most tasks, instead of working separately with no communication. During the times when I or someone else were left behind, the team would always make sure that everyone is caught up.

Leadership is important because some sort of hierarchy has to be established in a team working environment. Not everyone can be the boss, there has to be a designated leader for different projects and parts. To be a good leader you need to be ablet manage the team and assign tasks effectively. I was the team lead for the nozzle, not the most challenging part of the engine for sure but still I feel like I fulfilled my role.

Planning is very important in capstone projects such as this, where many interconnected components are included and any delay would cause another delay and etc. We as a team tried to set early deadlines so that in case of changes being made there would be plenty of time for revisions.

Vincent Shi

Attendance and preparation are two important aspects when working as an engineering team. Frequent absences can cause delays in the design process and can lead to engineering issues being unresolved for extended periods of time. I would rank myself a 4.5/5 at most, as while I was present for the majority of the semester, I ended up missing a handful of days due to research conferences and facility visits.

Inclusion is important in a team setting because it allows for multiple perspectives when working on a project. This is important because someone may point out an issue that was overlooked by other members of the team, allowing for a more concise and thought-out solution. In our team, we took turns sharing out design progress to make sure we could address issues early on. This allowed for a more fluid design process, as my team could point out mistakes that I made and give advice on certain design choices.

Leadership provides teams with a way to delegate tasks to team members so that they can work together to reach the same goal. Effective leadership helps teams ensure the collective success of the project. When I modeled the engine, I reached out to each team member to collect measurements of engine components and provided feedback when things didn't look right. This allowed us to develop a model of the engine that was accurate.

A project such as the design of a propulsion system requires a lot of planning. By setting deadlines and objectives, our team was able to go through the design process without experiencing major hiccups. Specifically, we tried setting earlier deadlines for reports to have an extra day for formatting and checking for errors.

Appendix D: Detailed Station Data

Cycle:

Table 13**:** Engine Station Parameters at Design Point

	MATLAB Design Tool		**AEDsys Outputs**	
Engine Station Number	Total Temperature (K)	Total Pressure (kPa)	Total Temperature (K)	Total Pressure (kPa)

0	311.17	121.60	311.17	121.60
2	311.17	121.36	311.17	121.60
13	337.58	157.76	337.59	157.77
19	337.58	154.61	337.59	154.62
2.5	461.12	424.74	461.13	424.77
3	1095.00	6674.56	1095.03	6674.89
4	1778.00	6407.58	1777.77	6407.89
4.1	1773.40	-	1777.32	-
4.4	1227.99	-	1234.04	-
4.5	1226.14	1091.45	1233.86	1106.31
5	849.62	186.61	857.13	191.46
9	849.62	186.05	857.13	190.89

Inlet:

Table 14: Takeoff vs Cruise Comparison

	Takeoff	Cruise
M_0	0.10	0.85
P_0	101.33 kPa	18.82 kPa
T_0	327.59 K	216.65 K
$\dot{m}_0$	1578.84 kg/s	631.00 kg/s
$\dot{m}_{0,corr}$	1673.28	1964.53
A_0	40.37 m^2	8.31 m^2
M_1	0.50	0.65
P_1	85.76 kPa	22.70 kPa
T_1	312.35 K	228.55 K
M_{th}	0.53	0.70
P_{th}	84.21 kPa	21.76 kPa
T_{th}	310.72 K	225.83 K
M_2	0.45	0.55
P_2	85.25 kPa	23.60 kPa
T_2	315.47 K	233.81 K

Table 15: Takeoff Condition

Parameter	Station 1	Throat	Station 2
Static Temperature (K)	312.4	310.7	315.5
Static Pressure (kPa)	85.76	84.21	85.25
Total Temperature (K)	328.2	328.2	328.3
Total Pressure (kPa)	102.1	101.9	97.95
Mach	0.50	0.53	0.45

Table 16: Cruise Condition

Parameter	Station 1	Throat	Station 2
Static Temperature (K)	228.6	225.8	233.8
Static Pressure (kPa)	22.7	21.76	23.59
Total Temperature (K)	248.0	247.9	328.2
Total Pressure (kPa)	30.19	30.16	28.98
Mach	0.65	0.70	0.55

Fan:

Table 17: Degree of Reaction- Fan

DoR	Value
Hub	0.40
Meanline	0.87
Tip	0.95

LPC:

Table 18: Stage Characteristics - LPC

Stage	NoB (Rotor)	NoB (Stator)	Load Coeff	Flow Coeff @ St 1	Flow Coeff @ St 2	$\Delta\alpha$	$\Delta\beta$
1	40	36	-0.46	0.63	0.69	-33.44	19.68
2	46	42	-0.46	0.73	0.80	-29.66	19.68
3	50	42	-0.39	0.81	0.85	-24.67	15.32

Table 19: Degree of Reaction - LPC

Stage	Hub	Mean	Tip
1	0.52	0.79	0.90
2	0.59	0.76	0.84
3	0.67	0.76	0.82

Table 20: Health Assessment - LPC

Stage	DH (Rotor)	DH (Stator)	DF_bar (Rotor)	DF_bar (Stator)
1	0.74	0.87	0.04	0.43
2	0.78	0.88	0.03	0.38
3	0.81	0.90	0.04	0.32

HPC:

Table 21: Stage Characteristics - HPC

Stage	NoB (Rotor)	NoB (Stator)	Load Coeff	Flow Coeff @ St 1	Flow Coeff @ St 2	$\Delta\alpha$	$\Delta\beta$
1	74	60	-0.35	0.47	0.55	-32.47	15.27
2	108	82	-0.35	0.59	0.65	-28.16	14.57
3	110	93	-0.35	0.67	0.65	-28.30	11.24
4	110	94	-0.35	0.70	0.65	-28.30	10.13
5	90	84	-0.34	0.66	0.67	-27.18	12.21
6	88	79	-0.33	0.71	0.67	-26.22	9.52

Table 22: Degree of Reaction - HPC

Stage	Hub	Mean	Tip
1	0.81	0.86	0.89
2	0.80	0.83	0.85
3	0.89	0.91	0.92
4	0.85	0.86	0.87
5	0.90	0.91	0.92
6	0.84	0.84	0.85

Table 23: Health Assessment - HPC

Stage	DH (Rotor)	DH (Stator)	DF_bar (Rotor)	DF_bar (Stator)
1	0.77	0.90	0.13	0.38
2	0.79	0.90	0.11	0.34
3	0.76	0.94	0.13	0.30
4	0.75	0.90	0.14	0.34
5	0.78	0.95	0.10	0.28
6	0.77	0.89	0.12	0.34

HPT + LPT:

Table 24: Stage Characteristics - Turbine

Stage	NoB (Rotor)	NoB (Stator)	Load Coeff	Flow Coeff @ St 1	Flow Coeff @ St 2	$\Delta\alpha$	$\Delta\beta$
HPT	45	51	2.00	0.87	1.00	62.00	-90.61
LPT – 1	33	38	2.10	1.42	0.81	50.00	-88.62
LPT – 2	61	66	2.00	0.97	0.90	53.00	-80.76

Table 25: Degree of Reaction - Turbine

Stage	Hub	Mean	Tip
HPT	0.33	0.15	0.58
LPT – 1	0.38	0.48	0.69
LPT – 2	0.43	0.76	0.76